UNIVERSITÀ DEGLI STUDI DI PADOVA

Dipartment of Industrial Engineering

Master's degree in Energetic Engineering

Master's Thesis

DEVELOPMENT OF CONTROL STRATEGIES FOR HYBRID ENERGY STORAGE

SUPERVISOR: PROF. ANNA STOPPATO

CO-SUPERVISOR: DR. MARCOS LAFOZ PASTOR

STUDENT: LUCIO PANARISI

number 1128880

Academic year 2017/2018

SUMMARY

1 INTRODUCTION ON HYBRID ENERGY STORAGE SYSTEMS (HESS)

The share of energy from renewable sources has grown strongly in recent years. This trend is confirmed by European statistics [1] which state that this share was the 16.7% of the gross final consumption of energy in 2015. Furthermore, the Directive 2009/28/EC of the European Parliament sets this value at 20% for all the member states. This new scenario drives the attention to problems that were easily solvable, such as power quality and consequently system stability. In fact, many of these sources are not predictable and the mismatch between power demand and production leads to voltage and frequency fluctuation, making the grid instable. For this reason, energy storage is becoming a topic of primary interest since the function of an energy storage system is to provide power when the demand exceeds the production or vice-versa when the production exceeds the demand.

The applications of such a system are infinite: nowadays the most common and used one is relative to the hybrid or full electric vehicles, where a pack of batteries and supercapacitors work together with the combustion engine (in the hybrid case) to run the vehicle and improving the total efficiency. In this picture, since distributed generation from unpredictable sources is gaining more and more attention, energy storage can be an effective mean to reduce the unbalance between production and consumption of electrical energy in the power system, reducing the load on less economical peak-generating facilities. Load leveling allows for the postponement of investments in grid upgrades or in new generating capacity. Then, this system made of a renewable source and an energy storage can be connected through a converter to larger networks, such as microgrids (in AC or DC) or the main grid in AC. The control of source and energy storage is achieved through power electronic interfaces and must ensure the power quality of the small system itself as well as the larger one connected. In fact, if the power injected into the main grid by the plant is not controlled and smoothed, voltage and frequency of the grid may be subjected to variations respect their rated values and exceed the safety limits. In this dissertation, such a system working in DC is considered since the energy storage devices (and many renewable sources plants) work in DC, so only one AC/DC converter is necessary and energy dissipation associated with AC/DC conversion can be avoided. Finally, the complexity of the system is reduced.

Whatever the application is, the design of an effective energy storage should take into account peak of power as much as peak of energy. This fact leads to a problem relative to the technologies available: nowadays there is not an energy storage device with both high specific energy and high specific power. Batteries are certainly the most used type of energy storage since their cost is lower than other technologies but they are not the ideal device for every application, especially for those involving high powers. A comparison between technologies is provided by the Ragone plot in Fig. (1.2).
Supercapacitors and flywheels can provide very high peak of power but their specific energy is low. On the other hand, clearly not considering methanol and gasoline, Lithium Ion (Li-Ion) and hydrogen fuel cell have high specific energy but low specific power. This trade-off between energy and power leads to the reflection which inspired this work: combining two different technology, one with high power and the other with high energy, is far more convenient than using only one of them. In fact, the use of one device only means the need of oversizing the entire system in case peak of power or energy occur: choosing for example the Li-Ion batteries, the sizing should carefully look at the peak of power even if a few batteries would be sufficient to cover the energy demand. An effective combination of batteries and supercapacitors would be less expensive and would improve the efficiency and lifetime of the batteries. Such a system is called hybrid energy storage system, HESS. Hydrogen fuel cell and flywheels are other two possible choices, but the first has very slow dynamic performance and both are technologies under development, not completely mature.

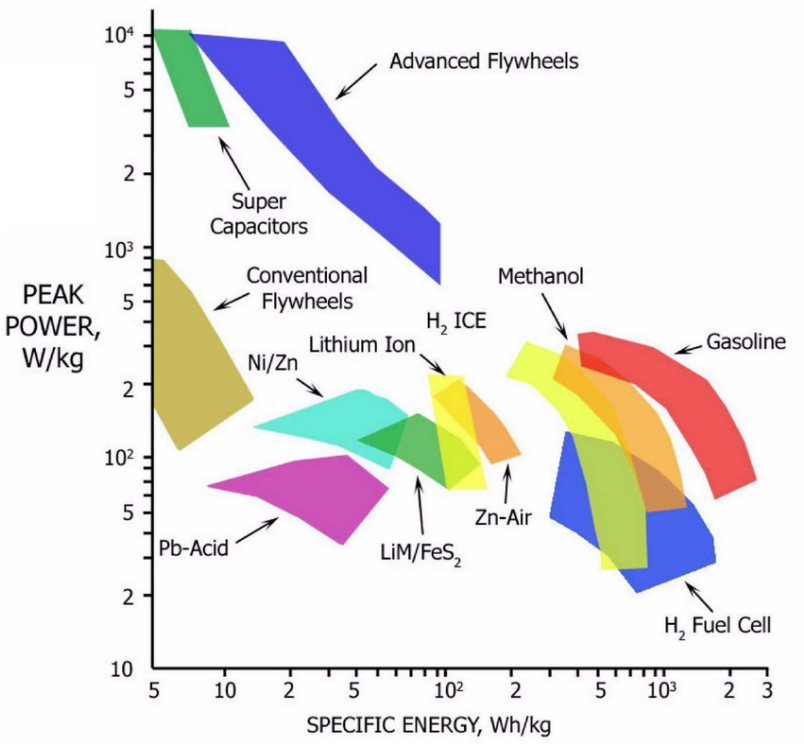

Figure 1.1: Ragone plot for different technologies [2]

Thus, this study considers a HESS made of supercapacitors and lithium ion batteries to smooth the power fluctuation in a DC bus connected to a renewable energy plant that extracts energy from waves motion. The plant does not exist yet and is part of a project under study at CIEMAT, therefore the data of power are generated by a software that uses data collected in the Cantabrian Sea. The aim is proving that an HESS (if effectively controlled) can be cheaper and more efficient than an energy storage system made of batteries only.

Once the energy storage devices are chosen, it is necessary to decide how the power is shared between them and here is where the control strategy acts. An effective strategy should be able to consider the different characteristics of the devices, in order to make them work as close as possible to the nominal conditions specified by the constructor. In fact, if these conditions are not respected, the device lifetime may be reduced and the device itself replaced after a short period. Therefore, after giving some basic concepts regarding the possible topologies of such a system, the battery and the supercapacitor are modelled using the software Simulink and connected to the bus in a parallel active scheme. Then, two different types of control strategies are investigated. All the models are built in Simulink ambient using blocks, declaring the nominal parameters by means of scripts in MATLAB. Since the role of the supercapacitor is to extend the lifetime of the battery, more attention is given to the model of the latter, while a simplified model of the entire DC electric system is used in the simulations. Finally, the comparison between results is presented and each strategy is assessed. However, these results are strictly related to the application and the energy storage devices chosen, so the dissertation wants also to provide the tools to select the appropriate strategy and its parameters in case of other types of systems. In fact, a strategy appropriate in case of supercapacitor and batteries with wave energy as source, may not be adapt in a different system and especially the tuning of the parameters is strongly dependent on the technologies involved. For these reasons, the procedures and equations used are always explained before being applied to the specific case.

2 DESCRIPTION OF THE SYSTEM

This chapter shows the possible configurations that the HESS can assume. Then, the operation of the DC/DC converter is explained in order to implement a simplified model of the grid by using blocks, instead of elements from the Simscape Electronics Libraries of Simulink.

2.1 TOPOLOGY

The topology is the arrangement of the various elements of the system and underlines how they are connected. Specifying the topology is necessary due to different topology will lead to consider different control strategies, which in some topology are possible while in others are not. As explained in the previous chapter, this dissertation considers the HESS and the renewable energy plant connected to a common DC bus, which is then connected to an inverter as connection to the main AC grid. For this reason, the bus voltage should be maintained as close as possible to the reference value to not compromise the operation of the inverter. Since the HESS purpose is to smooth the power fluctuations, the system is connected in parallel to the bus. This means that the main elements of the scheme are the power source, the energy storages (two or more), the DC common bus and the DC/DC converter(s) if present. As stated before, in this paper the energy storage chosen are batteries and SCs. Fig. 2.1 shows the four main possible configurations for the energy storage system, considering how the power is allocated [3]:

a) The first and simplest is the passive topology, in which battery and SC are combined together without using any DC/DC converter. The bus voltage is fixed by the battery voltage, that can be considered quite stable in a certain range of the battery state of charge. On the other side, the SC stored energy can not be utilized efficiently due to the voltage is fixed
b) In the supercapacitor semi-active topology, the battery is still connected directly to the bus so the voltage is fixed, but the SC uses a DC/DC converter, which allows fluctuations of its voltage in a wide range increasing its efficiency, controlling its current
c) The battery semi-active topology is the opposite of the previous one: the SC interfaces the DC bus directly, while the battery uses a DC converter. In this way, it is possible to control the battery current flow that can be maintained at a constant value, increasing the lifetime and energy efficiency of the device. In other words, the converter protects the weaker element. The main drawback is the variation of the bus voltage, which follows the SC voltage
d) Finally, the parallel-active topology is able to solve all the problems spotted above. In fact, by using 2 DC/DC converters, it allows flexible operating voltages, explicit power sharing control for both sources and bus voltage control, which is the key of power quality for such a system. The main drawback of using two DC/DC converters is the higher cost.

Clearly, this classification is valid only in the case of two different energy storage devices used as energy storage system. In the case of batteries only, just one DC/DC converter is necessary to connect the pack with the bus.

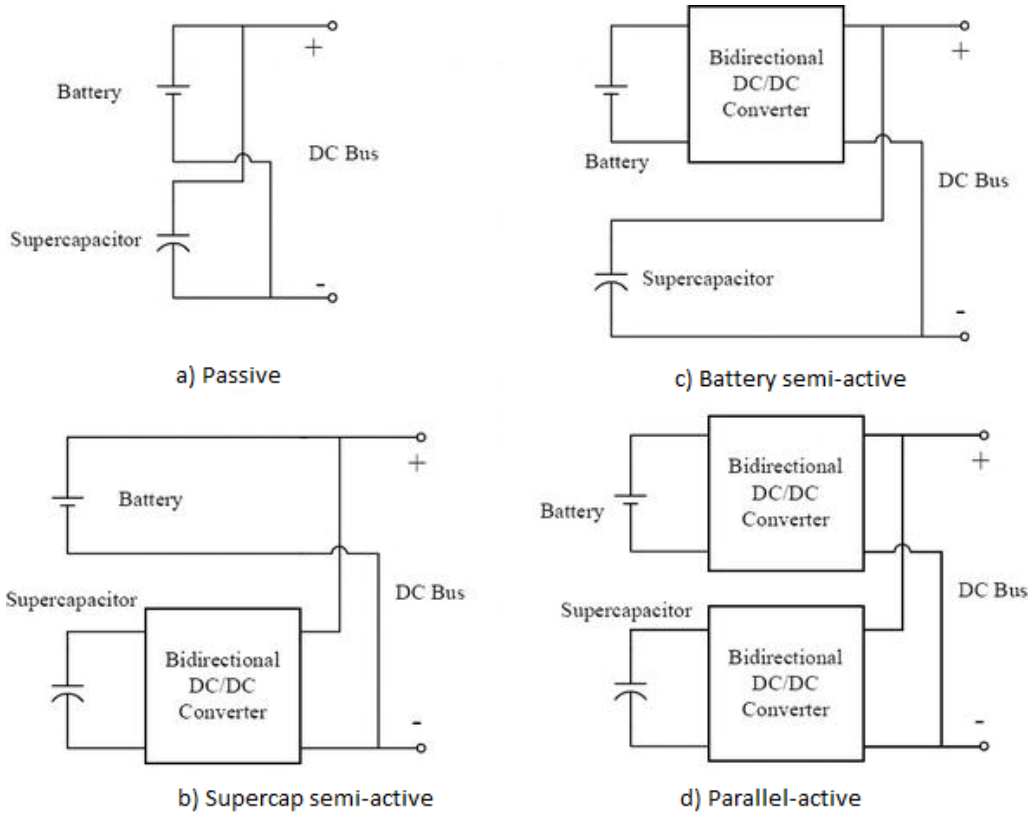

Figure 2.1: different topologies of HESS [3]. The controlled variables are: a) None b) I batt c) I sc d) I batt, I sc, V bus

The most studied and utilized topologies are the supercapacitor semi-active and the parallel-active. The first one is widely utilized in electric vehicle since one converter less means the vehicle is less heavy and less expensive. In fact, in this type of application, weight and cost are the two key factors. The second one instead can be used in stationary application since weight is not an issue and the initial higher cost is justified by a better regulation and higher efficiencies for the two devices (by using the appropriate control strategies). Since this study investigates control strategies that regulate the voltage of the bus and provide reference signals to both the energy device storages, only the full-active topology is considered.

In this dissertation, the price of the converter is considered in terms of €/kW. Therefore, since the total amount of power managed by the energy storage system is always the same, the price of the converter when using only batteries is the same as the price of two smaller converters connecting the supercapacitor and battery packs to the bus. This consideration is close to the reality since the main cost component of the converter is the number of brunches in parallel which determine the total amount of power it can manage: the more the branches, the higher the rated power and the cost.

Finally, the system studied in this dissertation can be represented with the scheme in Fig. 2.2 where two DC/DC converters are used to connect the two devices to a common DC bus. The main grid could be a DC or AC grid and the renewable energy source (RES) any type of plant producing non-constant power. As previously stated, the RES in this case is wave energy and the data analysis will be conducted in chapter 3.

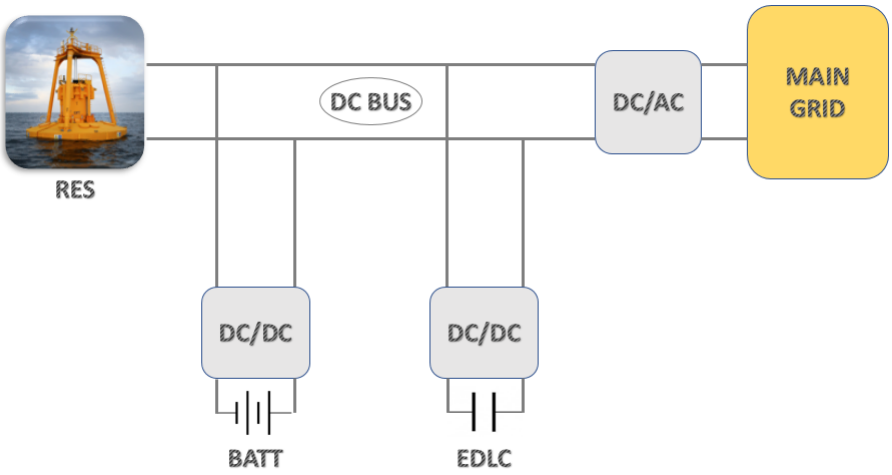

Figure 2.2: scheme of the system considered in this dissertation

2.2 DC/DC CONVERTER AND SIMPLIFIED MODEL OF THE SYSTEM

As previously stated, two DC/DC converters are considered for the topology chosen. They are used as interfaces to the bus and are bidirectional, since the power flow can occur in both directions as the system works to smooth power fluctuation, and they are subjected to the control strategy chosen which acts on an upper level. Since their model is quite complex and requires a large amount of time to be simulated, this dissertation will consider the converters as simple current/power sources that perfectly follows the directive of the control strategy, extracting more or less power from their respective energy storage device. In order to explain why such a simplification is reasonable, it is useful to briefly explaining their principle of operation.

A DC-to-DC converter is an electronic circuit which is able to convert a source of direct current from one voltage level to another. It is widely used in many electronic devices that use batteries since it allows to use one battery only instead of multiple batteries to provide power. Furthermore, as discussed later, the voltage of energy storage devices usually decrease as the energy is drained so the DC/DC converter allows to have a constant voltage at the desired level. Converters that are able to step up the voltage level are called 'Boost converters' while converters that reduce the voltage level are called 'Buck converters'. A third type is the one which is both buck and boost, that is the 'Buck-Boost'. Finally, those whose operation is based on switching, can be made bidirectional to move power in either direction.

Switching is the most efficient conversion method. When the switch of the converter is in the On-state, the voltage source is directly connected to the inductor L, which acts as an energy storage (a magnetic field storage). The longer the switch is in On-state, the higher is the output voltage since the inductor is charged for a longer period. The energy is accumulated in L while the capacitor C supplies energy to the output load. When in Off-state, the inductor is connected to the output and C, inverts its polarity and transfer its energy to the load and C. So, thanks to this energy transfer mechanism, the load can be powered at any voltage which will be equal to $V_{in} + V_L$. Since the voltage of the inductor during the On-state and that of the capacitor during the Off-state are not constant but slightly decrease as the element is discharged, the output voltage is not properly constant but will be a ripple signal related to the repeated change of state of the switch (see ref. [4], [5] for detailed information).

Fig. 2.2 shows the current flows during the modes. The state of the switch depends on a reference value given by the control strategy and, as the last step, is regulated by a PWM generator, which

basically compares an error signal with a waveform generated by a function generator. The frequency of this waveform is high, usually between 100kHz and 5MHz, and is called 'commutation frequency'. The last comparison provides a modulated signal between 0 and 1 which correspond to the Off and On-state. The duty cycle is the amount of time (in percentage of commutation period which is the inverse of the frequency) during which the switch is in On-state. In other words, the PWM output is a rectangular wave between 0 and 1 and the thickness of each rectangle is the duty cycle of that single period. This means the output voltage is related to the density of the rectangles.

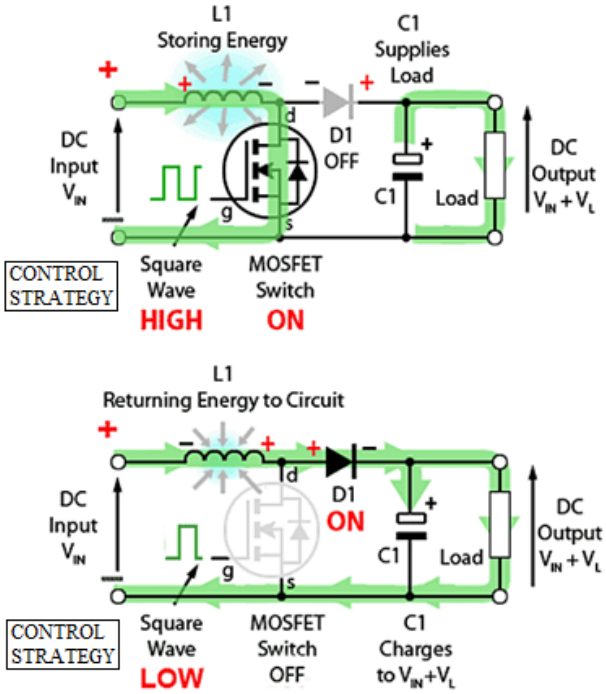

Figure 2.3: current flow during On/Off-state [4]

The element that processes the error signals and indirectly controls the state of the switch is the proportional–integral–derivative controller (PID), widely used in control systems [6]. A PID controller continuously calculates an error value as the difference between a desired setpoint and a measured process variable and applies a correction based on proportional, integral, and derivative terms (denoted P, I, and D respectively), which give the controller its name.

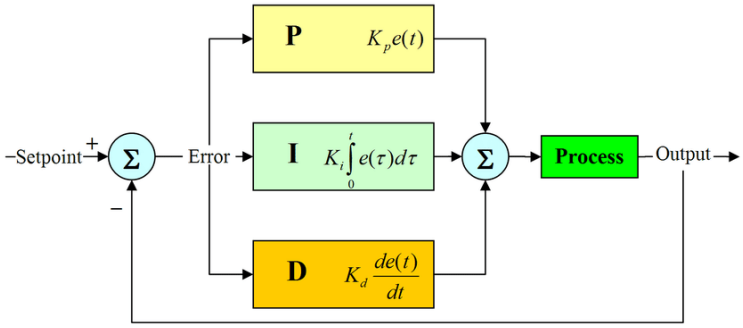

Figure 2.4: block diagram of a PID controller in a feedback loop

When applied to converters, two PI (without the derivate term) loops are usually implemented as control mechanism. As previously explained, the first loop compares the reference voltage with the actual voltage of the bus and the difference is elaborated by the first PI. Its output is a current signal that is compared with the inductor current of the converter (so the current provided by the energy

device). Through a waveform, the duty cycle is calculated and the converter eliminates this error by regulating the on-off state time of the switch. The control strategy operates on an upper level and controls the signal references to the PI controllers, in order to modify the operation of the DC/DC accordingly to the wanted output.

Once the principle of operation is clear, the model can be simplified. In fact, as stated above, the output (as well as the inductor current) will be a rippled signal around the reference voltage provided by the control strategy: the difference between the ripple and the reference is very small due to the high frequency of commutation so the ripple can be neglected and the output considered constant, equal to the reference (during steady state). The higher the frequency, the smaller is the ripple as shown in Fig. 2.4. In other words, the converters work in a far smaller time domain (10^{-4}s) than that where the energy storage and source operate. Hence, the converter can be substitute by the first and slower PI controller of the control loop, which establishes the current that the energy device has to provide.

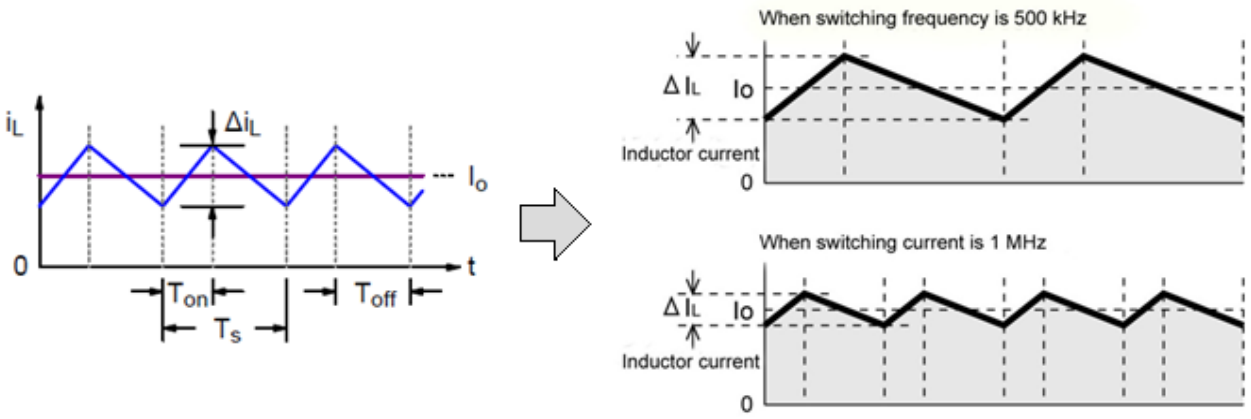

Figure 2.5: inductor current during On/Off-state for different switching frequency. The average value does not change

This simplification is equivalent to assume that the reference current and the actual current in the inductor (so of the device) are always equal. In this way, the PI controller regulates the bus voltage by controlling the power of the device and is manually tuned for each strategy. In order to know the actual voltage of the bus, it is possible to implement a transfer function that gives the voltage of the bus once is known the difference between the generated power and the power of the energy storage. Such a function can be obtained considering the law correlating the voltage and the current of a conductor. In this case, the conductor is the capacitance of the bus and the current is the current crossing it, resulting from the imbalance of powers. Clearly, not all the amount of power generated is handled by the HESS since part of it is dispatched to the main grid (as better explained in the next chapter).

According to Fig. 2.5, the imbalance is given by the difference between the remaining generated power (Pnet) and the HESS power.

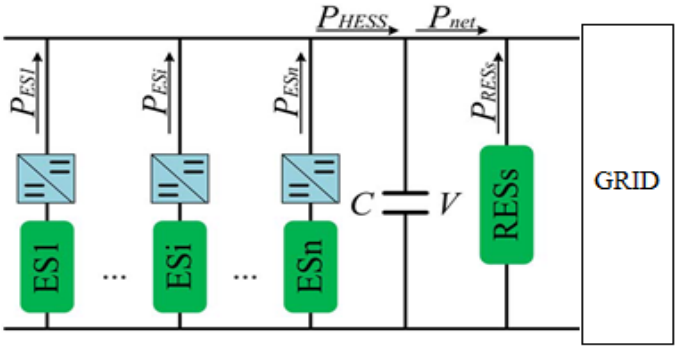

Figure 2.6: power flow direction in a scheme with n energy storages

Then, the resulting equation is [7]:

Equation 2.1

$$Cbus \cdot \frac{dV(t)}{dt} = \frac{P_{HESS}(t) - P_{net}(t)}{V(t)} = I_{capacitance}$$

Then, the new model is that shown in Fig. 2.5, where the bus voltage deviation from the reference value is used as input of the PI controllers, one for each converter. In this way, the system can be built by using simple blocks and simulation time can be far larger.

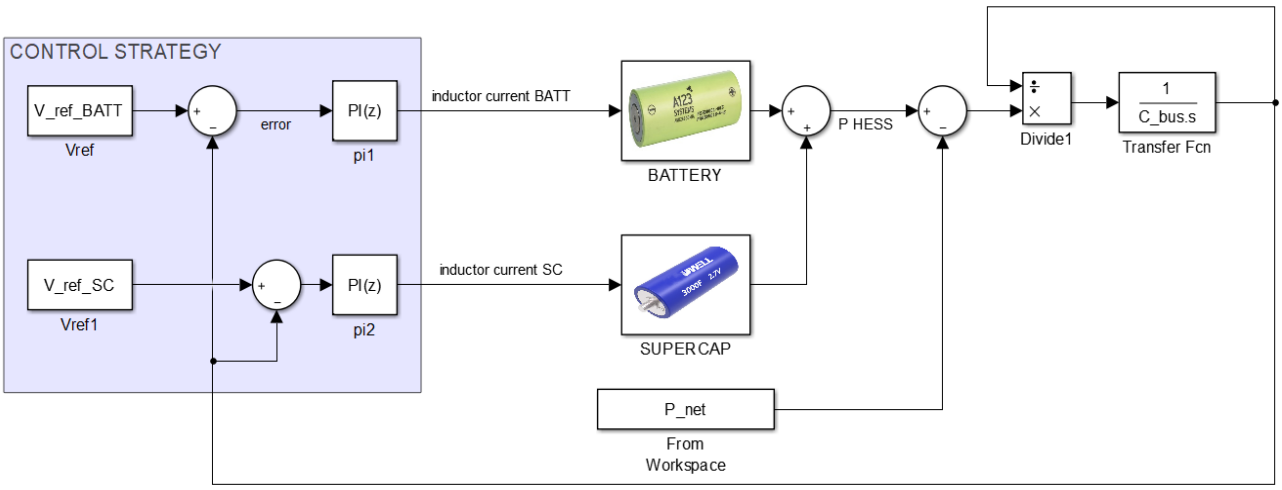

Figure 2.7: scheme of the simplified system in Simulink. Transfer function implemented by using Laplace transform

3 WAVE GENERATION DATA ANALYSIS

This chapter briefly describes the extraction of energy from ocean waves and the approach used to analyze data of power generated by a wave park. The same approach can be applied to other data from a different power plant. The key of the analysis is the ramp rate limitation of power dispatched towards the grid.

3.1 WAVE POWER

Although the aim of this study is to provide general procedures to develop the control strategies investigated, data are necessary in order to size the energy storage devices and consequently verify the behavior of the system. For this reason, a generation profile from a renewable energy plant is used as input. Clearly not all the power generated is directed to the storage: part of the power is dispatched to the grid and the aim of the storage is smoothing the variation of this profile, in order to not induce voltage or frequency variations in the main grid due to fluctuations of power generated. In this case, the plant considered exploits the energy from waves since CIEMAT has been studying this topic recently, collecting data in the Cantabrian Sea that washes the northern coast of Spain and the southwest side of the Atlantic coast of France. These data have been elaborated by a software which gives the total power generated by a hypothetical park located in that area.

Research in this area is driven by the need to meet renewable energy targets, but is relatively immature compared to other renewable energy technologies. Despite this, in 2008, the first experimental wave farm was opened in Portugal at the Aguçadoura Wave Park. Wave power is distinct from tidal power, which captures the energy of the current caused by the gravitational pull of the Sun and Moon. Waves and tides are also distinct from ocean currents which are caused by other forces such as the Coriolis effect, cabbeling, and differences in temperature and salinity. In fact, the waves are produced by wind action and are therefore an indirect form of solar energy. As long as the waves propagate slower than the wind speed just above the waves, there is an energy transfer from the wind to the waves. The main disadvantage is the largely random variability in several time-scales, as with the wind from which is originates: from wave to wave, with sea state, and from month to month (although patterns of seasonal variation can be recognized). Hence, it is the ideal application for an energy storage system.

Generally, the power of the wave energy flux is given in kW per unit of wave-crest length and is proportional to the wave height, its period and the water density. Since this section wants to introduce only some basic physical concepts regarding wave energy, the equations used to work out power and energy are not discussed (see ref. [8]). On the other hand, it is useful explaining which type of device the software considers to generate the data. Nowadays there are several technologies available to capture the energy of the waves [9] and the one considered in this case is the point absorber, shown if Fig. 3.1: this device floats on the surface of the water, held in place by cables connected to the seabed. Buoys use the rise and fall of swells to generate electricity in various ways including directly via linear generators or hydraulic pumps. Because of their small size, wave direction is not important. The linear generator is an electrical generator working by the principle of electromagnetic induction that works with linear motion, instead of rotary motion. It is directly coupled with the buoy and the stator, containing windings, mounted in a stationary structure (or fixed to the sea bed).

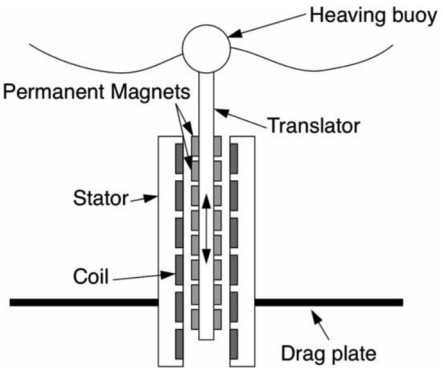

Figure 3.1: point absorber device

Focusing on the power generation, the software considers 50 devices aligned of 5 different lines. Every device is 600 m distant from the other on the same line, while the lines are 520 m distant from each other. Furthermore, in order to not have interaction between devices in different lines, the buoys are not aligned with those on the neighbor lines, but slightly shifted.

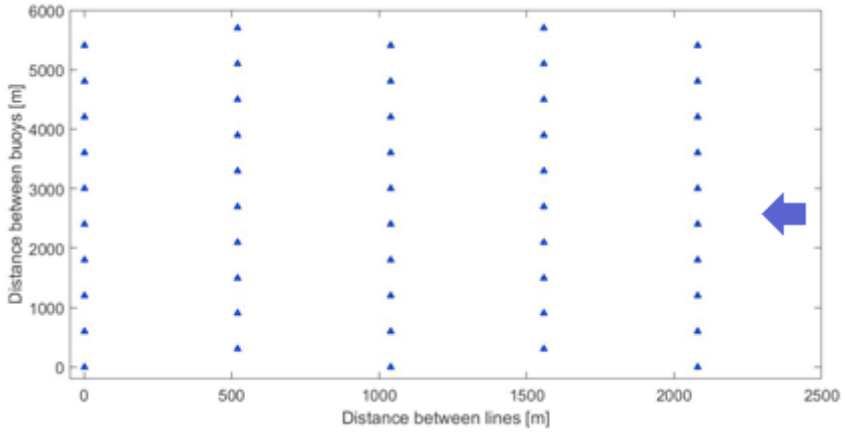

Figure 3.2: buoys disposition considered by the software

3.2 DATA ANALYSIS

The peak of power of the entire park is in the order of MW, with a high variability and for this reason an energy storage is necessary. In fact, renewable energy electricity installations have priority over other installations in terms of dispatching electricity to the system. However, the priority is subject to the secure operation of the national electricity system so the safety of the system needs to be guaranteed under all circumstances. This leads the power dispatched to be limited in terms of ramp rate. Since there is not yet a legislation for these types of plants, the ramp rate limit used in this dissertation is that commonly used for other types of renewable plants such as wind farms [10]. In this case, the ramp rate limitation is given in terms of maximum variation of instant power which should be within the range of 5-10% of the average power of the previous minute. This approach is also used by authors [11]. So, once the profile of the moving average per minute is obtained, the power profile to the energy storage system is given by the difference of the generated power and the moving average. A MATLAB script is used to generate the moving average, setting the maximum variation at 5% and the results are shown in Fig. 3.3.

The difference between the power generated and the moving average in Fig. 3.3 is the power reference of the energy storage system and is shown in Fig. 3.4.

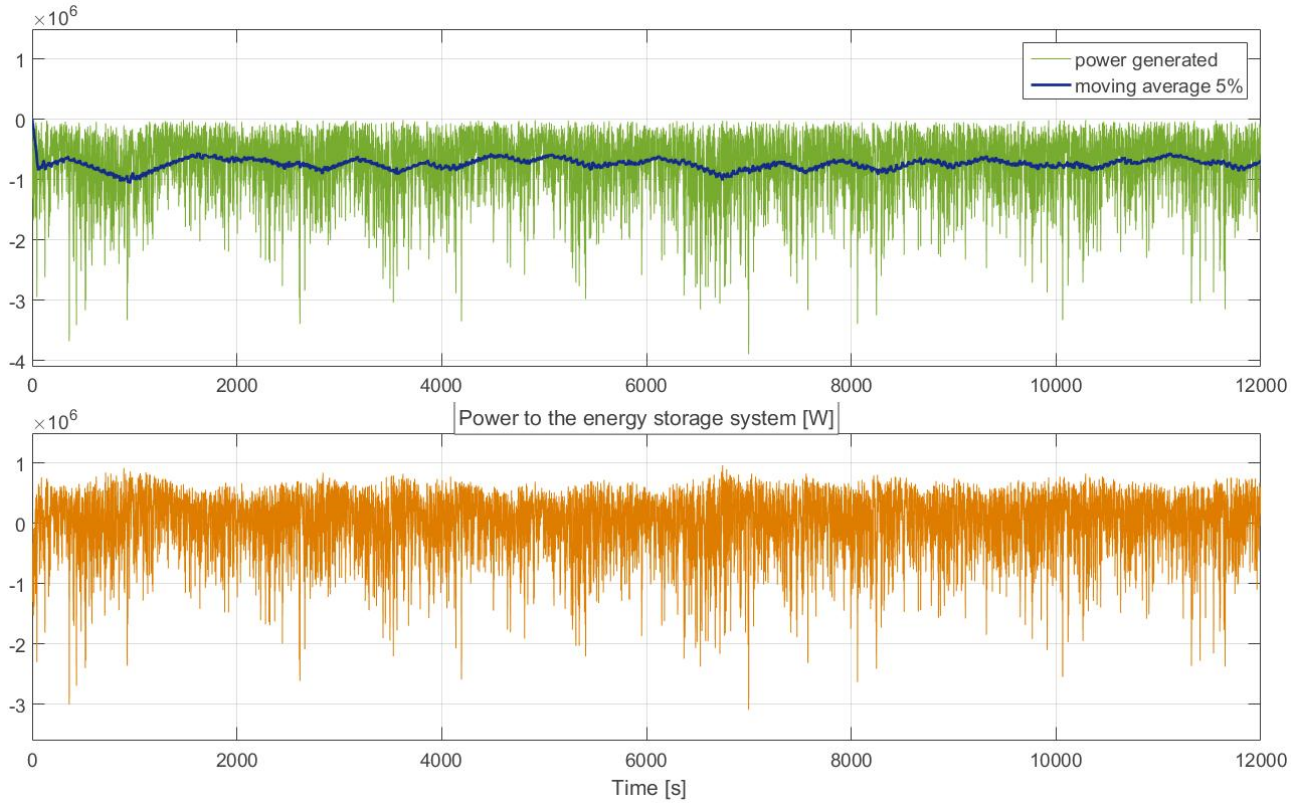

Figure 3.3: total power generated, moving average of total power generated by the park considering a maximum ramp rate of 5% and their difference

Finally, Fig. 3.6 shows the energy profile obtained by integration of the power profile. In fact, in order to size the system, both the maximum energy and power demand must be considered. The maximum energy required is:

Equation 3.1

$$E_{storage} = |E_{max} - E_{min}|$$

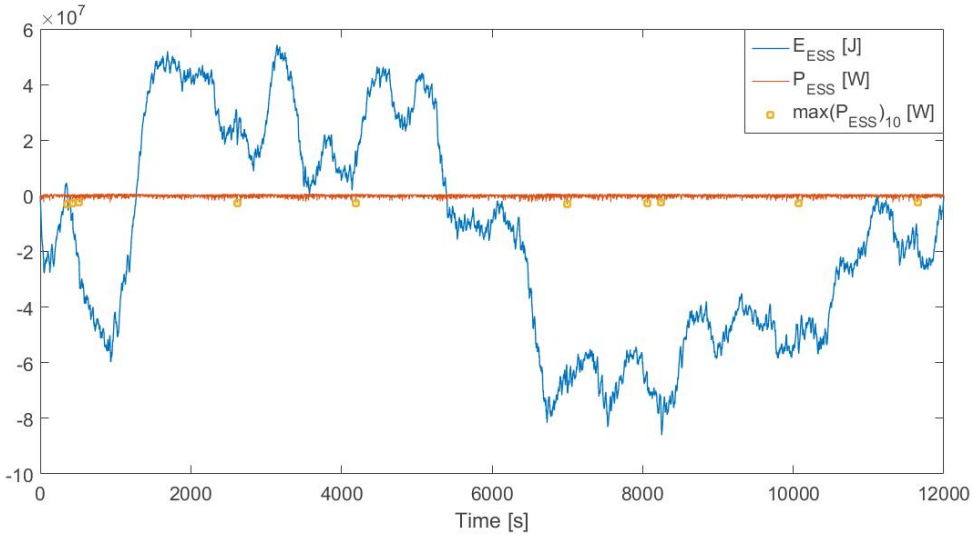

Figure 3.4: energy and power references of the energy storage system. The yellow spots show the 10 maximum power values which are all negative

According to this analysis, the values obtained are:

- E_{max} = 1.4031e + 08 J
- P_{max} = −3.0877e + 06 W

Therefore, the choice of using two DC/DC converters is justified by the fact that the system handles a power in the order of MW and it is important to use in the most efficient way the energy storage system.

Finally, the same analysis can be conducted using any desired source and other ramp rate limits.

4 THE BATTERY

This chapter provides a brief introduction about the chemistry of batteries to understand why Li-Ion are those chosen for this study. The definitions of parameters in the second section will be used for supercapacitors as well. After this part, the model is explained in detail, taking into account the temperature effect as well as the loss of capacity due to the aging of the device.

4.1 CHEMISTRY OF BATTERIES

A battery is an indirect electrical energy storage device that means it does not store electric energy in electromagnetic field, but in another form which is chemical through the electrochemical conversion. It comprises of two electrodes: an anode and a cathode, with an electrolyte between them. Their definition is related to the type of reaction that takes place on the electrode. Therefore, it must not be confused with the polarity assigned to the terminals (+ and -) which are connected to the electrodes. The reactions that take place are redox reactions. The electrode where reduction occurs is called cathode, the one where oxidation occurs is the anode.
When two dissimilar metals are put in contact through an electrolyte, there is a tendency for electrons to pass from one material to another, according to their different affinities for electrons. A potential difference between the two electrodes is thus built up until it balances the tendency of the electron transfer between the metals. Therefore, when connecting a load, redox reactions occurs spontaneously and the battery acts as an energy generator. Electrons flow from the anode to the cathode in the external circuit of the cell and a current is produced. This means that the positive pole is the cathode and the negative pole is the anode. To close the circuit, an electrolyte with a semipermeable membrane (a separator) is used: it is a substance that produces an electrically conducting solution when dissolved in a polar solvent, such as water. The dissolved electrolyte separates into cations and anions so, if an electric potential is applied to such a solution, the anions and cations move in opposite directions within the solution and this amounts to a current. The separator keeps the two electrodes apart, letting only positive or negative ions pass through.

Batteries which can work in discharge mode only are called primary batteries, while batteries that can be discharged and recharged many times are called rechargeable or storage batteries. For the purposes of this study, it is considered the rechargeable type only. When the cell potential is depleted, they can be recharged connecting an electric energy source: the battery acts as a user. When the current is applied to the cell in the opposite direction, the anode becomes the cathode and vice versa, so the charge reverses the direction and the ions flow from the cathode to the anode. For this reason, during charge the positive pole is the anode and the negative pole is the cathode. Redox reactions of opposite type occur, so the electrode that was oxidized upon discharge is now reduced and the electrode that was reduced is now oxidized: they are returned to their former state, ready to be discharged again.

Cell voltage is determined by the chemical reactions which take place at the anode and cathode. Considering a general redox reaction, it is possible to work out the Gibbs free energy. The equilibrium voltage of the cell can be calculated as [12]:

Equation 4.1

$$w_{max} = n \cdot F \cdot E_0$$
$$E_0 = -\frac{\Delta G}{n \cdot F}$$

with *n* being the number of transferred electrons and *F* the Faraday constant. This value should clearly be positive for a spontaneous reaction, such in the case of a battery in discharge mode.

These equations do not consider the polarization effects within the battery [13]. They can be seen especially when the battery is fully charged or close to its discharge limit, so when there is lack of equilibrium in the reaction, and they are referred to as polarization resistances since they introduce voltage deviation from the theoretical value. In fact, to proceed the reaction, all the reactants must be physically present in one location, which for a battery is the electrode. The process involves the transport of the reactants to the site of the chemical reaction and this means that, at the beginning, the reaction rate is slow due to the lack of catalyzation. Similarly, close to the discharge limit, the concentration near the electrode continues to drop as the battery discharges, so the reaction can not proceed. Besides, the processes described depend on both temperature and discharging/charging rate. In fact, temperature increases the kinetic energy of the reactants consequently decreasing the polarization effect, since the transport so the reaction is faster. Discharging at higher rate instead, increases the losses due to mass transport, decreasing the concentration of reactants at the electrodes surface. All the batteries suffer these effects, despite the specific mechanism of reduction and oxidation depends on the type of cell, so on the combination of materials used for the electrodes and electrolytes.

Nowadays, the most common rechargeable batteries are [14]:

- Lead–Acid Batteries: the spongy lead works as the negative active material of the battery, lead oxide is the positive active material and diluted sulfuric acid is the electrolyte. For discharging, both positive and negative materials are transformed into lead sulfate
- Nickel–Metal Hydride (NiMH): the NiMH battery uses an alkaline solution as the electrolyte. The battery is composed of nickel hydroxide on the positive electrode while the negative electrode consists of an engineered alloy of vanadium, titanium, nickel, and other metals
- Nickel–Cadmium (Ni–Cd): the active components of a rechargeable NiCd battery in the charged state consist of nickel hydroxide (NiOOH) in the positive electrode and cadmium (Cd) in the negative electrode. For the electrolyte, usually potassium hydroxide is used
- Lithium-Ion: all Lithium-ion technologies are based on the same principle. Lithium ions are stored in the anode (or negative electrode), and transported during the discharge to the cathode (or positive electrode) in an organic electrolyte. The most popular materials are the graphite for the anode, and a metal oxide for the most cathode, based on Nickel, Manganese and Cobalt

Since Li-ion are the batteries used in this study (for reasons that will be explained in the next paragraph), it is useful to study more in deep their chemistry. Li ions are the working ionic component of electrochemical reactions and they are transferred back and forth between the anode and the cathode through the electrolyte. The storage of these ions occurs via intercalation, which is defined as the reversible inclusion or insertion of a molecule (or ion) into materials with layered structures. These materials are usually graphite and transition metal. A generic intercalation reaction can be written as follow:

$$Li + xMN_y \rightarrow LiM_x + xyN$$

with *N* the component eventually extruded from the alloy compound.
The intercalations/deintercalation reactions correspond to the two half-reactions which are:

$$LiC_6 \leftrightarrow Li^+ + e^- + 6C \qquad negative\ electrode$$
$$Li^+ + e^- + FePO_4 \leftrightarrow LiFePO_4 \quad positive\ cathode$$

The overall/full reaction for a LiFePO4 battery is:

$$LiC_6 + FePO_4 \leftrightarrow 6C + LiFePO_4$$

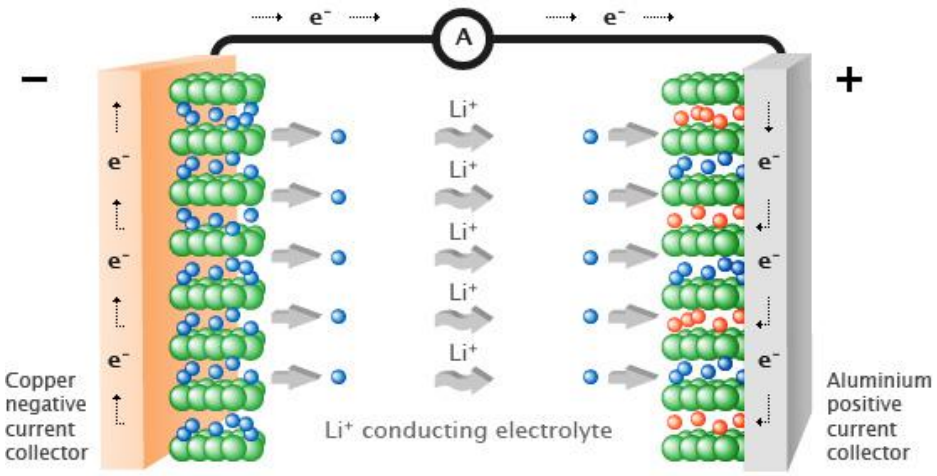

Figure 4.1: redox reactions within a Li-Ion cell

The negative electrode (anode during discharge, cathode during charge) is usually graphite. It is the most used particularly in Li-ion batteries thanks to its low cost, good electrochemical performance, low volume expansion and its availability. By adding small amounts of metals with high theoretical energy densities, such as silicon, the overall energy density can be increased thanks to alloying reactions. On the contrary, the selection of the positive electrode material (cathode during discharge, anode during charge) is strongly dependent on the application itself. The choice depends on which key property is the most important for the application. An overview of the most used cathode materials can be found in the following table [15]:

Cathode Material	Energy density (Wh/kg)	Cost	Lifetime
LiCoO2 (LCO)	546	Medium	Medium
LiMn2O4 (LMO)	410–492	Low	Low
LiNiMnCoO2 (NMC)	610–650	High	High
LiFePO4 (LFP)	518–587	Medium	High

4.2 BATTERIES PARAMETERS AND COMPARISON

In order to choose the appropriate battery, it is necessary to take into account several parameters related to the chemistry of the device, to specify the performance or to describe its present operating conditions. The main quantities are:

- Capacity (nominal, effective), SOC and DOD
- Voltage (nominal, during discharge/charge)
- Energy and power (specific, density)
- Life time (cycle life)
- Efficiency (Coulomb, energy)

CAPACITY, SOC, DOD

Capacity is the energy stored in a battery and is usually measured in [Ah], which is the amount of electric charge it can deliver at the rated voltage for one hour. The nominal capacity Qn is the effective capacity obtained for a discharge time equal to the standard time Td specified, correlated to the type of battery. The ratio Qn/Td gives the *standard discharging current* in terms of C-rate, where the C-rate is the discharge current divided by the theoretical current draw under which the battery would deliver its nominal rated capacity in 1 hour. If the battery is being discharged very quickly (high C-rate), then the amount of energy that can be extracted from the battery is reduced and the battery capacity is lower. This is due to the fact the necessary components for the reaction to occur do not necessarily have enough time to either move to their necessary positions so only a fraction of the total chemical energy is converted. Fig. 4.2 provides a representation of this behavior, which can be described using the Peukert's law for certains types of batteries:

Equation 4.2

$$Qnew = Qn \cdot \left(\frac{Qn}{I \cdot Td}\right)^{k-1}$$

where *Qnew* [Ah] is the new capacity when discharging the battery at the current *I* [A] and *k* is the Peukert coefficient (related to the type of battery). This law is not effective for Li-Ion batteries since the capacity does not change significantly with the discharging rate [16], so it will not be considered in the model.

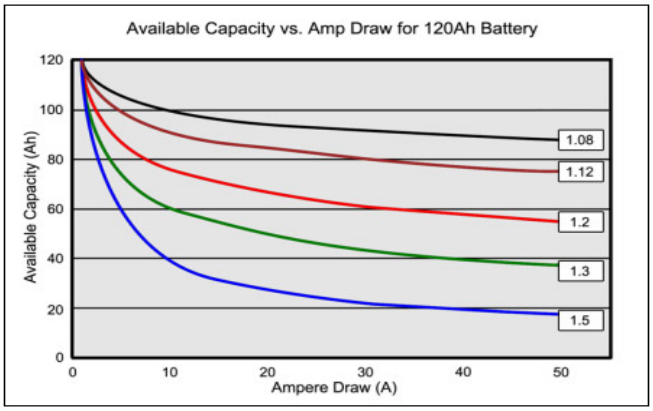

Figure 4.2: reduction of capacity according to Peukert's law

Related to the battery capacity, the *state of charge* (SOC) is defined as the fraction of the total energy or battery capacity that has been used over the total available from the battery. In other words, it is the ratio of the amount of energy currently stored in the battery to the nominal rated capacity. The battery cannot be fully discharged without causing serious and often irreparable damage to it. So, the *depth of discharge* (DOD) of a battery determines the fraction of power that can be withdrawn from

the battery. This means that the actual energy that can be extracted from the battery is significantly less than the rated capacity. Lead-Acid batteries for example are not suitable for discharges over 20% of their rated capacity. This value determines their "cut-off voltage" since the voltage is strictly correlated to the state of charge. Clearly, the relation between DOD and SOC (in Ah) is the following:

Equation 4.3

$$SOC(\%) = 100 \cdot \frac{(1 - \int i \cdot dt)}{Qn}$$

$$SOC + DOD = 100\%$$

VOLTAGE

The *voltage* of a battery can be considered constant only within a certain range of its state of charge. This range is used to define the nominal voltage (usually at 25°C and 0.2C) since the central area of the operative range is characterized by a plateau, index of the equilibrium reached by the chemical reaction within the battery. The theoretical equilibrium voltage is different from this nominal voltage due to the polarization effects. Furthermore, it is necessary to consider the voltage drop introduced by the ohmic resistance, which depends only on the material chosen and the temperature, increasing with it. Despite this, voltage rises with temperature since the polarization resistance decrease is predominant on the ohmic resistance. The voltage-capacity discharge characteristic of the battery is shown in Fig. 4.3. The two resistances described form *internal resistance*.

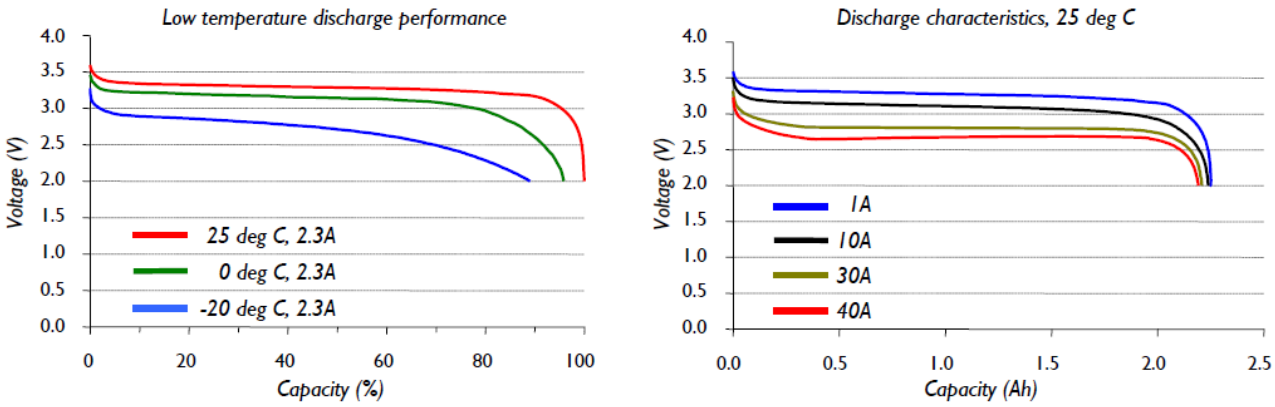

Figure 4.3: voltage characteristic for a Li-Ion cell at constant C (left) and at constant temperature (right) [17]

During charging, a similar process occurs, except that charging increases the concentration surrounding the electrode so a higher voltage is required to charge the battery than expected by equilibrium calculations. For this reason, hysteresis is always observed between the charge and discharge curves. In addition, the ohmic resistance leads to a drop in potential (drop in IR) between the end of charge and the beginning of discharge.

SPECIFIC ENERGY

It is equal to the product of the specific capacity of the electrode materials and the working voltage. Similarly, the *specific power* delivered is conventionally given by the product of the specific nominal voltage and the standard discharge current (C-rate). These parameters are strictly related to the materials. For instance, Lead-Acid batteries have low values due to the weight of the lead collector, while lithium (in Li-Ion batteries) is the lightest of all metals and has the greatest electrochemical potential so it provides the largest specific energy per weight.

LIFE TIME

It is the elapsed time before the battery becomes unusable because it does not more exhibit acceptable performance in terms of capacity (reduction of the capacity of 20% or 30% respect the initial value [18]). Life time depends on the utilization conditions that, therefore, must be specified. In fact, some deterioration occurs on each charge–discharge cycle. They usually occur because electrolyte migrates away from the electrodes or because active material detaches from the electrodes. This means that batteries lose capacity as the number of charge cycles increase and critical conditions such as deep discharge, fast charge/discharge or overcharge shorten battery lifespan. The loss of capacity can be related to the memory effect as well since, when the battery is repeatedly recharged after being only partially discharged, it may gradually lose its maximum capacity. Especially NiMH batteries suffer this effect. Generally, life time is expressed in terms of *cycle life* so in number of discharge-charge cycles under specific charge and discharge conditions.

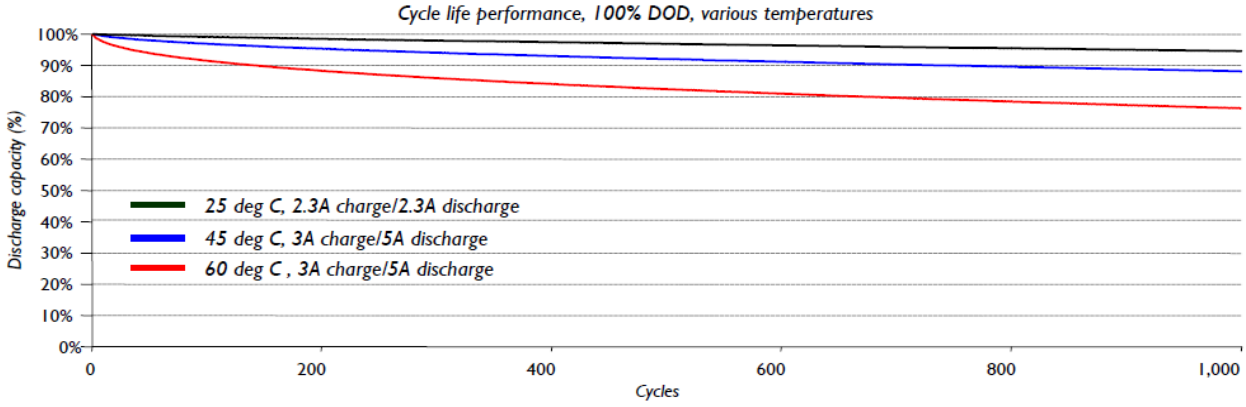

Figure 4.4: capacity reduction for a Li-Ion cell under different conditions

EFFICIENCY

The efficiency can be referred to the coulomb or the energy efficiency. The *Coulomb efficiency* is the ratio between the charge (amp-hour) delivered by the battery during the discharge process (effective capacity) and the charge absorbed during the preceding charge process. It is in the range 0.95-1 and decreases when the charge is done quickly. On the other hand, the *energy efficiency* is the ratio between the energy delivered during the discharge process and the energy absorbed during the preceding charge process so it can be interpreted as a 'roundtrip efficiency' The energy efficiency is in the range 0.85-0.9, lower than the Coulomb efficiency due to the presence of the internal resistance that wastes energy during both the discharge and the charge process. Since this last one represents the real performance of the device, the term efficiency will indicate the energy efficiency whose equation is [19]:

Equation 4.4

$$\eta_e = \frac{\int_0^{td} Ed \cdot id \cdot dt}{\int_0^{tc} Ec \cdot ic \cdot dt} = \frac{W_d}{W_e}$$

The following table resumes all the properties described above, providing a comparison between the most used types of secondary batteries [20].

Specificatios	Lead Acid	NiCd	NiMH	Li-ion		
				Cobalt	Manganese	Phosphate
Cell voltage (nominal)	2V	1.2V	1.2V	3.6V	3.8V	3.3V
Discharge cutoff voltage (1C)	1.75V	1V		2.5-3V		2.8
ohmnic resistance (m Ω)	<100 12V pack	100-200 6V pack	200-300 6V pack	150-300 7.2V	25-75 per cell	25-50 per cell
energy density (Wh/kg)	30-50	45-80	60-120	150-190	100-135	90-120
Cycle life (80% discharge)	200-300	1000	300-500	500-1000	500-1000	1000-2000
Fast-charge time	8-16h	1h	2-4h	2-4h	1h or less	1h or less
Overcharge tolerance	High	Moderate	Low	Low		
Peak load current	5C	20C	5C	>3C	>30C	>30C
Charge temperature	-20 to 50°C	0 to 45°C		0 to 45°C		
Discharge temperature	-20 to 50°C	-20 to 65°C		-20 to 65°C		
Self-discharge/ month (room temperature)	5%	20%	30%	<10%		
Maintenance requirement	3-6 months	30-60 days	60-90 days	Not required		
In use since	Late 1800s	1950	1990	1991	1996	1999

The data provided underline that Li-ion batteries are the most performing. In particular, LiFePO4 (phosphate) is the type chosen for this study. Applications for which they will be used require a wide range of operability in terms of DOD due to the possible large power fluctuations. So, to not compromise the lifetime of the devices, ‘deep cycle’ batteries are necessary. Furthermore, Lithium has high specific energy, its cell reaction provides higher voltage than other cells and is able to work with higher temperature than other materials. On the other hand, these batteries can pose unique safety hazards since they contain a flammable electrolyte and may be kept pressurized. Because of these risks, testing standards are more stringent than those for acid-electrolyte batteries.

Apart from safety, cost is the main issue related to this technology since it is new relatively to the others. Obviously, the two most costly components are the positive and negative electrode, which constitute almost the 60% of the total production cost since they require noble materials and are used in high quantities in a battery pack. In any case, the price has already decreased sensibly since 2011 [21]. Fig. (3.5) shows the prices of sale of the major producers which are beginning to converge on the trendline.

Regarding the environmental impact, the major components of a Li-ion cell require the mining of lithium carbonate, copper, aluminium, and iron ore. Lithium mining specifically is resource intensive, but lithium is only a minor portion of the battery cell by mass, so the aluminium and copper environmental impacts are much more significant. The lithium-ion recycling industry is only in its infancy right now, but the cell materials have shown high ability for recovery and recyclability, so it is expected that lithium-ion recycling rates will increase.

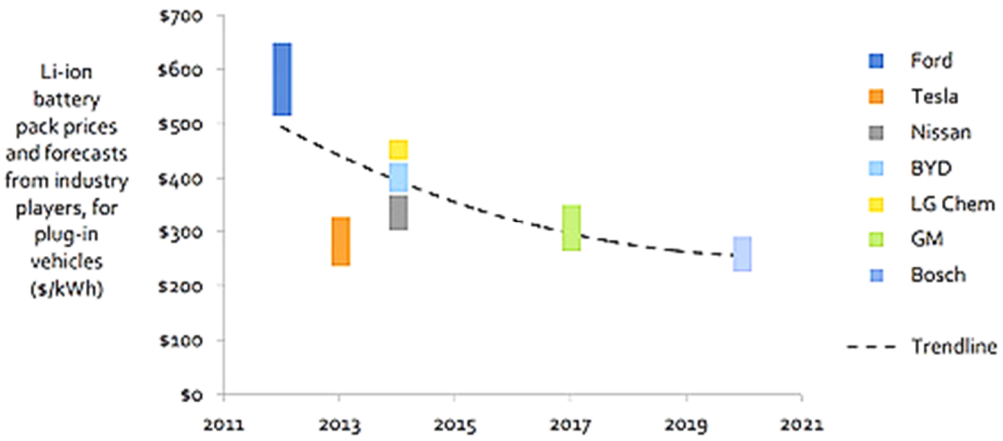

Figure 4.5: trend of price of Li-ion batteries [21]

4.3 THE SHEPERD MODEL

A good prediction mechanism of the battery performance has many advantages. It increases the battery lifetime by preventing over (dis)charging the battery, it allows utilizing the entire capacity of the battery and it offers an access to the user to know the amount of energy in the battery pack. In this study, it is assumed that every cell has the same behavior so the operation of one cell does not influence that of the others. Thus, once one cell is modelled, the voltage of the entire pack will simply be the voltage of the single cell multiplied by the number of cells in one branch, while the total current provided will be that of the single cell multiplied by the number of branches in parallel. This assumption is made in order to simplify the model and reducing the number of parameter, but clearly parameters such as the cell temperature may modify the performance of the cells nearby.
The starting point of a model is to define the voltage of the battery as a function of current, SOC and temperature to minimize the error between the model voltage and the true voltage. As previously explained, it is possible to identify a nominal working area as well as an exponential zone, so the equation used to work out the voltage should follow as much as possible the profile in Fig. (4.6).

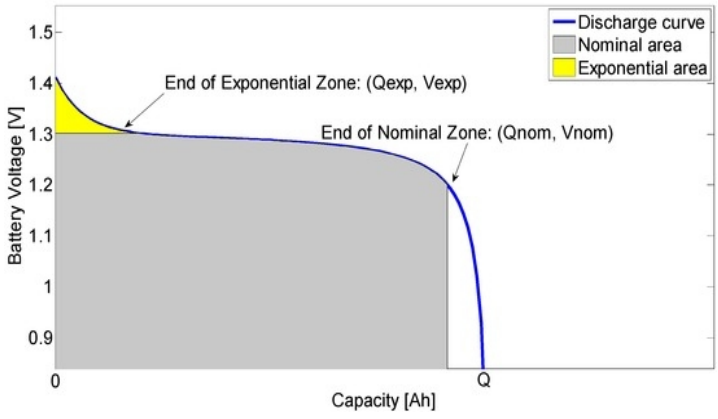

Figure 4.6: discharge characteristic of a Li-ion battery

There are two families of battery model that can be used [22]:

- Electrochemical: based on the chemical processes that take place in the battery. They use a set of coupled non-linear differential equations to describe the pertinent transport, thermodynamic, and kinetic phenomena occurring in the cell. This makes these models the most accurate available. However, the highly detailed description makes the models complex and difficult to configure

- Electric: they represent a compromise solution between precision and complexity. The battery is modelled through an equivalent circuit which is developed by using resistors, capacitors and voltage sources to form a circuit network. Typically, an ideal voltage source is selected to describe the open-circuit voltage (OCV). The accuracy can be improved by complicating the circuit.

For the purpose of this study, an electric model will be sufficient due to the strategies of control will require more efforts. There are several electric circuits that can be used to represent a battery. Since we are interested in a rechargeable type, polarization resistance will play a key role so it must be considered. Furthermore, it should be a model easily implementable in Simulink by a block diagram, without testing the battery to obtain parameters (datasheet information is sufficient). For these reasons, the choice falls on the Sheperd model, that allows to work out the terminal voltage of the battery knowing the current/power demand. The general Sheperd equation in discharging mode has the following form [22], [23]:

Equation 4.5

$$E(t) = E0 - K \cdot \frac{Q}{Q - \int idt} \cdot i(t) - R0 \cdot i(t)$$

where *E0* is the open-circuit constant voltage, *K* is polarization constant [V/Ah], *Q* is the battery capacity [Ah], *R0* the ohmic resistance, $\int idt$ is discharged capacity [Ah], and *i(t)* is the dynamic current [A] at time t. The nonlinear term in equation (4.5) states how the voltage is varied by real charge and current of the battery. In order to expose the exponential battery behavior in more detail, the previous equation is usually modified by adding an exponential term:

Equation 4.6

$$E(t) = E0 - K \cdot \frac{Q}{Q - \int idt} \cdot i(t) - Rohm \cdot i(t) + A \cdot e^{-B \cdot \int idt}$$

where *A* represents the amplitude [V] and *B* the time constant inverse in the exponential zone [Ah^{-1}]. All the previous parameters can be founded by using the discharge curves provided in the battery datasheet, identifying the end of exponential and end of nominal zones as shown in the idealized discharge curve above. In this case, the battery had already been tested in another study conducted within the organization and the experimental values obtained are:

Parameter	V nom	E0 (V)	Qn (Ah)	R ohm	I max	K	A	B
Value	3.3 V	3.4 V	2.3 Ah	0.014 Ω	70 A	0.005 V/Ah	0.2415 V	13.0435 (Ah^-1)

Equation (4.6) does not provide an effective dynamic behavior of the system since when a step of current is applied, the voltage varies instantaneously while, in real battery, the polarization effects act like a filter for the variations of current. For this reason, another change has to be made, considering the current filtered through the polarization resistance.

Since this resistance is different during discharge and during charge, two different equations will be used [22], [23]:

Equation 4.7

$$\begin{cases} E(t) = [E0 - K \cdot \dfrac{Q}{\int idt - 0.1Q} \cdot (i(t) + i^*) + A \cdot e^{-B \cdot \int idt}] - Rohm \cdot i(t) \quad (charge) \\ E(t) = [E0 - K \cdot \dfrac{Q}{Q - \int idt} \cdot (i(t) + i^*) + A \cdot e^{-B \cdot \int idt}] - Rohm \cdot i(t) \quad (discharge) \end{cases}$$

Clearly the filtering effect depends on the dynamic of the battery and it is simulated using a low pass filter (LPF). The value of the filter time constant (τ) is obtained from experimental data and is equal to 10s.

Fig. (4.7) represents the equivalent electric circuit of the model and explains how it works in Simulink. The charge and discharge equations (without the ohmnic resistance) define the internal voltage of the battery once the current demand is known. Then, the external voltage is obtained adding the voltage variation introduced by the ohmnic resistance.

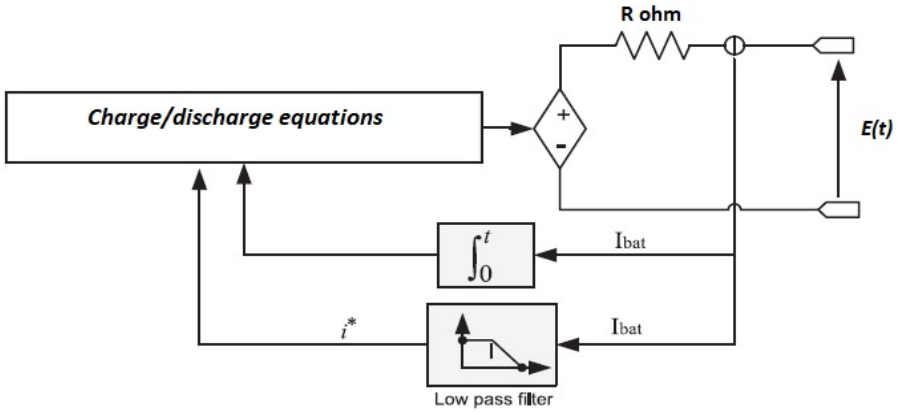

Figure 4.7: schematic representation of the battery model implemented in Simulink

4.4 THERMAL MODEL

Until now, the temperature has not been considered in the model and it has been supposed constant, but the performance of the device strongly depends on this factor, therefore it should not be excluded in the analysis. To simplify the model, temperature will be assumed uniform within the cell as well as its variation. Values of parameters that depend on temperature can be updated, according to its variation, by using the following empirical equations [24]:

Equation 4.8

$$\begin{cases} E0(T) = E0(T0) + \dfrac{dE}{dT} \cdot (T - T0) \\ K(T) = K(T0) \cdot e^{\alpha(\frac{1}{T} - \frac{1}{T0})} \\ Rohm(T) = Rohm(T) \cdot e^{\beta(\frac{1}{T} - \frac{1}{T0})} \end{cases}$$

where *dE/dT* [mV/K], α and β [1/K] are obtained from experimental data. The values of α and β have been found equal to 2.6176e+03 and 3.7726e+03 respectively. One the other hand, the temperature coefficient *dE/dT* is not constant but depends on the battery SOC [25]. For this reason, the look-up table in Fig. 4.8 is used in Simulink to select the correct values, once the SOC is known.

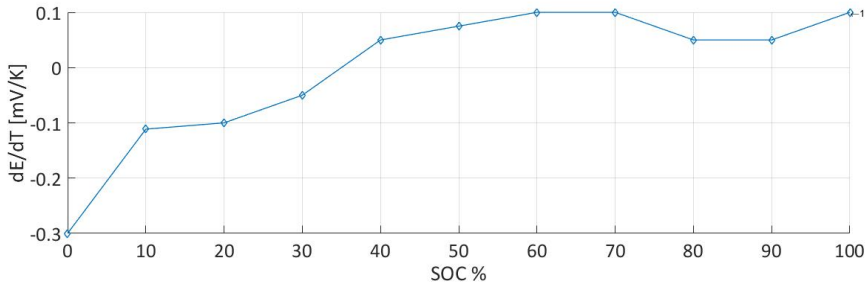

Figure 4.8: dE/dT coefficient for a Li-ion battery

Equations (4.8) would be sufficient for a model that does not include the temperature calculation and simply assumes it as an input. Such a model can be improved by adding a real-time temperature calculation, made with certain assumptions such as uniform cell temperature and heat generation.
The first part of the calculation is based on the equation developed in 1985 by Bernardi [26], who used the first law of thermodynamics for an isobaric system to work out the rate of heat generation for a single cell, which general equation is:

Equation 4.9

$$q = \sum_j I_j \cdot \left(U_j^{av} - T \cdot \frac{dU_j^{av}}{dT} \right) - I \cdot V + enthalpy\ of\ mixing\ term + phase\ change\ term$$

where *Ij* is the volumetric partial reaction current resulting from electrode reaction j, *Uj* is the corresponding open-circuit potential with superscript av referring to the value evaluated at the average composition, *I* the total current $[\frac{\mathrm{A}}{\mathrm{cm3}}]$ and *V* the cell potential. The first term on the right side represents the enthalpy of charge-transfer reactions, the second stands for the electrical work done by the battery, the enthalpy-of-mixing term is the heat effect associated with concentration gradients developed in the cell while the phase-change term the heat effect due to phase transformations. This heat generated results positive is produced by the cell, negative if consumed.
The equation used in the model does not deepen the chemical processes within the cell so the last two terms of equation (4.9) will not be consider. Furthermore, only one total current in [A] is considered, so the first term is simplified. The actual equation implemented is [27]:

Equation 4.10

$$q = I \cdot (E0 - E - T \cdot \frac{dE}{dT})$$

This heat generated corresponds to the cell loss of power so it will be used to work out the energy efficiency.

The second part of the thermal model represents the heat evacuation for a single cell and for a whole battery pack. In fact, the temperature variation is strictly connected with the difference between the heat generated heat evacuated. Then, it is possible to write the equation [24], [28]:

Equation 4.11

$$Cp \cdot \frac{\partial T_{in}}{\partial t} = q_{gen} - q_{out}$$

where *Cp* the specific heat capacity of the cell $[\frac{\mathrm{J\,kg}}{\mathrm{K}}]$. The predominant transport mode within the battery is the conduction, while convection and radiation are the more likely modes in the surrounding air. Since the temperature is considered uniform, the only heat transfer to be modelled is that from the cell surface to the ambient. Neglecting the radiation, the previous equation can be written as:

Equation 4.12

$$Cp \cdot \frac{\partial T}{\partial t} = q_{gen} - h \cdot A \cdot (T - T_{amb})$$

where h is the convective heat transfer coefficient $[\frac{\mathrm{W}}{\mathrm{m2\,K}}]$ and A is the external area [m2]. It is interesting to notice that this equation can be modelled as an equivalent electric circuit, where capacitors and resistors work as heat capacity and heat transfer resistance, respectively, and the current source is the equivalent of the heat source term. The circuit resulting from this equation is quite simple and is shown in Fig. (3.9). Since the temperature is considered uniform, that on the surface is equal to that within the cell so the internal thermal resistance $R_{th\ int}$ (which represents the conductive heat transfer) is zero while the external resistance R_{out} (which represents the convection mechanism, inversely proportional to h) is not. Equivalent circuits with different degrees of complexity can be chosen.

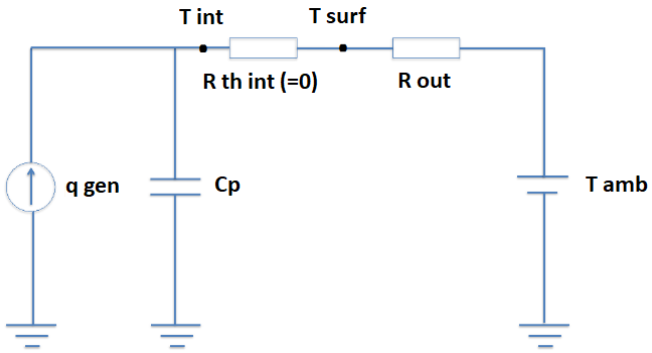

Figure 4.9: equivalent thermic circuit of the cell [28]

Finally, using the Laplace notation, it is possible to explicit the temperature as:

Equation 4.13

$$T(s) = \frac{q_{gen} \cdot Rout + Tamb}{1 + m \cdot cp \cdot Rout \cdot s} = \frac{q_{gen} \cdot Rout + Tamb}{1 + t_{th} \cdot s}$$

where t_{th} is the thermal time constant [s] of the cell obtained from experimental data.
The external resistance can be modified to consider the effect of the cells nearby with the following empirical equation [28]:

Equation 4.14

$$Rout(Ns) = \sqrt[6]{\frac{Ns}{2} \cdot Rout}$$

where Ns is the number of cells in series. Note that *Rout* affects both the steady-state temperature of the cell and the time needed to reach steady-state, increasing both.

4.5 AGING CALCULATION

In order to estimate the cycle life of the battery, aging is included into the model. In this model, aging is referred to the loss of capacity related to how the battery is working and does not consider the calendar aging. Temperature and current rate are the two main factors determining the lifetime reduction so, to model their influence, the choice falls on the Arrhenius equation. This equation is a succinct, but precise characterization of the temperature dependence of the rate of a chemical reaction and its equation is [29]:

Equation 4.15

$$k = A \cdot e^{-\frac{Ea}{R \cdot T}}$$

where k is the constant rate of a reaction, A is the pre-exponential factor or pre-factor [s^{-1}], E_a is the activation energy [KJ/mol], R is the universal gas constant (8.314×10^{-3} KJ/mol·K) and T is the temperature [K]. The equation indicates that the increase of the reaction rate occurs either by increasing the temperature or by decreasing the activation energy (i.e., using a catalyst). When this equation is applied to the capacity loss of the battery, k becomes the rate of cell capacity change. Then, by integrating the equation, it is possible to obtain an explicit form for the loss of capacity [24], [29]:

Equation 4.16

$$\nabla Q = A \cdot e^{-\frac{Ea}{R \cdot T}} \cdot (n \cdot DOD \cdot Qn)$$

where the last factor in brackets throughput in Ah. By applying the logarithm, the equation linearized form of the equation results to be:

Equation 4.17

$$\ln(\nabla Q) = \ln(A) - \left(\frac{Ea}{R \cdot T}\right) + z \cdot \ln(Ah)$$

Thanks to this syntax, the coefficients A, Ea, z can be extrapolated from experimental data. This is typically done by means of a multi-dimensional regression analysis, which takes multiple capacity curves for different current rates and temperatures into account. This analysis provides the expressions for Ea and B as a function of the current rate C and, in case of LiFePO4 batteries, the correlations are [24]:

Equation 4.18

$$Ea(C) = 31500 - 370.3 \cdot C$$

$$ln(B) = 1.226 \cdot e^{-0.2797 \cdot C} + 9.263$$

This empirical model behaves as follows:

- The higher the temperature, the faster the capacity loss
- Aging with moderate current rates (2C-4C) is slower than aging with low current rates, which in turn is slower than aging with high current rates (> 6C)
- The model does not consider the DoD influence, since 1 Ah discharged at 100% SOC implies the same capacity loss than 1 Ah discharged at 10% SOC

These equations are intended for constant C cycling since they are derived from data obtained at constant charge/discharge. On the other hand, the application will not have a constant power demand profile so after running the simulation is necessary to collect the current data and sort them by rate C.

Then, the MATLAB script will apply the previous equations to each current rate, weighing each loss of capacity by the frequency of that C to obtain the final loss.

4.6 MODEL RESPONSE AND VERIFICATION

In order to verify the goodness of the battery model before using it in a more complex system, its response to different inputs is reported. Voltage, SOC and temperature of one single cell are monitored and, thanks to the theoretical knowledge and the characteristic curves in the datasheet, the model is assessed.

At first, a constant current demand is given as input to verify the discharge time of the cell. Three different discharging rates are used, clearly with different simulation time. In fact, using a discharging rate of 1C (2.3 A for this cell) the voltage should fall to zero in almost one hour while, if the rate is doubled, the time before total discharge is approximately halved and so on:

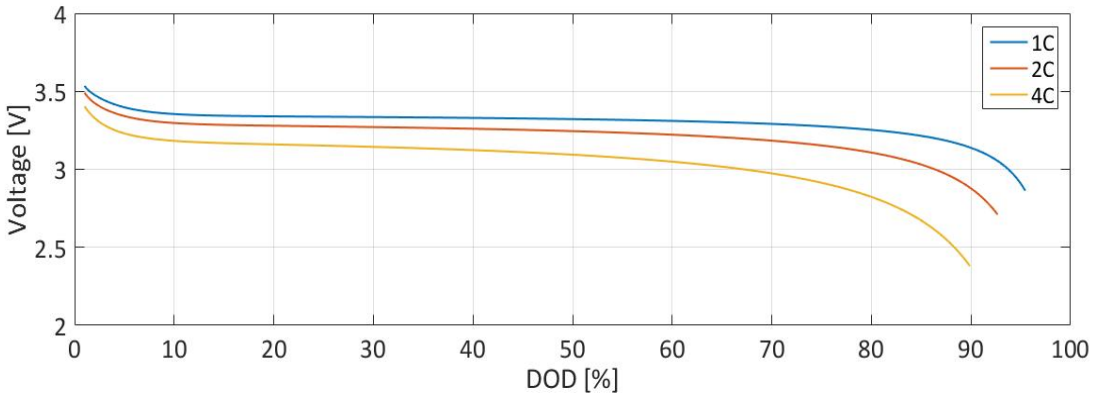

Figure 4.10: Voltage-DOD characteristic for the cell implemented in the model

Since temperature is not fixed, to each characteristic corresponds a specific temperature profile. Higher current rates should lead to higher peak of temperature and the simulation confirms this fact:

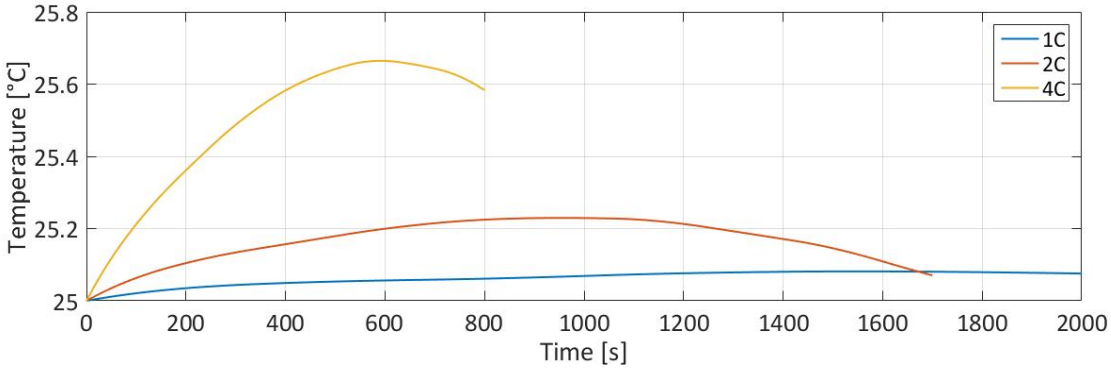

Figure 4.11: temperature variations of the cell at different discharge rate

Finally, it is useful to prove the dynamic performance of the cell, using a pulsed demand of power. The dynamic behavior should be seen during the steps of current, when the polarization resistance act as a low pass filter determining a slower voltage variation. The voltage variation and the current demand are reported as functions of time in Fig. 4.12.

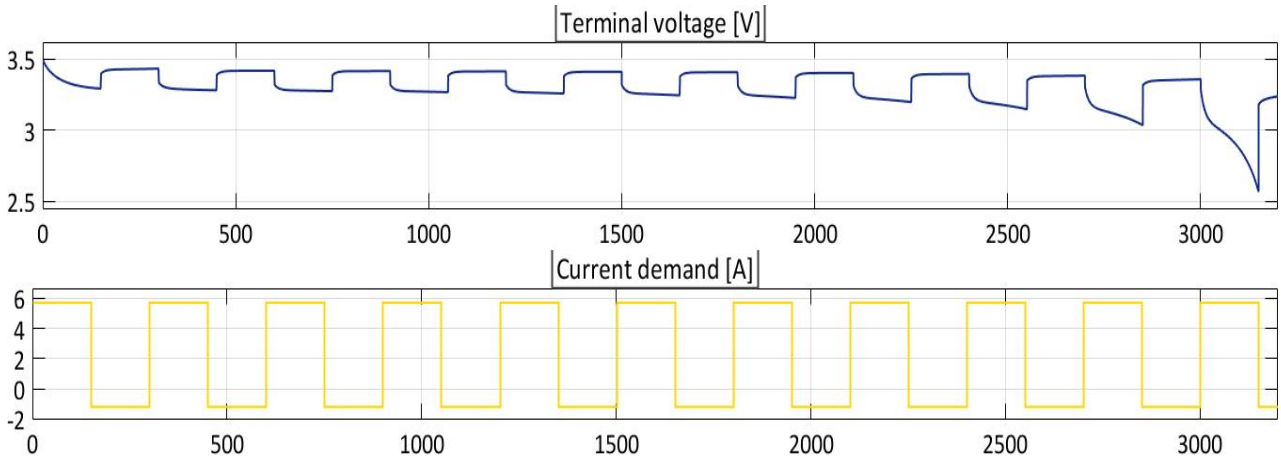

Figure 4.12: voltage response of the battery at pulsed current demand

5 THE SUPERCAPACITOR EDLC

This chapter provides basic information regarding the chemistry of supercapacitor, with a focus on the EDLC type. After this first part, the model used in Simulink is explained in detail, without considering the temperature effect and aging.

5.1 CHEMISTRY OF SUPERCAPACITORS

Capacitors and inductors are direct electrical energy storage devices that means they store energy directly by mean of the electromagnetic field in a defined volume. This field could be predominantly electrostatic (electric) field and magnetic field. Devices that use the electric field are known as capacitors, while those that use the magnetic are known as inductors. Since the capability of capacitors is insufficient for most power conversion applications, ultra-capacitors and super inductors have been developed. However, super inductors are for very short term and very high-power applications so they will not be considered in this study.
Focusing on electrostatic systems, they are composed of two metallic bodies and a dielectric between them. When charging the bodies, charges of opposite signs are attracted to the surface of each electrode, creating an electric field which allows capacitor to store energy. The capacity of the device is given by the ratio between the charge stored and the voltage:

Equation 5.1

$$C = \frac{Q}{V}$$

For this type of capacitor, C is proportional to the surface of the plates, the distance between them and the permittivity of the dielectric, which usually is not linear so it depends on the voltage. Voltage and current are linked via differential equations and the amount of energy stored of a nonlinear capacitor charged to the voltage U0 is [30]:

Equation 5.2

$$W = \int_0^{Q0} u(q) \cdot dq = \int_0^{Q0} \left(C(u) + \frac{\partial C(u)}{\partial u} \cdot u\right) \cdot u \cdot du$$

If the dielectric is linear this energy is computed as:

Equation 5.3

$$W = \frac{1}{2} \cdot C0 \cdot U0^2$$

Clearly the higher the voltage and the capacitance, the higher the energy capability will be. This aspect depends on the technology used and the technology used in supercapacitors allows to have capacitance of thousands of farads. The principle used to store energy determines the type of supercapacitor [30]:

- The electric double layer capacitor (EDLC) is composed of two porous conducting electrodes immersed in an electrolyte and separated by a separator. Each electrode forms a capacitor with a layer of the electrolyte's ion. Since this surface is in the range of thousands of square meters and the ion's diameter in the range of angstrom, the capacitance is in the range of thousands of farads. No chemical reaction is involved in the process
- The pseudo-capacitor relies on an electron charge transfer reaction at the electrode-electrolyte surface to store energy. It is very similar to rechargeable electrochemical batteries so is better than EDLC in terms of specific energy but worse in terms of specific power

- A combination of these two types is the so-called hybrid capacitor, which uses electrodes with different characteristics, one exhibiting mostly electrostatic capacitance and the other mostly electrochemical capacitance
- High voltage capacitors are multi-layer ceramic capacitors proposed in 2006 to replace batteries and EDLC but because of their low specific energy they have not been used very often

The EDLC are certainly the most used and for this reason their name is commonly used to denote the entire category. The first who studied the double layer was Helmholtz in 1853 [31]. According to Helmholtz, when an electronic conductor is brought in contact with a solid or liquid ionic conductor (electrolyte), a common boundary (interface) among the two phases appears. The electrode holds a certain amount of charge that is balanced by ions of opposite charge in the electrolyte solution. The movement of ions in the solution creates a non-faradic current. These ions are not directly in contact with the electrode due to a layer of molecules of solvent between them which creates a difference of potential. The line that crosses the centers of the solvated ions forming the layer is called Outer Helmholtz Plane (OHP) and the thickness of the layer is equal to the molecule diameter. The area between these ions and the electrode acts as a capacitor whose capacitance, created by these two layers of opposite polarity (double electric layer), is considered constant and depending only on the permittivity and thickness of the layer.

From this first model, others were used to better describe this phenomenon to better fit the experimental data. Gouy-Chapman's model considers a diffuse model where the charge distribution of ions is a function of distance from the metal surface. Therefore, the capacitance is not constant but dependent on the ions concentration. Another widely used model is that developed by Stern [31] [32]. He combined the two previous models so that there is a rigid layer where Helmholtz's model is valid (Stern layer) and the potential linearly varies with the distance from the electrode. On the other hand, in the diffused layer, the potential varies exponentially according to Gouy-Chapman. In this way, the system is described as two capacitances in series, once between the electrode and the OHP, the other related to the diffused charge. All these models underline that no chemical reactions are involved within the EDLC and for this reason its lifetime is longer than that of secondary batteries.

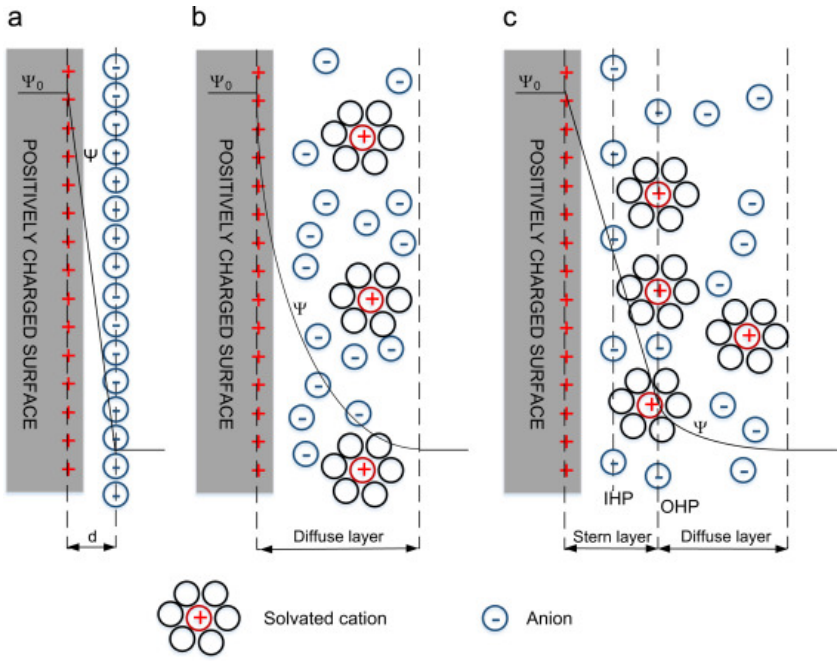

Figure 5.1: EDLC models. (a) Helmholtz, (b) Gouy-Chapman, (c) Stern

On the other hand, a pseudo-capacitor has a chemical reaction at the electrode. Accompanied by the electric double-layer, some de-solvated electrolyte ions pervade the separating solvent layer and are adsorbed by the electrode's surface atoms. They are specifically adsorbed and deliver their charge to the electrode. In other words, the ions in the electrolyte within the Helmholtz double-layer also act as electron donors and transfer electrons to the electrode atoms, resulting in a faradaic current. The adsorbed ion has no chemical reaction with the atoms of the electrode (no chemical bonds arise) since only a charge-transfer take place. This faradaic charge transfer, originated by a fast sequence of adsorption reactions, is called pesudocapacitance which adds to the double layer capacitance. However, they can be effective with very different parts of the total capacitance value since a pseudocapacitance may be higher by a factor of 100 as a double-layer capacitance with the same electrode surface. Electrodes' ability to produce pseudocapacitance strongly depends on the electrode materials' chemical affinity to the ions adsorbed on the electrode surface as well as on the electrode pore structure and dimension. The performance of this type of supercapacitor are between that of a EDLC and that of a battery since (thanks to the pseudocapacitance) it can store more energy than a EDLC but its discharge, charge time is slower. Finally, research regarding electrodes materials is still going on and price is higher than conventional EDLC. For this reason, EDLC are the one used in this study.

The material used for the electrodes is usually activated carbon, a form of carbon processed to have small, low-volume pores that increase the surface area available for adsorption or chemical reactions. In fact, its cost is lower than that of other materials with the same active surface and it is widely available. Carbon-based electrodes exhibit predominantly static double-layer capacitance, even though a small amount of pseudocapacitance may also be present depending on the pore size distribution. Pore sizes in carbons typically range from micropores (less than 2 nm) to mesopores (2-50 nm), but only micropores (<2 nm) contribute to pseudocapacitance. The size of these pores is related to a phenomenon called *relaxation*, due to which diffusion of ions in small pores is characterized by longer time constants, leading to a dynamic variation of the EDLC properties especially during fast charge/discharge at strong frequencies. Basically, it is an effect on a nonhomogeneous repartition of charge on the electrodes. Because of aging, this phenomenon is reinforced by impurities.

5.2 CHARACTERIZATION OF A SUPERCAPACITOR

The relation between voltage and current of discharge/charge is strictly related to the capacitance of the device and for an ideal capacitor can be expressed by the following equation:

Equation 5.4

$$I = \frac{dQ(t)}{dt} = C \cdot \frac{dV(t)}{dt}$$

The capacitance C is generally not constant but depends on voltage according to the behavior of the electrolyte dielectric constant that increases and the variation of the thickness of the double layer. Therefore, the internal structure of the supercapacitor is affected by an increased accumulation of charge and as the charge and voltage increase, the effective dielectric constant increases. Usually this dependence is approximated by a first-order function [30]:

Equation 5.5

$$C(u) = C0 + kc \cdot u$$

where *C0* is the initial linear capacitance and *kc* is a positive coefficient [F/V] which multiplies the voltage *u* and can be derived from the capacitance-voltage curve of the device.

Furthermore, the maximum voltage sustainable by the device is related to the breakdown voltage of the electrolyte, that is the voltage at which the current flows through the electrical insulator. This results in the insulator becoming electrically conductive. Electrical breakdown may be a momentary event (as in an electrostatic discharge) or may lead to a continuous arc and is always a disruptive event for the device. Therefore, depending on the electrolyte used, the maximum voltage of charge is established: aqueous electrolytes have a breakdown voltage around 1.2 V per electrode (2.4 V for the cell), lower than that of organic electrolytes which is 1.4 V (2.8 V for the cell).

To characterize a supercapacitor, the galvanostatic curves is usually adopted: it plots the voltage versus time at constant discharge/charge. The curve includes two parts: a capacitive part produced from voltage change owing to the energy change in the supercapacitor, and a resistive part representing the voltage change due to the internal resistance of the supercapacitor. This equivalent series resistance (ESR) is related to the conductivity of the electrolyte and the ohmic resistance of the electrodes and contacts. The ESR value is very low (less than 1mΩ) and gives the power loss during charge and discharge. On the other hand, a second resistance can be spotted, the equivalent parallel resistance (EPR), which gives the leakage current when no load is applied to the device and its value is in the order of MΩ since it is usually modelled as a parallel resistance. The resistive part associated with the ESR is visible in Fig. (5.2) at the initial stage of the discharging curve. Clearly, the greater the current, the greater the drop and the shorter the time needed to charge-discharge the device.

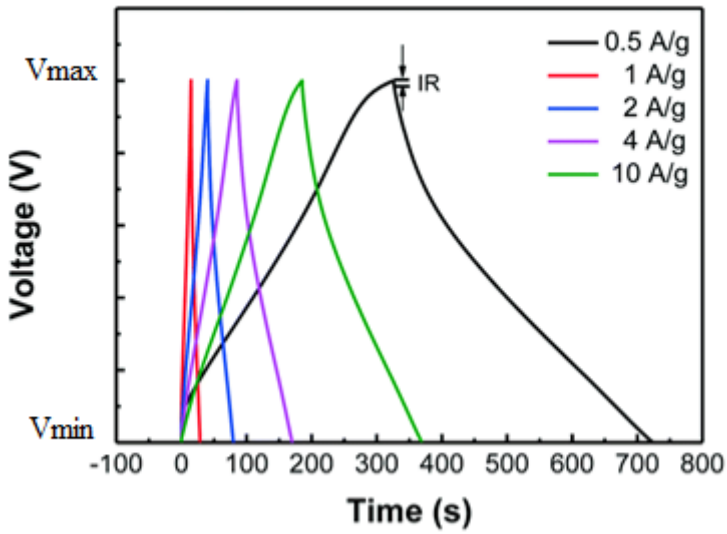

Figure 5.2: galvanostatic curve of a EDLC at different current density [32]

ESR and capacitance are frequency dependent properties, but since the model works in DC operational mode (zero frequency) these relations are not studied and showed. Finally, temperature is another factor which may have an influence on these values. ESR decreases when temperature increases while capacitance shows a less significant dependence. As shown in Fig. 5.3, the capacitance variation is not even visible while that of the ESR is important at low or high temperature. Furthermore, its value is usually very small and its analytic determination as a function of the cell temperature is difficult [30]. For all these reasons, ESR and capacitance are assumed independent from the temperature. Despite this assumption, it is necessary to remember that even if supercapacitors have a longer lifetime than secondary, their lifetime is not infinite. Prolonged exposure to elevated temperatures, high applied voltage and excessive current will lead to increased ESR and decreased capacitance.

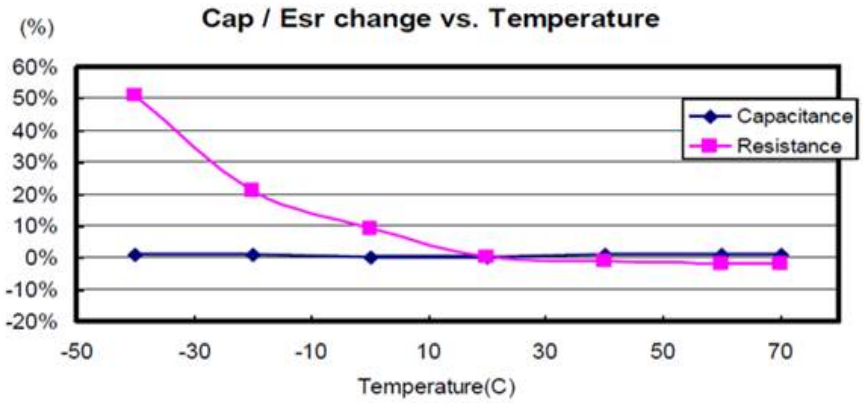

Figure 5.3: capacitance and ESR variation with temperature

5.3 THE MODEL

As in the case of battery models, there are several models of different complexity that can be used to represent an EDLC. The most complete and complex is that represented by a transmission -line with a finite number of RC branches. In fact, in order to represent the slow phenomena such as relaxation (strongly related to frequency), every branch has a different time constant and a different resistance value, which increase as the diffusion of ions inside the pores is slower and more difficult. However, using such a complex model is not practical as there are many parameters to extract from experimental tests and, in this case, frequency dependency on parameters is neglected since a DC system is considered. Therefore, the EDLC is usually represented by a simpler first order circuit, with an internal DC resistance and a linear voltage-dependent capacitance. The RC slow branches are neglected since typically the short-term time constant is in the order of seconds while the long-term time constant in the order of minutes.

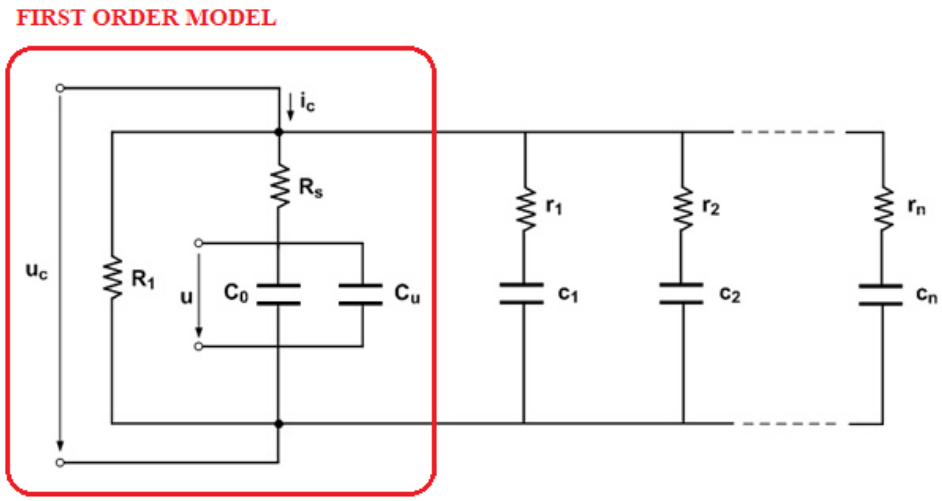

Figure 5.4: transmission-line model of a EDLC. In red, the simplified model used in the dissertation

Fig. (5.4) represents the electric circuit that has been modelled in Simulink by blocks. *Cu* is the part of capacitance that linearly varies with voltage according to equation (5.5). *Rs* is the ESR and *R1* the self-discharge resistance which, as done for the battery, is neglected as important only in the long-term period. As done for the battery, every cell is considered equal to the others in terms of performance and parameters so knowing the number of cells in series and the number of branches, the voltage of the entire pack and the total current provided are determined.

The EDLC used for this study is a Maxwell 3000F, whose parameters are [33]:

Parameter	C nom	V max	Vmin	ESR	I max	I max continuous	C0	Kc
Value	3000 F	2.85 V	1.6 V	0.29 mΩ	1900 A	210 A	1850 F	350*4/3 F/V

C0 and kc are obtained from the voltage-capacitance characteristic of the cell which, as stated previously, can be approximated as linear. Therefore, the voltage is calculated using equation (5.4), integrating the voltage variation in time, where the capacitance is the total capacitance linearly dependent on voltage. Finally, the ESR leads to loss of power so the cell has to provide more power than that demanded, since the input of the model is the power signal. For this reason, the current demand is divided by the instantaneous efficiency or, in other words, the power efficiency defined as:

Equation 5.6

$$\eta_p = \frac{P_{provided}}{P_{provided} + Ploss} = \frac{U \cdot id}{U \cdot id + ESR \cdot id}$$

On the other hand, the energy efficiency is defined in the same way as it is defined for the battery using equation (4.4).
The loop used in Simulink is:

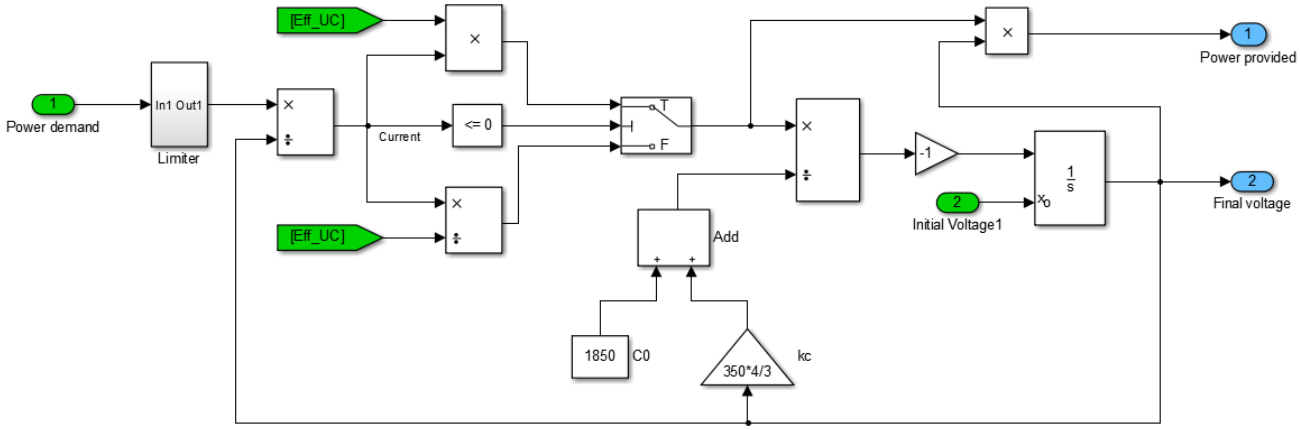

Figure 5.5: concept of the blocks scheme implemented in Simulink

The energy stored in such a device charged on voltage *U0* is obtained combining equation (1.2) and equation (1.5) and is equal to:

Equation 5.7

$$W = \frac{1}{2} \cdot (C0 \cdot + \frac{4}{3} \cdot kc \cdot U0) \cdot U0^2$$

For the EDLC, the state of charge defined in term of total energy is estimated by:

Equation 5.8

$$SOC(\%) = \frac{W - Wmin}{Wmax - Wmin}$$

where *E*, *Emin*, *Emax* denote respectively the energy currently stored, the minimum energy (corresponding to the recommended cut-off voltage) and the maximum energy (corresponding to the maximum voltage). Knowing the initial SOC, equation (1.7) allows to work out also the initial voltage of the cell. It should be noticed that, according to this equation, when the voltage is equal to the cut-off voltage, the SOC is zero.

5.4 MODEL RESPONSE AND VERIFICATION

In order to verify the goodness of the EDLC model, its response to different inputs is reported. Since temperature is considered constant, voltage and SOC of one single cell are monitored as well as the dynamic response to different power steps. In fact, according to Fig. (4.2), the charge/discharge time has to be slower if the power demand is greater. The model is then verified.

First, a power corresponding to the half of the maximum cell power is used as pulsed input. When the cell reaches the minimum voltage established, its SOC is zero so the limiter block sets the input at zero and the voltage remains at this level. On the other hand, when the input is negative, the cell can be charged till it reaches the maximum voltage allowed, corresponding to SOC 100%. Voltage immediately changes when the step is applied, since the model considers the EDLC infinitely fast.

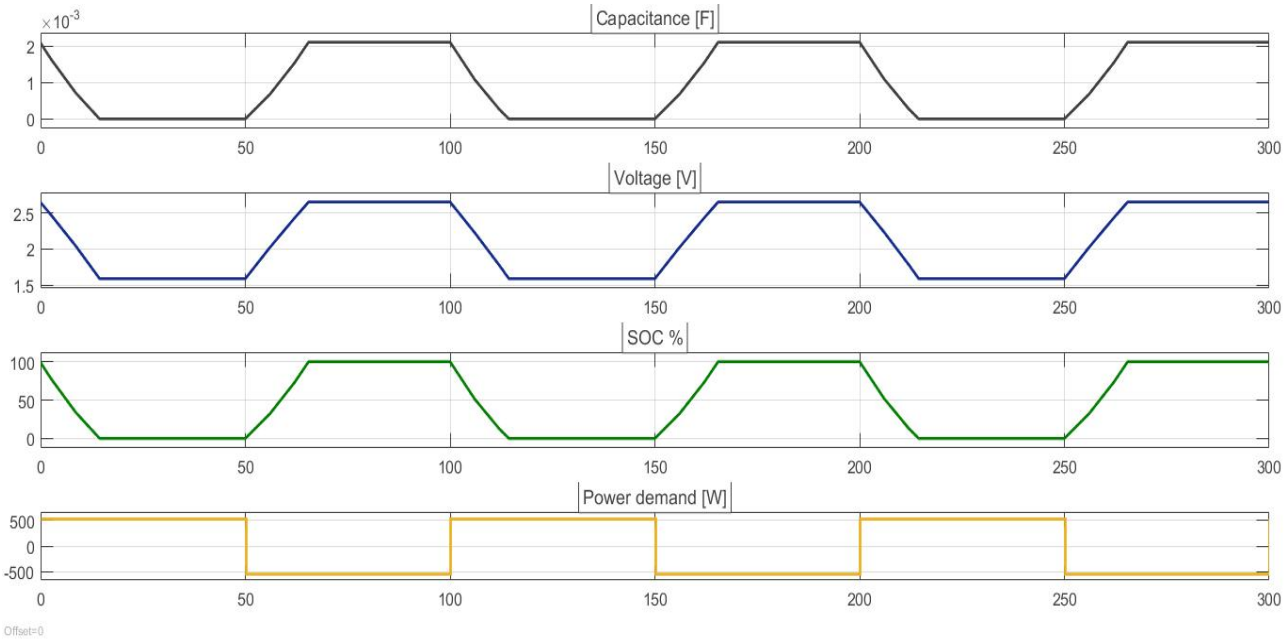

Figure 5.6: results of simulation of the EDLC model under pulsed discharge/charge

The same simulation is then repeated using a different step of power, to verify if the cell charge/discharge time is larger. In fact, using a power corrisponding to ¼ the maximum cell power, the lapse between fully charge and fully discharge is greatly increased and the limiter acts only for a short period of time. The results are shown in Fig. 5.7.

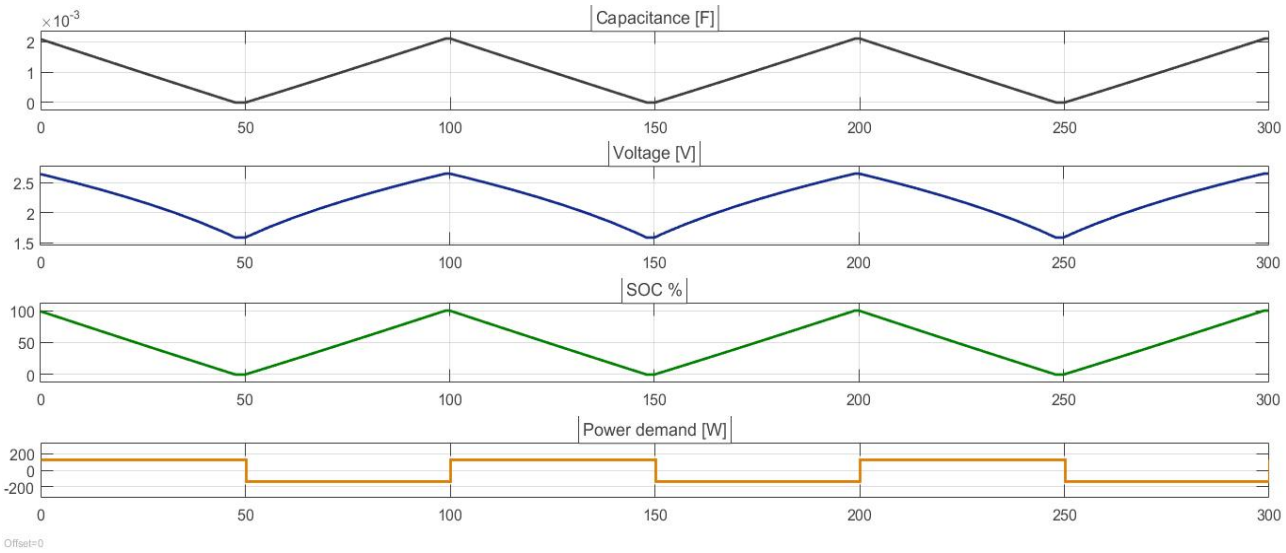

Figure 5.7: results of simulation of the EDLC model under lower pulsed discharge/charge than Fig. 5.6

6 CONTROL STRATREGIES

This chapter introduces the general features of a good control strategies and investigates on two different strategies, one centralized and the other decentralized. The working principles of both are then explained, focusing on the choice of the parameters. Besides the strategy, a control block to ensure the safe operation of the devices is always necessary and it is implemented using the data provided in the datasheet of the device.

6.1 OVERVIEW OF CONTROL STRATEGIES FOR HESS

The control strategy manages the power flow of the HESS based on the real-time system conditions. It is usually complex and required to operate continuously in order to fulfill the multiple objectives. Optimal control of the HESS is crucial to optimize the energy utilization and sustainability to a maximum extent. The common aims of the control strategies are listed as following:

- To prevent the deep discharge of the battery
- To reduce the peak power demand, charge/discharging cycle, and dynamic stress level of battery
- To maintain a stable DC voltage
- To reduce the total sizing cost of the system
- To reduce the loss of power supply possibility and the operational and maintenance. To improve the overall efficiency of the system

To achieve these goals, the EDLC is used as support of the battery to extend its lifetime as well as reducing the total cost of the system. In fact, as explained in the previous chapter, this device has very high power density and faster dynamic response than the battery, as well as longer life-cycle. However, the EDLC has a low energy density, which means its SOC easily decreases after short periods of time. Therefore, in order to not be subjected to peaks of power, the battery should be able to maintain the SOC level of the EDLC around the wanted value to prevent it from being fully discharged.

With regard to the architecture of a power system's control, two very distinctive opposite approaches can be identified: centralized and decentralized.
A fully centralized control relies on the data gathered in a dedicated central controller that performs the required calculations and determines the control actions for all the units at a single point, requiring extensive communication between the central controller and controlled units. On the other hand, in a fully decentralized control each unit is controlled by its local controller, which only receives local information and is neither fully aware of system-wide variables nor other controllers' actions [34]. Interconnected power systems that cover extended geographic areas are not suitable for a fully centralized approach but, in this case, it only comprises an energy storage and a renewable energy source so no extensive communication is needed and such a strategy can be implemented. It consists of a central controller which establishes the current references of each DC/DC converter, obtained by filtering the total current required to keep constant the bus voltage.
At the same time, a fully decentralized approach is never possible due to the strong coupling between the operations of various units in the system, requiring a minimum level of coordination that cannot be achieved by using only local variables. Therefore, a second strategy based on a hierarchical control scheme is tested. It is a compromise between fully centralized and fully decentralized control schemes, consisting of two control levels, primary and secondary. The first is already implemented in the controller while the second is performed by a central unit and modifies the voltage reference of each DC/DC converter to take into account the voltage variations introduced by the primary level.

When communications fail, the control can still rely on the primary level, even if this condition should only be temporary.

In any case, the control strategy is not able to consider all the status variable of the device so the current reference of the converter must be checked before being translated as effective current of the device. This control can be done by management system block, located just before the input port of the device model.

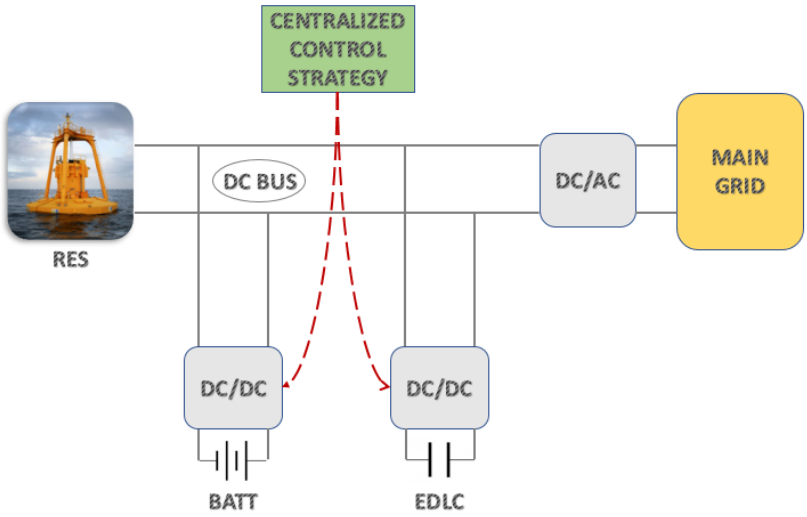

Figure 6.1: scheme of the fully centralized control strategy

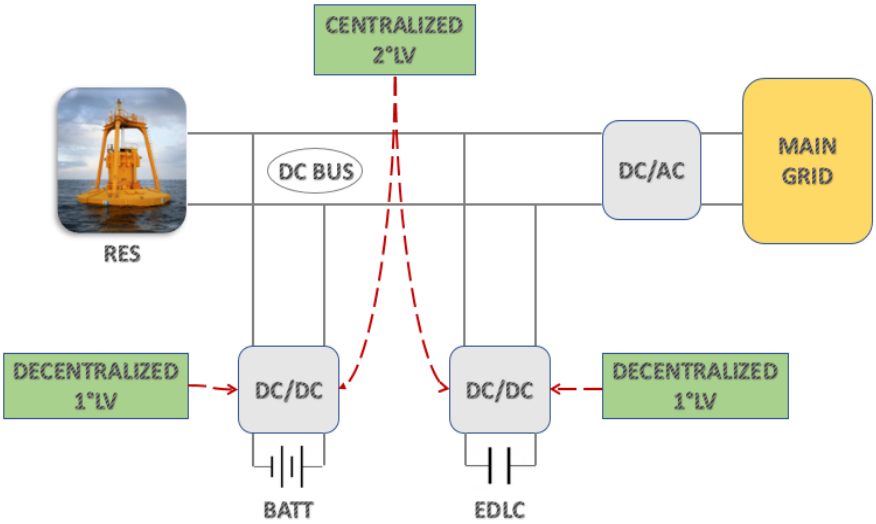

Figure 6.2: scheme of the partially decentralized control strategy, based on a two levels control

6.2 SAFE OPERATION CONTROL

The datasheet provided by the constructor contains the safety specifications of the cell. These limits should be respected in order not to reduce its lifetime and therefore taken into account in the model of the system. Usually, they refer to the maximum current, temperature and minimum voltage allowed. It should be noticed that the voltage is correlated to the SOC of the device, so the same specification can be given in terms of minimum SOC.

The battery specifications are reported in tables in sections 4.2 - 4.3 and since temperature is known from its model, it is possible to manage the input according to all the three parameters. This control block is basically the battery management system, or 'B.M.S.'. The current can be limited using simple saturation block having the higher and lower limit equal to the maximum current during charge and discharge respectively. Instead, the temperature calculated by the model can be compared with the maximum allowed and, in case it exceeds this value, the current is set at zero to let the battery cool. The same comparative procedure can be repeated for the SOC). Fig. 6.3 reports the scheme of the B.M.S.

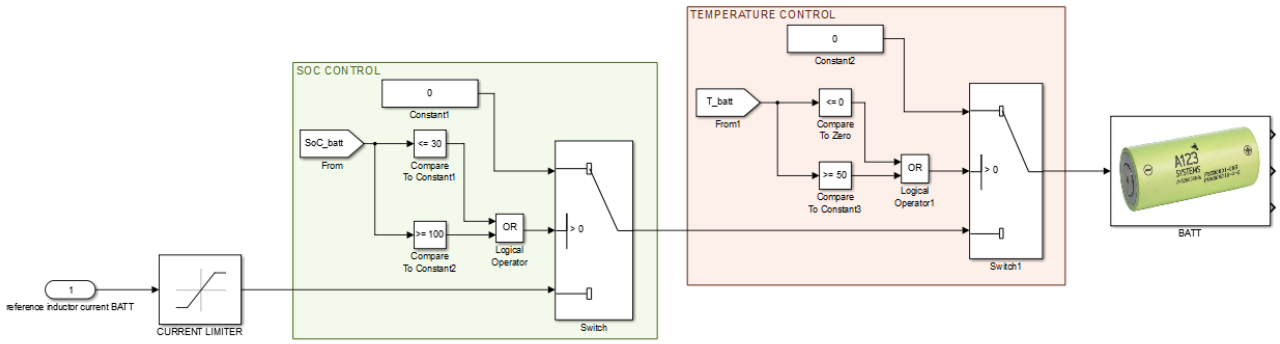

Figure 6.1: components of the B.M.S.

The EDLC specifications are reported in table in section 5.3 but since its model does not contain temperature calculation, only the current demand and the voltage can be checked. Then, the EDLC management system has the same scheme of the B.M.S. but without the temperature control.
Finally, Fig. 6.4 shows the location of the two management systems respect the control strategy.

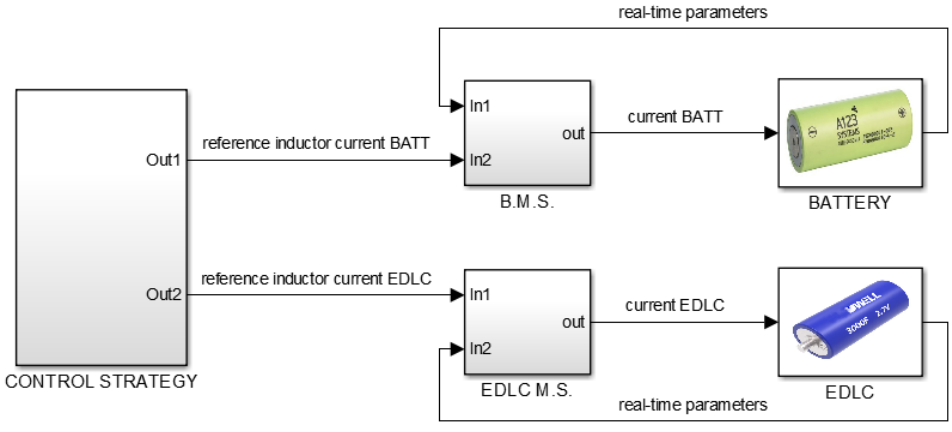

Figure 6.2: control strategy and management systems location

6.3 CENTRALIZED HIGH PASS FILTER STRATEGY

6.3.1 PRINCIPLE OF OPERATION

The first strategy investigated achieves power sharing through the energy storages by mean of a high pass filter (HPF). In electronics, a filter is a circuit which processes a signal modifying its amplitude and phase by introducing high attenuation above a specified frequency and little or no attenuation below that frequency. The frequency at which the transition occurs is called the "cut-off" or "corner" frequency.
In this study, passive filters are only considered: they are made of passive components such as resistors, capacitors and inductors and have no amplifying elements (such as transistors) so have no signal gain, therefore their output level is always less than the input. The order of the filter is given by the number of reactive component so a circuit made of a resistor and a single capacitor acts as a first order filter. The arrangement of the two components instead establish whether the filter is a low pass filter (LPF) or high pass filter (HPF). In practice, a low pass filter is a RC circuit that allows only signals of frequency below the cut-off frequency pass, while a high pass filter is a CR circuit that allows only signals of frequency above the cut- off frequency pass.

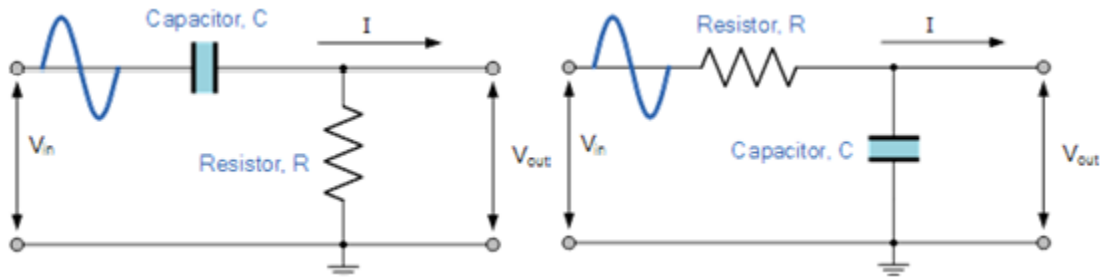

Figure 6.3: circuits of a HPF (on the left) and LPF (on the right)

The explanation of this behavior derives from the capacitor reactance. Since the reactance depends on frequency, it behaves as an impedance only if the signal varies in time, otherwise behaves as an open switch. In fact, the reactance can be calculated as:

Equation 6.1

$$Xc = \frac{1}{2\pi \cdot f \cdot C}$$

where *f* is the frequency of the signal [H] and *C* the capacitance [F]. Its value is inversely proportional to the frequency. The property of capacitive reactance makes capacitors ideal for use in AC filter circuits or in DC power supply, to reduce the effects of any unwanted ripple as the capacitor applies a short circuit signal path to any unwanted frequency signals on the output terminals. Focusing on the HPF, the equations describing the circuits are [35]:

Equation 6.2

$$\frac{Vout}{Vin} = \frac{R}{R + Zc} = \frac{R}{R - j \cdot \frac{1}{wC}} = \frac{1}{1 - j \cdot \frac{1}{wCR}} = \frac{1}{1 - j \cdot \frac{1}{wCR}} = \frac{1}{1 - j \cdot \frac{fc}{f}}$$

$$gain = \frac{1}{\sqrt{(1 + (\frac{1}{wCR})^2}}$$

The ‘cut-off’, ‘corner’ or ‘breakpoint’ frequency is defined as being the frequency point where the capacitive reactance and resistance are equal so its value is:

Equation 6.3

$$fc = \frac{1}{2\pi \cdot C \cdot R}$$

When this occurs, the output signal is attenuated to 70.7% of the input signal value or -3dB of the input. At high frequencies, *w* is large so the gain is approximately 1, while at lower frequencies the gain decreases. Furthermore, due to the time taken to charge the plates of the capacitor, the output is delayed compared to the input signal. The Bode plots in Fig. 6.6 can be used to represent the frequency response of the system in terms of magnitude and phase.

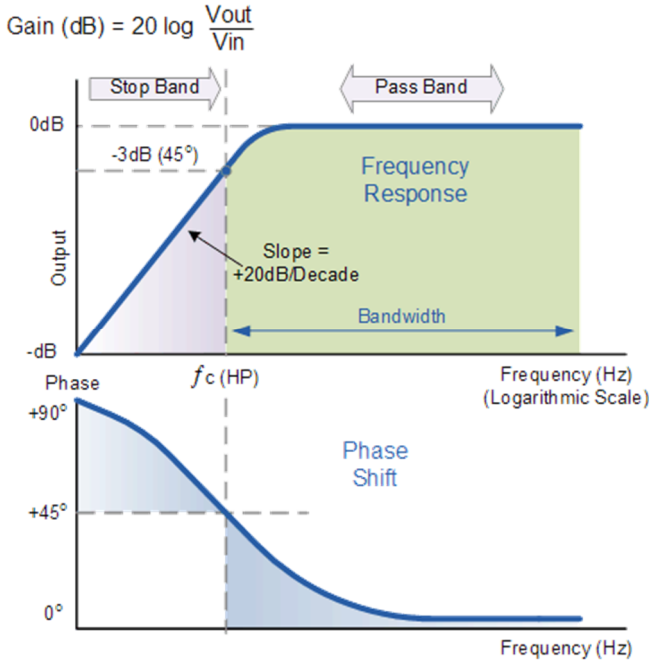

Figure 6.4: Bode plots of magnitude and phase against frequency

Then, by carefully selecting the correct resistor-capacitor combination, it is possible to create a RC circuit that allows only a range of frequencies above a certain value to pass through the circuit. The component of the signal within this ‘pass band’ is the input signal of the EDLC since it is able to handle fast fluctuations of power without overheating and decreasing its lifetime. On the other hand, the difference between the original signal and the high frequency component is the input of the battery, which is more suitable to handle slower variations of power.

6.3.2 HPF STRATEGY

The strategy based on HPF is been investigated by several authors [36], [37], [38], which approaches differ in selecting the cut-off frequency or SOC control of the supercapacitor. The general block scheme instead is common to all of them, even if in this case it has been simplified.
This strategy is relatively simple to implement. The objective of the devices is to coordinately control the DC bus voltage, whose variations are index of imbalance between power sent to the grid and power provided by battery and EDLC. For this reason, the central unit measures the DC bus voltage, then compares it with the reference value and this difference, which corresponds to an error, is sent to the PI controller. This proportional PI controller generates a current signal, which is the reference current of the entire storage system. At this point, the reference current is split in two parts using the HPF, generating a high frequency signal and a low frequency signal. From the control system, the

two references are sent to the corresponding DC/DC converters which, by mean of the faster PI controller, track this value and generate the duty cycle. The input current multiplied by the current voltage of the device is equivalent to the output power and the sum of the two powers gives the total amount of power provided by the storage system. If this power is equal to the power demand, no voltage fluctuation is registered in the bus.

The scheme in Fig. 6.1 can be implemented in Simulink by using the block scheme in Fig. 6.7. this simplified model only considers the PI controller of the central unit since (as previously explained) the devices are supposed to perfectly follow their current reference.

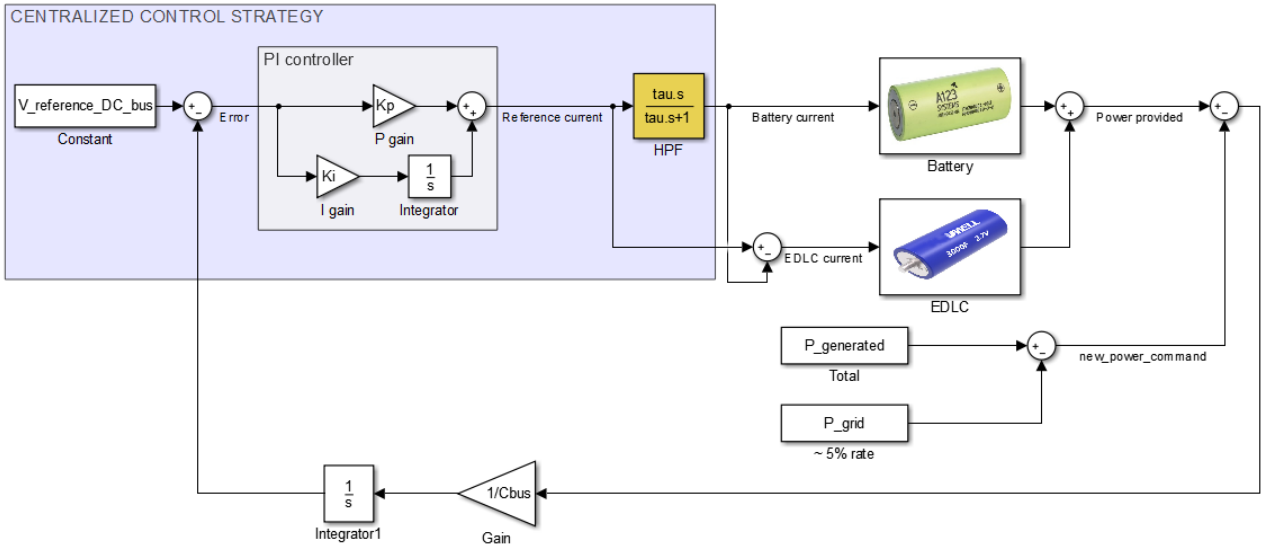

Figure 6.5: blocks scheme of the HPF strategy

The selection of the appropriate cut-off frequency is crucial for the optimal operation of the system. In fact, the same frequency may be considered too weak or too strong depending on the data to which it is applied. In literature many different approach can be founded. Some authors [39] propose a brute-force approach to select the cut-off frequency which gives the lower annual cost, but it does not consider the aging of the battery and the simulation time in this case would be too long. Authors [40] relate the number of operations of the battery in proportion to the entire life time of the HESS and use this value to calculate the cutoff frequency from the cumulative density function of the energy storage power profile. Others simply use a frequency ten times lower than the frequency of the AC grid [36].

In this dissertation, a mixed approach between authors [39] and [40] is considered. Firstly, to see the variability of data, the fast Fourier transform (FFT) is used. It is an algorithm that samples a signal over a period of time and divides it into its frequency components. These components are single sinusoidal oscillations at distinct frequencies each with their own amplitude and phase. Fig. 6.8 shows the FFT applied to the power reference of the energy storage. The range of frequencies is clearly visible and it is already possible to have an idea of which one must be selected for the filter. In fact, two different regions are visible, divided by a frequency value of about 0.1 Hz.

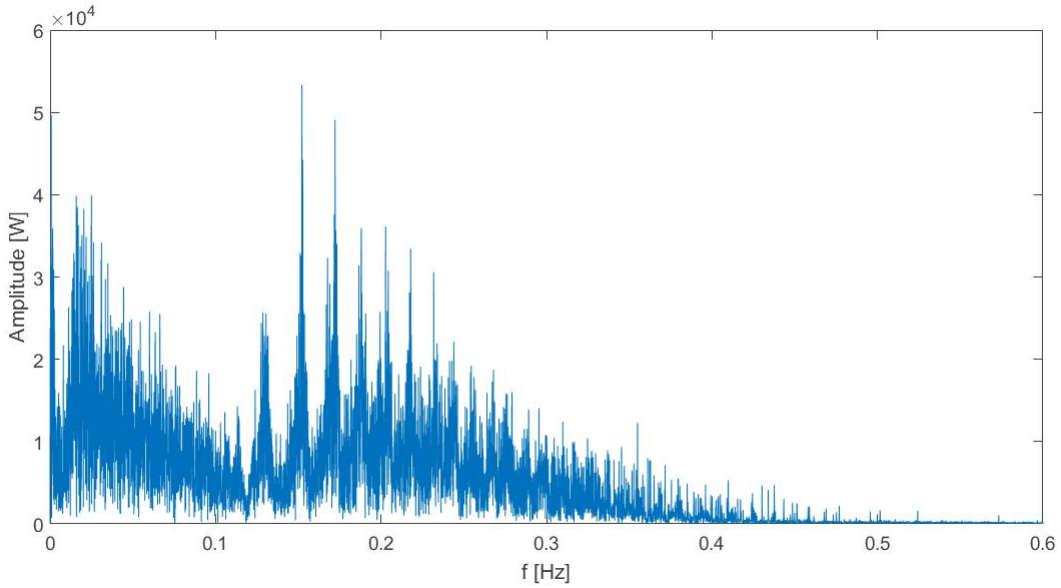

Figure 6.6: fast Fourier transform of the power profile

Secondly, to be more accurate, a cumulative function can be used to obtain the probability of a certain frequency to occur. In fact, according to authors in [40], the cut-off frequency is the frequency at which the cumulative probability is equal to *r*, where *r* is the ratio between the number of operations of the battery and the entire number of operations of the HESS:

Equation 6.4

$$r = \frac{Lifetime_{BATT}}{Lifetime_{BATT} + Lifetime_{EDLC}}$$

Possibly, with the help of the EDLCs, the battery will last more than 2000 cycles. Supposing a value of 5000 cycles for the battery and 1000000 for the EDLC, *r* results to be equal to 0.005. Introducing this value in the cumulative curve, it results a frequency value of about 0.008 Hz. Fig. 6.9 shows a detail of the cumulative curve.

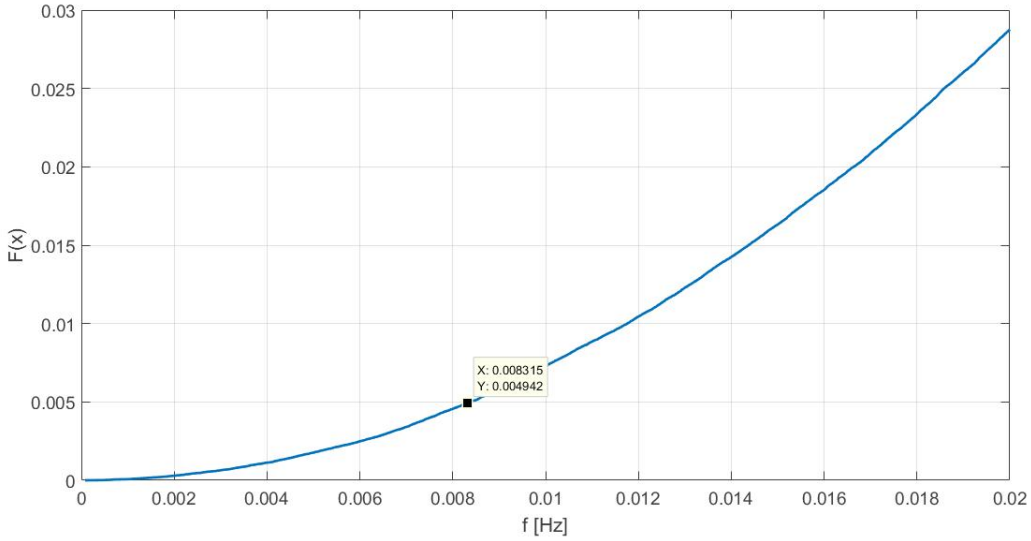

Figure 6.7: frequency cumulative curve. The cursor shows the X value corresponding to the Y value 0.005

In other words, frequencies under 0.008 Hz have the 0.5% of probability to occur so the device that manage the frequencies under 0.008 Hz, the battery in this case, is used 0.005 times out of 1.

Clearly this value is just an indication of the possible optimum frequency *fc*, so it is possible to circumscribe the range of possible frequencies around it and to use a brute-force approach to select the best one according to the criteria chosen, such as minimum battery aging, minimum total cost, minimum energy losses.

However, as explained in the first section, the SOC of the EDLC decreases faster than that of the battery and should be constantly restored in order not to collocate high currents on the latter. This means the power reference of both is slightly different from that obtained with the simple HPF since this restauration occurs after the filter block. The problem can be solved following the procedure proposed by [37], which studies the transfer function related to the new power allocation to find the energy restauration coefficient *Ke* of the EDLC. The relations between *Ke*, the reference frequency *fc* and the new frequency *a* due to the introduction of the factor *Ke* are [37]:

Equation 6.5

$$\begin{cases} \dfrac{1 + 2 \cdot a \cdot Ke}{a} = fc \\ \gamma = \dfrac{Ke}{a} \\ a = \dfrac{fc \pm \sqrt{fc^2 - 4\gamma}}{2 \cdot \gamma} \end{cases}$$

Therefore, γ has to satisfy the condition:

Equation 6.6

$$0 < n < 0.25$$
$$n = \frac{\gamma}{fc^2}$$

The closer γ is to the right limit, the faster will be the restauration of the EDLC energy and the response of the battery while, closer to the left limit, restauration is slower and the cut-off frequency is almost unchanged from its original value. The choice of this value depends on the application and, since in this case the power demand is not always positive but continuously fluctuates around zero, the EDLC is never completely discharged so γ can be smaller. In any case, its influence will be assessed in the simulation chapter.

Finally, the scheme if Fig. 6.10 can be modified to take into account the SOC restoration and, focusing on the filter section, results to be:

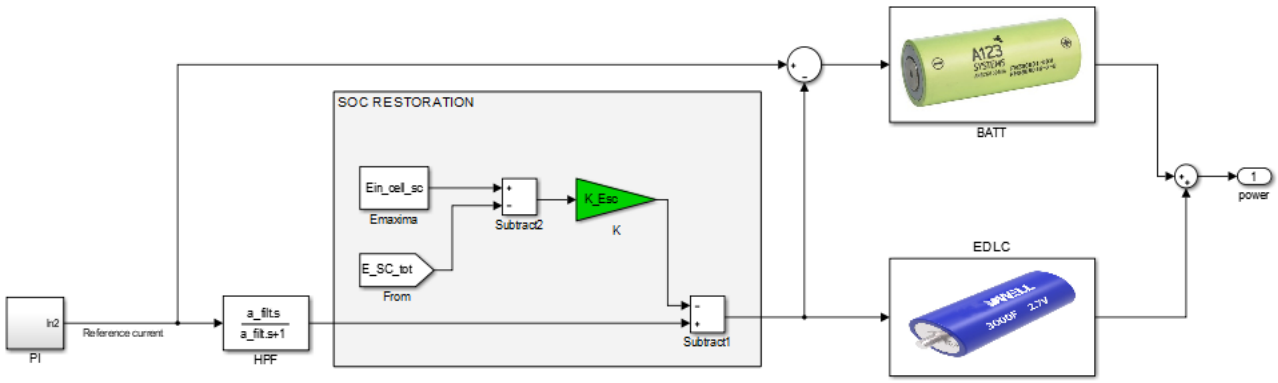

Figure 6.8: particular of the HPF strategy model with SOC restoration

6.4 DISTRIBUTED DROOP CONTROL

This chapter explains the hierarchical droop control strategy for DC systems making a comparison with the AC grid case. The equations of the first and second level of the strategy are explained, focusing the attention at the droop coefficient and at the SOC recovery of the EDLC.

6.4.1 FREQUENCY CONTROL IN AC GRIDS

Droop control is one of the most used technique to control DC systems, but in order to understand the idea behind the strategy, it is useful to explain its origin. In fact, it is very similar to the hierarchical control strategy used by AC systems to maintain the frequency at the nominal value. As a consequence of sudden load/generation changes, the frequency decreases/increases if there is a negative/positive mismatch between the power demand and the power generated. Thus, frequency deviations are index of poor regulation of active power and affect the operation of asynchronous generators and other devices. The hierarchical scheme is composed of a primary and secondary regulation.

During the primary regulation, each generator responds proportionally to the frequency variation injecting more power if the variation is negative, vice-versa if it is positive. In fact, each turbine-generator group is provided with a mechanical regulator, sensible to the frequency of the grid. When the power required by the load changes, the frequency (so the velocity) of the generator changes due to the variation of the resisting torque. The regulator leads the system to a new stable state, where the driving torque is again equal to the resisting torque. In this condition, the relation between power and frequency can be written as [41]:

Equation 6.7

$$\Delta P = -K \cdot \Delta f$$

where *K* is a proportional gain/droop coefficient. For this reason, the primary regulation is often called ‘droop control’. The coefficient has the dimension of an energy which can be expressed as [41]:

Equation 6.8

$$\begin{cases} K = \dfrac{Pn}{\sigma \cdot fn} \\ \sigma = (f0 - f1)/fn \end{cases}$$

σ is the statism degree of the regulator, *f0 f1* and *fn* the frequency at no load, the frequency at nominal power *Pn* and the nominal frequency respectively. According to equation (6.7), the greater gain *K*, the greater the response of the group in terms of power variation, while equation (6.8) states that K is proportional to the nominal power and inversely proportional to the statism degree.

After the imbalance is eliminated by the primary control, the frequency deviates from the nominal value so the assignment of the second level of this hierarchical strategy is to reestablish the nominal value of the frequency. In AC grids this is done by the RPM variator, which moves the static characteristic up or down according to the new frequency stable value, as shown in Fig. 6.11. Not all the generators participate: those that do, provide the total amount of power which initially generated the disturbance, reconducting the generators that act only during the primary regulation at their initial state. Usually, the secondary regulation has a slower dynamic, in order to prevent overlapping of the two level which may lead to problems of instability.

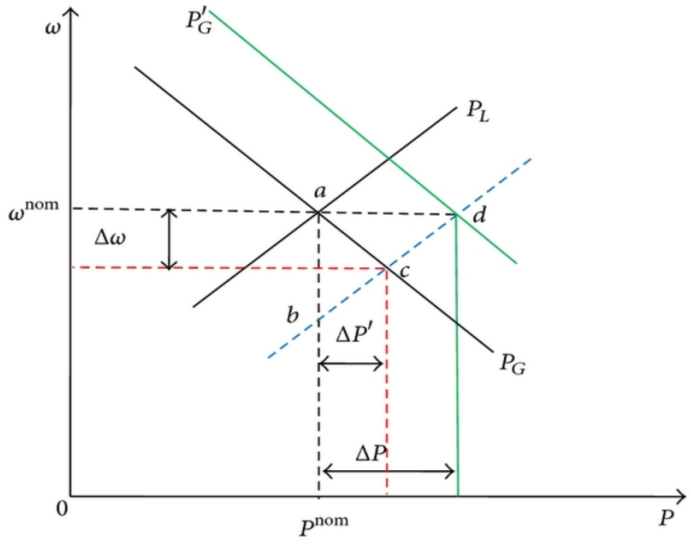

Figure 6.9: primary and secondary regulation. PG and PL are the static characteristics of the generator and the load respectively. After the transitory in c, the system frequency is restored in d, the new equilibrium point [42]

6.4.2 V-P DROOP CONTROL APPLIED TO DC SYSTEMS

The concepts explained in the previous section regard AC grids, but can be applied to DC systems as well, even if with some differences. In fact, AC voltages are characterized by three parameters: amplitude, frequency and phase. Voltage magnitude is directly related to reactive power, while frequency and phase are directly related to active power. On the other hand, in DC systems, voltages are characterized by only one parameter, the amplitude: there is no reactive power and both the power flow and the power imbalance are reflected into the voltage magnitude. For this reason, it is logical to give voltage amplitude the same function that frequency has in equation (6.7) so when voltage deviations occur, the regulator asks the energy storage for more or less power according to the sign of the deviation.

The regulator, in case of DC systems, is not mechanical but simply implemented into the converter electronics so it is faster and more reliable. Equation (6.8) also states that the droop coefficient is proportional to the rated power of the group: similarly, the droop coefficient in the DC grid case will be proportional to the rated power of the converter so to the rated power of the relative storage. The role of the statism degree instead is played, in the DC grid case, by the maximum voltage deviation desired in the DC bus, considering that too great deviations may lead to instability and malfunction of the inverter. For this reason, values of 5-10% are usually selected as maximum allowable deviation in percentage. Then, the droop coefficient *m* [V/W] of the storage *i* can be calculated as [43]:

Equation 6.9

$$\frac{1}{m_i} = \frac{Pn_i}{\Delta V\%_{max} \cdot Vref}$$

Since the current reference is provided by the PI controller of the converter (after comparing the reference value of the voltage with the actual output voltage of the converter), the droop control will act modifying the voltage reference value to vary the current so the power reference. Then, keeping the comparison with the AC grid case, the output power–voltage (P–V) relationship of the converter *i* in steady state results [43], [44]:

Equation 6.10

$$Vout_i = Vref - m_i \cdot P_i = Vref_{new\ i}$$

Since the bus is considered ideal, the output voltage of each converter is the same, so the *i* index is not necessary when referring to the voltage and it is possible to write the equivalence [44]:

Equation 6.11

$$Vbus = Vbatt_{out} = Vsc_{out} = Vout$$

Equation (6.10) is the equation of the V-P droop control. It describes the first level of the strategy at steady state and is used to establish the reference voltage of the converter $Vref_{new}$, different from *Vref*. Clearly, the *m* coefficient plays the key role in power sharing. In fact, equation (6.10) can be plotted to see how the output voltage of the converter varies with the power, as shown in Fig. 6.12. The droop coefficients are the slopes of the droop characteristic so the greater the value, the sharper the slope and the lower the contribution in terms of power to reach the new stable voltage level *V=Vout*, equal for all the converters. In fact, explicating power in eq. (6.10) it is possible to write:

Equation 6.12

$$\Delta P_i = -\frac{\Delta V}{m_i}$$

where ΔV is the voltage deviation equally experienced by all the devices connected to the bus. Then, the total amount of power provided by all the energy storage system is:

Equation 6.13

$$\Delta P_{HESS} = \sum \Delta P_i = -\Delta V \cdot \sum \frac{1}{m_i}$$

The equivalent droop coefficient of the HESS results to be:

Equation 6.14

$$m_{eq} = \frac{1}{\sum \frac{1}{m_i}}$$

$$Vout = Vref - m_{eq} \cdot P_{HESS}$$

Finally, the relation between power shared by the storage *i* in steady state is:

Equation 6.15

$$P_i = \frac{Vref - Vout}{m_i} = \frac{m_{eq}}{mi} \cdot P_{HESS} = \frac{Pn_i}{\sum Pn_i} \cdot P_{HESS}$$

Thus, the response of the energy storage which has the higher rated power will be greater than that of the other storage.

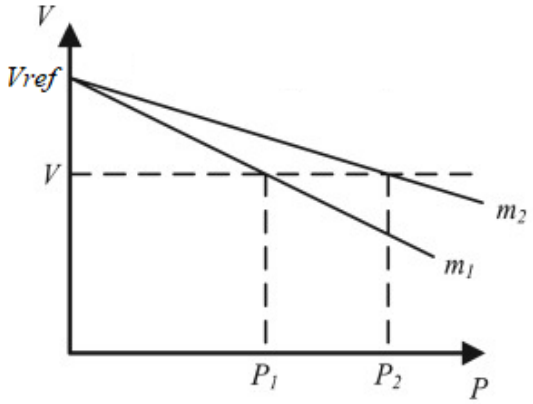

Figure 6.10: droop characteristic for different m coefficients (m2<m1)

Each local converter has its own droop control with a specific droop coefficient *m*, that depends on the rated power of the storage controlled. Therefore, there is no need for communication between them and each one responds proportionally to the available power of the device. Absence of the communication link at this first level improves reliability without adding any constraint regarding physical location of the module. On the other hand, the droop control deviates the voltage from its nominal value, as the primary regulation does with the frequency. Following this comparison, a second level is necessary to reestablish the initial value of the voltage and it has to be implemented by a communication link. In fact, this upper level monitors the output voltage of each converter which is generally different from one converter to the other due to the line impedance. However, as previously explained, the bus line is considered ideal.

If the line impedance can not be neglected, an average voltage of the bus is calculated and compared to the nominal value. Then, after receiving this value, the deviation from the nominal value is sent to a PI controller which finally acts at the primary level, modifying the voltage reference. The controller is not properly a PI but a simpler integral controller, so its output is calculated as [44]:

Equation 6.16

$$\Delta V = \frac{ki}{s}(Vref - Vbus) = \frac{ki}{s}(Vref - Vout)$$

Since the droop control at the first level is implemented with a simple equation and no integral calculation is done, the second level is slower and acts after the first, leading the system to the initial voltage reference.

Finally, the hierarchical control structure can be resumed by Fig. 6.13 as:

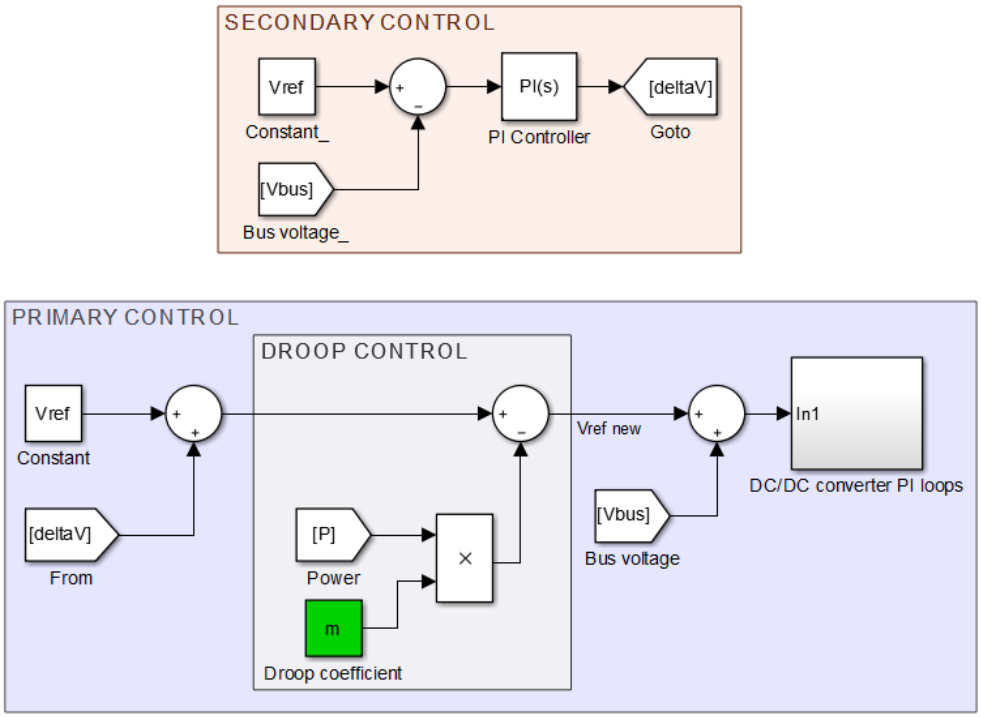

Figure 6.11: hierarchical control strategy of the droop control. The first level is decentralized, while the second is centralized

According to the scheme, the secondary control modifies equation (6.10), updating the reference voltage by introducing the bus voltage restoration term ΔV as follow:

Equation 6.17

$$Vref_{new} = (Vref + \Delta V) - m \cdot P = Vref - m \cdot \frac{s}{s + ki} \cdot P$$

This additional term moves up the P-V characteristic in figure, similarly to what the secondary regulation does in the AC grid case, consequently the voltage deviation is eliminated. Furthermore, it acts as a HPF, so the output voltage of the battery converter returns to reference value at steady state and voltage deviation is eliminated.

As done for the HPF strategy, the SOC restauration of the EDLC has to be implemented into the control. The SOC deviation from the reference value can be translated in a voltage signal, to change the voltage reference of the droop control and subsequently the current output of the PI loop. Fig. 6.14 shows the primary control level of the EDLC. If the SOC is below the reference value, the SOC block diminishes the signal *Vref new* and the difference between this value and the bus voltage will eventually give a negative result, so the current output of the inductor will be negative and will charge the EDLC. The *Ke* factor determines how fast is the recovery and can be calculated as:

Equation 6.18

$$Ke = \frac{\Delta V\%_{max} \cdot Vref}{\Delta SOC_{max}}$$

Therefore, *Ke* is related to the SOC limits of the device. The influence of this factor will be evaluated in the simulation, but usually the SOC of the EDLC can vary among a wide range without compromising the lifetime of the device.

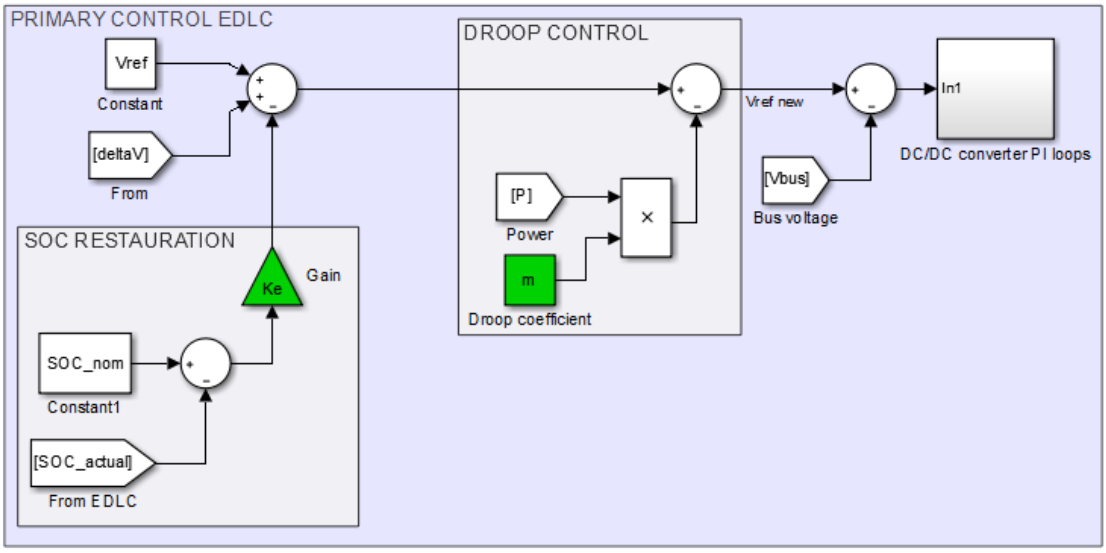

Figure 6.12: primary control of the EDLC considering the SOC restauration

As done for the HPF strategy in Fig. 6.7, the transfer function of the bus can be used to calculate the actual bus voltage. The scheme in Fig. 6.2 can be can be implemented in Simulink with the following block scheme:

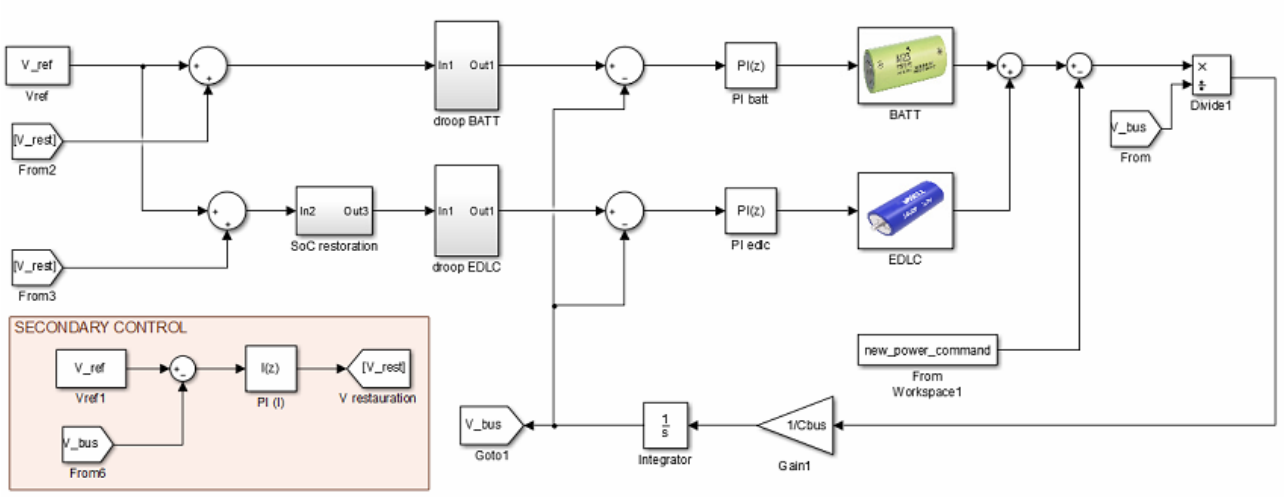

Figure 6.13: blocks scheme of the droop control strategy with SOC restoration

Once the rated power of each storage device is known, the *m* coefficient can be easily calculated and the strategy implemented. However, the number of branches of each storage system is still unknown at this point: the sizing is related to the amount of power and energy shared between the battery and the supercapacitor but, according to the strategy, these amounts depend on the *m* coefficient. Therefore, a brute-force approach is used to select the appropriate combination of numbers of batteries and EDLCs. In fact, thanks to the analysis previously conducted on the data of power generated by the plant, the maximum power and energy required are known. Then, considering the nominal power and energy of each battery and EDLC cell and by using a simple MATLAB script, it is possible to find the possible combination of minimum numbers of branches that satisfy the maximum power and energy demand. After that, each different combination is tested in the simulation and the response of the system in terms of battery aging, energy losses and bus voltage variations is monitored. This procedure is reported in the next chapter.

Finally, it should be noticed that equation (6.10) can also be written substituting the power output of the device with its current, as done by authors in [44], [45]. In this case, the droop coefficient assumes the dimension of a resistance and is calculated using the rated current, so it is commonly called 'virtual resistance' and V-I droop instead of V-P droop control. Similarly to eq. (6.9), this resistance is equal to:

Equation 6.19

$$R_i = \frac{\Delta V\%_{max} \cdot Vref}{In_i}$$

where *In* [A] is the maximum current provided by the *i* energy storage.
Since the output of the battery and EDLC models implemented is in Watts, for simplicity power is used instead of current. Other studies [46] investigate the stability of the system in one case or another by calculating the equivalent impedances of the converters but, since in this dissertation the grid model has been simplified and the converters are not considered, the choice of current instead of power would not give substantial differences.

Finally, some authors [44], [47] studied a hybrid approach between HPF strategy and droop control, called 'integral-droop (ID) control'. They apply the conventional V-P droop control to the slower

device (the battery), while EDLC is controlled by the ID. The equations, using the same terminology as ref. [44] that use a V-I droop instead of a V-P droop, are:

Equation 6.20

$$Vout = Vref - \frac{1}{C} \cdot \int I_{EDLC} dt = Vref_{new} \ (EDLC)$$
$$Vout = Vref - R \cdot I_{BATT} = Vref_{new} \ (BATT)$$

The first one is the equation of the ID droop. The two equations, combined together work as filter and split the power into low and high frequency components for battery and the EDLC. Furthermore, collocating the secondary voltage restauration only on the battery, the SOC of the EDLC is automatically restored. However, the enabled voltage and SOC restoration may impact the autonomous transient power split for EDLC and battery. Parameters should be carefully designed to decouple the processes to ensure expected system dynamics. For this reason, the strategy is not studied and implemented in this dissertation and will be object of future studies.

7 SIMULATIONS AND RESULTS

The chapter firstly shows the results of the simulation in case of batteries only, which is used as comparison for the two strategies. The methods used to size the system are then described and the results of the simulations shown, investigating the influence of the parameters which characterize each strategy.

7.1 CASE WITH BATTERIES ONLY

Since the aim of the dissertation is to prove that better results can be obtained combining two types of energy storage device, it is fundamental to evaluate the performance and in particular the cost of the system when only batteries are used as storage. In order to know how many batteries are necessary to supply the power demand, the following parameters has to be decided before sizing:

- Bus voltage and capacitance: the choice of the bus voltage should consider the voltage of the AC side, connected by an inverter to the DC system
- Voltage of the battery and EDLC packs on the other side of the DC/DC converters: even if the converter can theoretically provide any voltage desired, its duty ratio should be kept lower than 0.6 to avoid instability and not to ruin the converter itself
- Nominal power and energy of the battery cell: chosen considering their datasheet
- Nominal power and energy the EDLC cell: chosen considering their datasheet
- Maximum power and energy associated with the wave generation (not considering the part dispatched to the grid, see chapter 3): calculated from the data
- PI controller gains: manually tuned

Then, the bus voltage selected is 750V (considering the AC grid at 400V) and a typical value of the capacitance in these case is 0.5 F. From the value of the bus voltage, the battery pack voltage results to be 500V while for the EDLC pack is 550V since its voltage is not as constant as that of the battery. The nominal power can be found multiplying the nominal voltage by the nominal current. The datasheets report the maximum current allowed for the two devices but these values can not be set as nominal current since they refer to limits that can not be tolerated for too long. Therefore, for the battery a practice limit of 6C is used and for the EDLC a current of 200A, which is the maximum current that can be continuously provided without deteriorating the device. The nominal energies are associated with the maximum and minimum voltage/SOC of the cells and can be calculated from these limits. Finally, the maximum power and energy of the power profile are those in chapter 3 for the droop control strategy, while for the HPF one depends on the cut-off frequency chosen. This process will be better explained in the next section.

Parameter	V bus	C bus	V batt	V EDLC	Pn batt	Pn EDLC	En batt	En EDLC	Pmax	Emax
Value	750 V	0.5 F	500 V	550 V	47.5 W	540 W	3.96 Wh	2.1 Wh	- 3.087 MW	38.98 kWh

The initial SOC of the battery is set at 70%, that of the EDLC at 55%. In fact, the application mostly requires the storage to be able to absorb a great amount of energy, so they can not be fully charged at the beginning of the simulation.

Regarding the cost, the EDLC results more expensive than the battery. The following prices per kWh installed are used, considering the average price on the market for high power installations:

- 350 €/kWh for the battery
- 3500 €/kWh for the EDLC

Once these parameters are established, the battery pack can be sized to handle the entire power and energy of the energy storage system. The numbers of cells in series can be easily calculated as:

Equation 7.1

$$N\ cells\ in\ series = \frac{Vpack}{Vcell_n}$$

The result of this equation is also valid for the other strategies since the voltage required is always 500 V. Regarding the number of branches, the battery pack has to be able to provide both the maximum power and energy, so the number of branches will be the higher between the results of the equations:

Equation 7.2

$$N\ branches = \frac{Pmax_{demanded}}{Pmax_{branch}}$$

$$N\ branches = \frac{Emax_{demanded}}{Emax_{branch}}$$

The results of eq. (7.1) and (7.2) are:

- N cells in series batt: 152
- N branches: 428

The results of the simulation, which scheme is equal to the schemes of the two strategies without the EDLC and the control strategy block, are reported in terms of SOC variation and capacity fade in Fig. 7.1 and Fig. 7.2. The capacity fade is calculated after 2000 cycles.

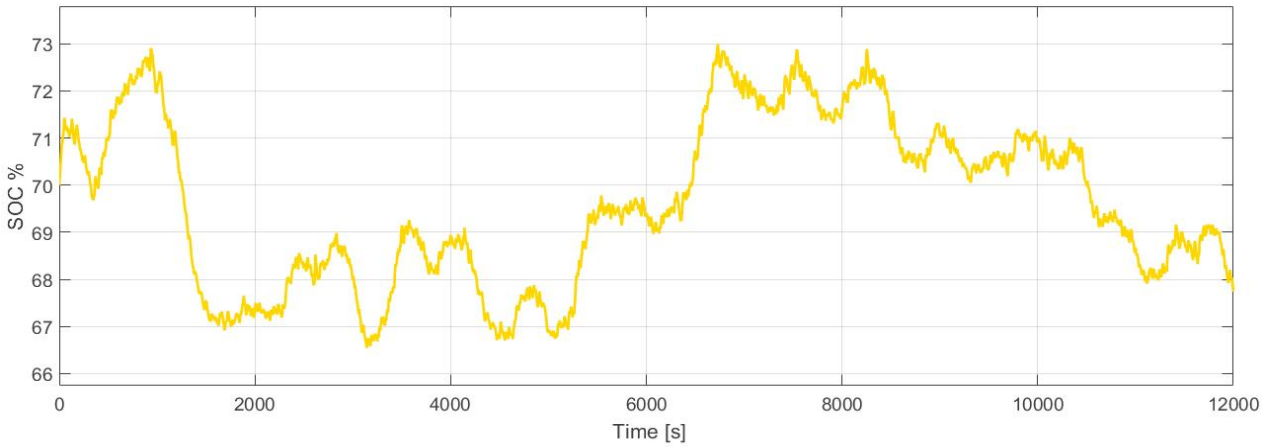

Figure 7.1: SOC variation of each battery cell

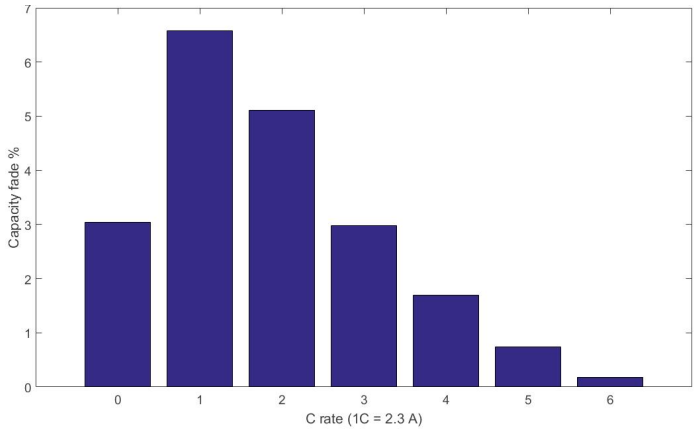

Figure 7.2: percentage of capacity fade introduced by each current rate. The overall capacity fade is the sum

The numerical results are:

- Capacity fade after 2000 cycles: 20.32 %
- Cost of the total pack of battery: 180340 €
- Energy losses: 23 kWh

It should be noticed that usually a battery is substituted when reaches a capacity fade of 20%, as in this case. If a higher nominal power value had been considered, the number of branches would have been lower as well as the total cost of the pack, but the lifetime capacity fade would have been far greater since the cell would have been subjected to higher current rates. Therefore, 6C represents a good value for comparing this case with the strategies.

7.2 HPF STRATEGY RESULTS

The size of the battery and EDLC packs can be easily calculated with equations (7.1) and (7.2) once the respective power and energy demand are known. In fact, eq. (7.1) applied to the EDLC gives:

- N cells in series EDLC: 204

Since the filter splits the power to the energy storage in high and low frequencies components, each device will have to manage its own power profile and will be sized according to it. So firstly, it is necessary to select the cut-off frequency then, by using a MATLAB script, the maximum power and energy of the profile will be calculated and finally each pack will be sized.

A brute-force approach is used to select the appropriate cut-off frequency, testing the value around that founded in Fig. 6.7, which is 0.008 Hz. Since a lower frequency means smoother reference power for the battery, it is expected the higher cut-off frequencies to give worse results in terms of capacity fade. On the other hand, too low frequencies may lead to a higher cost of the system since the EDLC pack has to be oversized to handle a greater energy and its cost is ten times higher than that of the battery. The optimal point should be found at a frequency where the battery pack is used to provide most of the energy and the EDLC pack to provide the peaks of power.

For the same configuration, the SOC restoration is tested with different values of the parameter n from eq. (6.6). As previously explained, the higher its value, the faster is the recovery but the higher the energy drained from the battery. In fact, eq. 6.5 assures that the cut-off frequency seen by the storage system is the frequency chosen, independently from n: this means n influences the average power provided by the battery, not the peaks which remain unchanged.

Firstly, in order to verify the operation of the filter, a simple step is used as power demanded to the energy storage system: the response of the EDLC should be immediate and fall to zero as the battery increases the power provided. Fig. 7.3 confirms this behavior for a step of 100 kW and a frequency of 0.008 Hz. Clearly, the velocity at which the EDLC response falls to zero is related to how strong is the filter: smaller frequencies give smoother and longer transients.

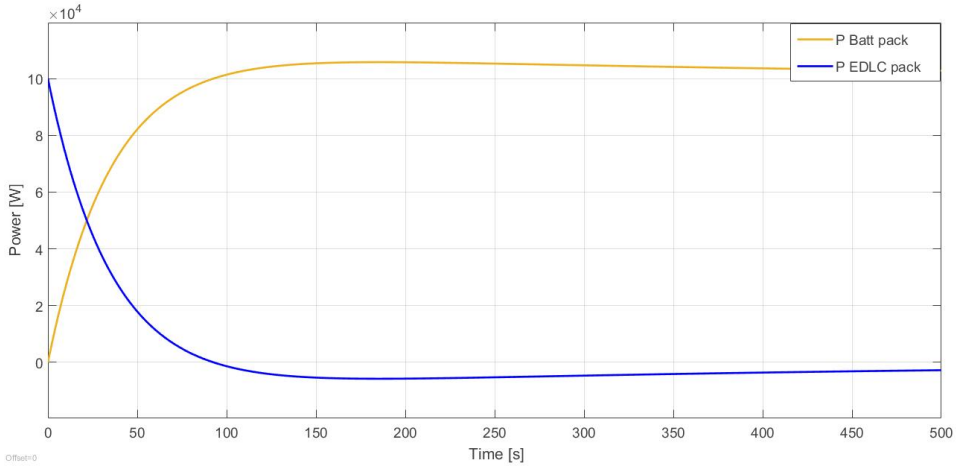

Figure 7.3: power response of battery and EDLC to a power step equal to 100 kW with fc 0.008 Hz

Once the good operation of the filter is proved, the different cut-off frequencies can be tested: Fig. 7.4 reports the results of the simulation in terms of capacity fade for the frequencies around the value 0.008 Hz. To each one corresponds a certain number of EDLCs and batteries which is reported in the following table:

Cut-off frequency [Hz]	0.001	0.002	0.003	0.004	0.005	0.006	0.007	0.008	0.009	0.01	0.11
N branches batt	55	58	59	60	60	65	69	72	75	80	83
N branches EDLC	41	28	28	28	28	28	27	27	27	26	26
Cost tot [€]	112090	85164	85585	86006	86006	88113	87630	88894	90158	90096	91360

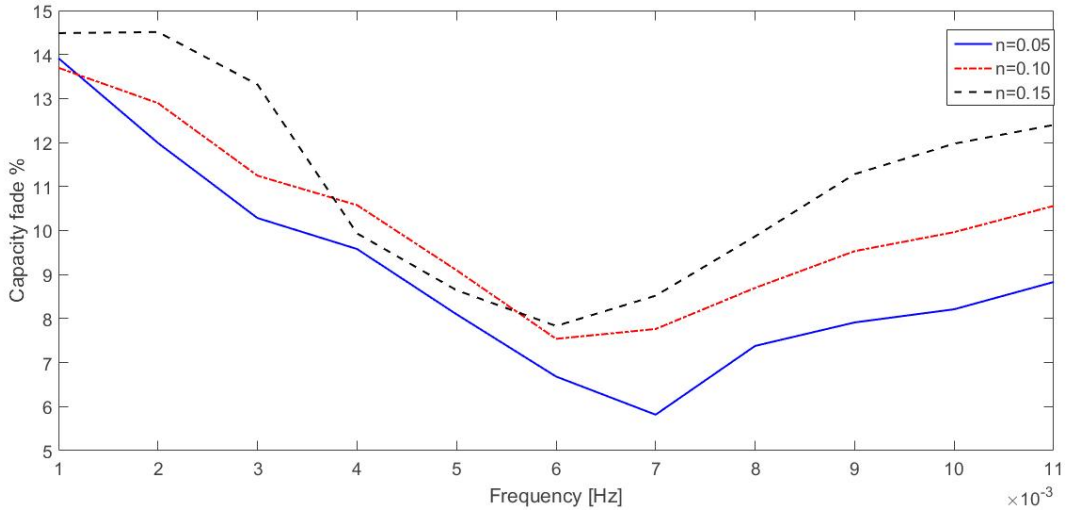

Figure 7.4: capacity fade at different frequencies for different n. Higher n give faster SOC recovery

As expected the lower capacity fade is obtained with the lower *n*. Since a value of zero is not safe for the operation of the storage, a value of *n*=0.05 is used as minimum possible value. It should be noticed that, for cut-off frequencies equal to 0.003 Hz and 0.004 Hz, the capacity fade is higher than the case with frequency 0.005-0.006-0.007 Hz. In fact, the lower peak of power does not mean the battery is less used, but simply that the power provided is more constant, following the smoother power profile given by the filter. In other words, as occurs with *n*, the number of branches is lower because the peak is lower (according to eq. 7.2), but the battery usage is more constant and the average power provided is higher. Another interesting aspect regards the energy losses: since the EDLC efficiency is higher than that of the battery, when the cut-off frequency is lower more energy is managed by the EDLC so less energy is lost.

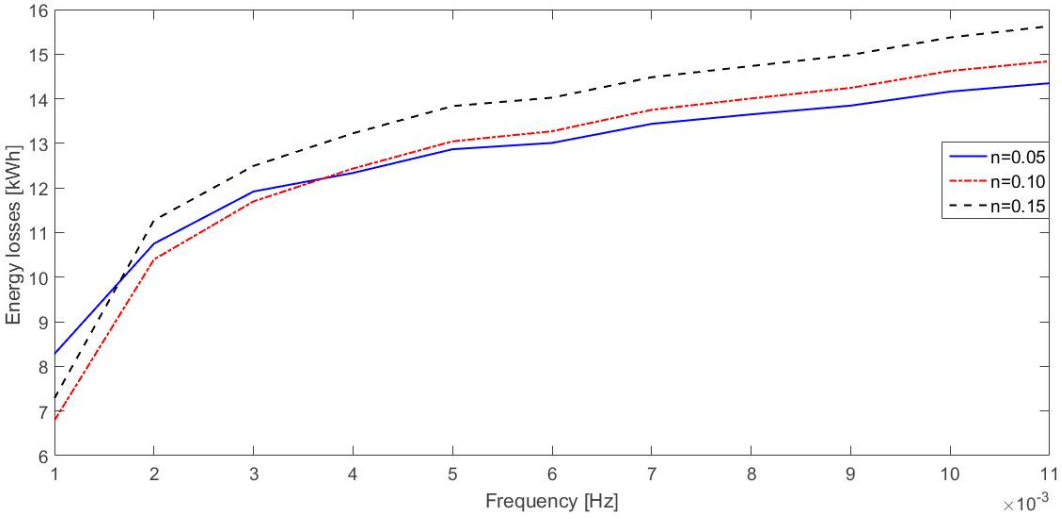

Figure 7.5: system energy losses at different frequencies for different n

Finally, considering the lower cost, capacity fade and energy losses, it is possible to state that the best result is obtained when:

- Cut-frequency: 0.007 Hz
- n: 0.05

These values give:

- Branches of batteries: 69
- Branches of EDLCs: 27
- Capacity fade after 2000 cycles: 5.8168 %
- Cost tot: 87630 €
- Energy losses: 13.437 kWh

Figures from 7.6 to 7.8 resume the results of these set of values in terms of power profiles, battery and EDLC SOC and capacity fade.

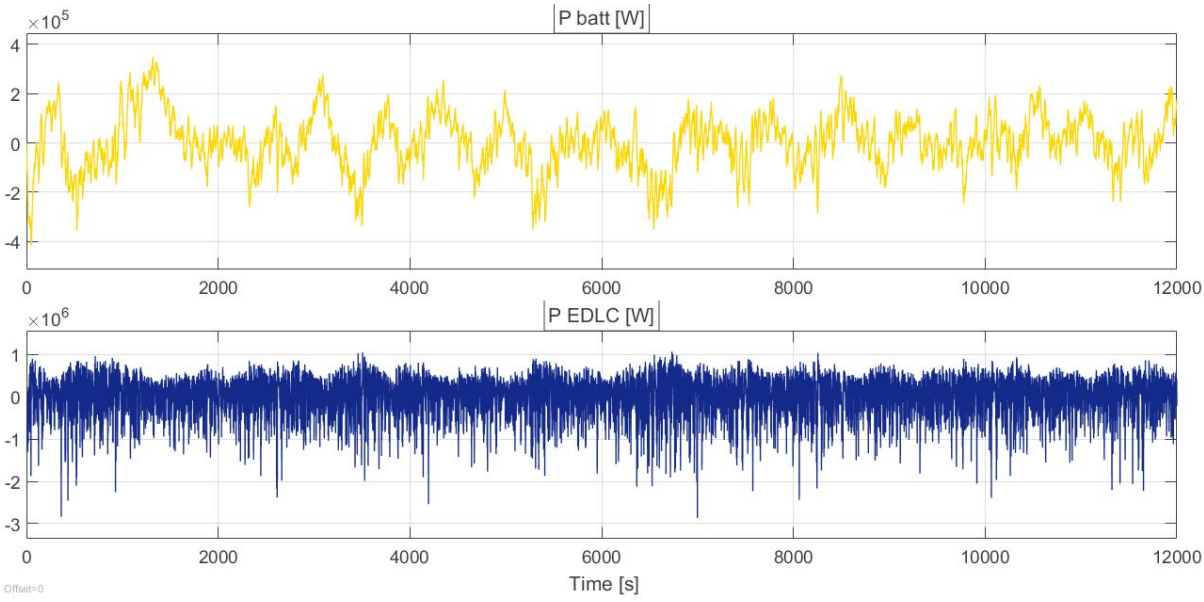

Figure 7.6: power response of battery and EDLC packs. The battery profile is smoother than that of the EDLC

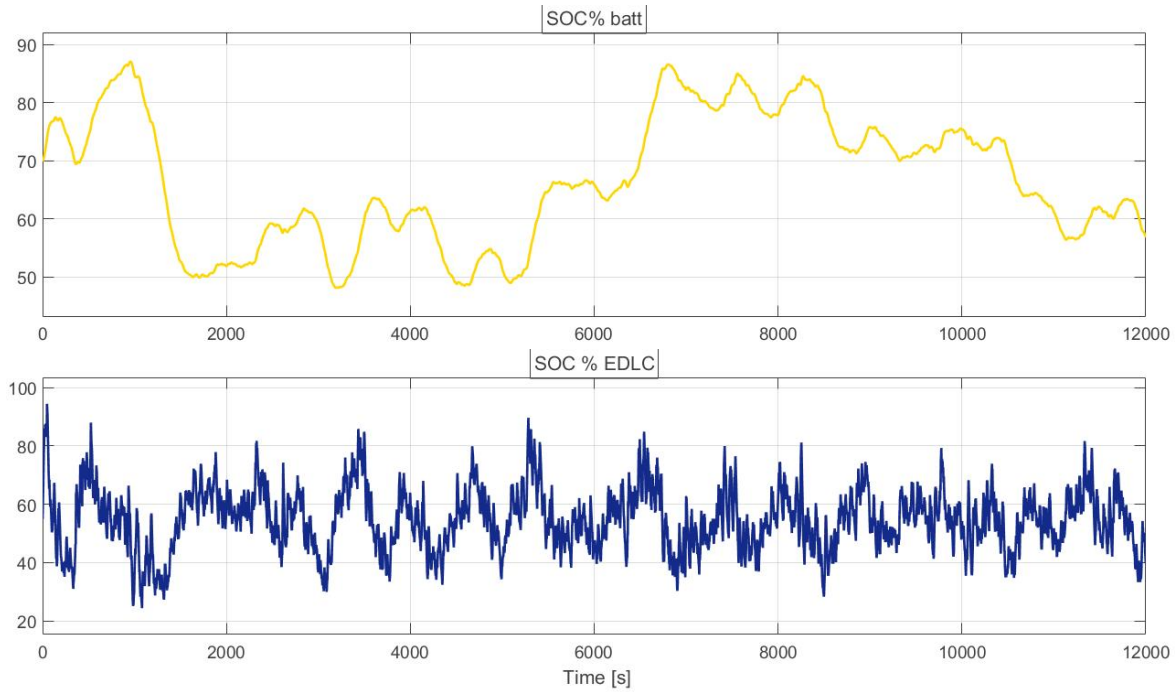

Figure 7.7: SOC variation of the battery and EDLC packs. The SOC variation of the battery is slower than that of the EDLC

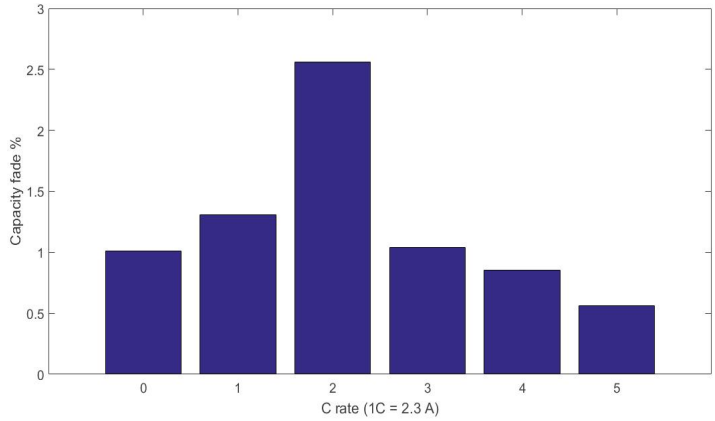

Figure 7.8: percentage of capacity fade introduced by each current rate. The overall capacity fade is the sum

Comparing Fig. 7.8 and Fig. 7.2 it is possible to state that, in the case with batteries only, the greater contribution to the overall capacity fade is given by the current rate 1C, while in the HPF case is given by 2C. This means the most frequent current rates in the two cases are 1C and 2C respectively. According to the aging model, the aging with moderate current rates is slower than aging with low current rates. Furthermore, the capacity discharged by 1C in the first case is higher than that discharged by 2C in the second. These two factors explain the higher capacity fade.

7.3 DROOP CONTROL STRATEGY RESULTS

The size of the system in this case is more complicated. In fact, it is not possible to know the power profile managed by each storage before knowing the number of branches of each storage since these profiles depend on the droop coefficient *m* (see eq. 6.9). A different approach respect that used for the HPF strategy is necessary. The only possible solution to this problem is testing various combinations of number of batteries and EDLC and then select the best one evaluating the cost, the capacity fade and the energy losses.

Among the infinite possible combinations, only those that are able to satisfy the power and energy demand with the minimum number of batteries and EDLC are tested. This approach guarantees the respect of the sizing conditions at the lowest cost possible. Then, a MATLAB script can be used to provide the combinations which are reported in Fig. 7.7: the script progressively calculates the number of EDLCs necessary when using 1,2,3…428 branches of batteries. Some of the values founded are able to satisfy the energy but not the power demand (or vice-versa) so they are not considered. Furthermore, to reduce the simulation time, the combinations with the same branches of EDLCs and different branches of batteries (or vice-versa) are not tested: a combination with 20 branches of EDLCs - 140 of batteries gives almost the same results of one with 20 branches of EDLCs – 141 of batteries. Therefore, from the 429 possible combinations, only 72 have been tested (the blue spots in Fig.7.7). From the figure, it is already possible to have an idea of which is the area of interest: the combinations on the left side, with high number of EDLCs, are in fact the most expensive, as well as those on the right side since they require a large number of batteries to satisfy the power demand. The optimum solution, from the point of view of the cost, are those in the middle.

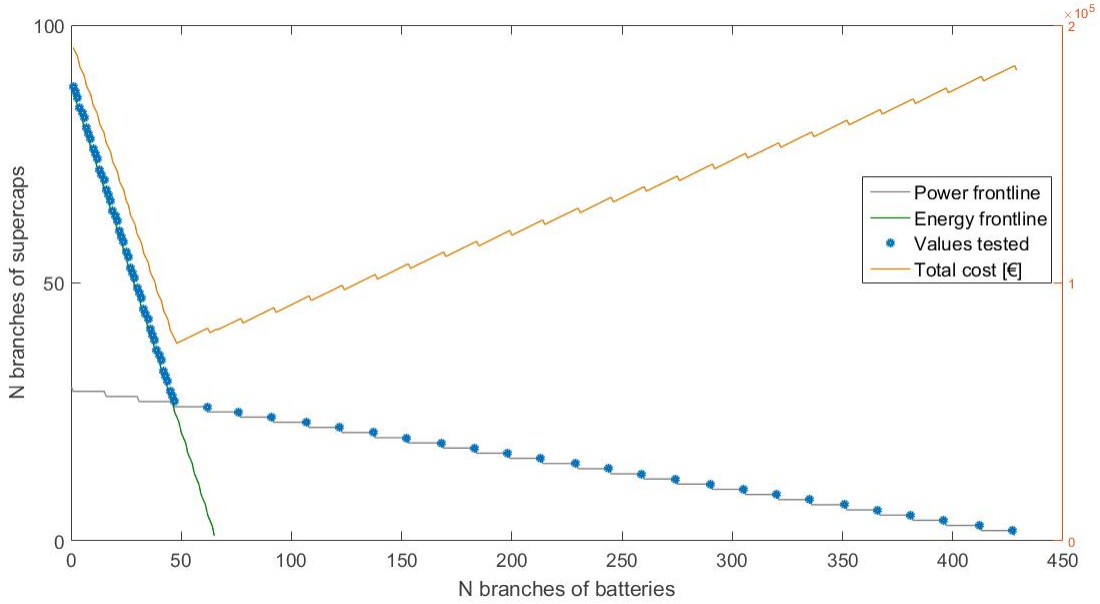

Figure 7.7: combinations of batteries and EDLCs that satisfy the power or the energy demand

For the same combination, the SOC restoration factor *Ke* (eq. 6.18) can assume different values so, as done for the HPF strategy, 3 different values are tested. It is expected that the higher is the *Ke*, the smaller the range of variation of the SOC of the EDLC and consequently the faster the response of the battery (so a greater capacity fade). In fact, according to eq. (6.18), a lower *Ke* is associated with a higher ΔSOC_{max}, so the SOC is allowed to change within a wider range. Since the initial SOC of the EDLC is set at 55%, the SOC can vary at most of nearly 50 from this initial value (+45 means fully discharged, -55 fully charged). Thus, the maximum ΔSOC_{max} is 50 in this case. This does not mean the system can not work with higher values, but that the EDLC energy recovery is slower and

eventually there will be moments during which it is completely discharged and the battery has to provide the entire power.

Firstly, in order to verify the operation of the power sharing mechanism, a simple step is used as power demanded to the energy storage system: the response of each storage device should be proportional to its installed power, according to eq. (6.15). Furthermore, using eq. (6.12) it is possible to predict the voltage deviation in case of no secondary control. As done for the HPF strategy, a step of 100 kW is used to test the behavior. The transients in this case are regulated by the PI controllers of the two DC/DC converters. In order to test the system, the number of branches of batteries (69) and EDLCs (27) found in the HPF strategy are used. Then, considering 10% as $\Delta V\%_{max}$, the m coefficients can be calculated as:

- $m_{batt} = \frac{\Delta V\%_{max} \cdot Vref}{Pn} = \frac{\Delta V\%_{max} \cdot Vref}{N_{branches} \cdot N_{series} \cdot Pn_{batt}} = \frac{0.1 \cdot 750}{69 \cdot 152 \cdot 47.5} = 0.1505 \frac{V}{kW}$
- $m_{EDLC} = \frac{0.1 \cdot 750}{27 \cdot 204 \cdot 540} = 0.02522 \frac{V}{kW}$

These values give the voltage deviation at the output of the converter when the pack has to provide 1 kW or, in other words, the voltage deviation necessary to have a response of 1 kW. Despite the fact that less branches of EDLC are used, the m coefficient is much lower than that of the battery pack. Using eq. (6.13), the voltage deviation after a step of 100 kW and without secondary regulation and SOC restoration is:

- $-\Delta V = \frac{100}{\frac{1}{m_{batt}} + \frac{1}{m_{EDLC}}} = \frac{100}{46.3} = 2.16\ V$

Therefore, the power contribution of each energy storage should be (from eq. 6.12):

- Battery pack: 14.35 kW
- EDLC pack: 85.65 kW

Fig. 7.7 shows the results of the simulation which confirm the predictions made. The short transitory at the beginning is given by the PI converters.

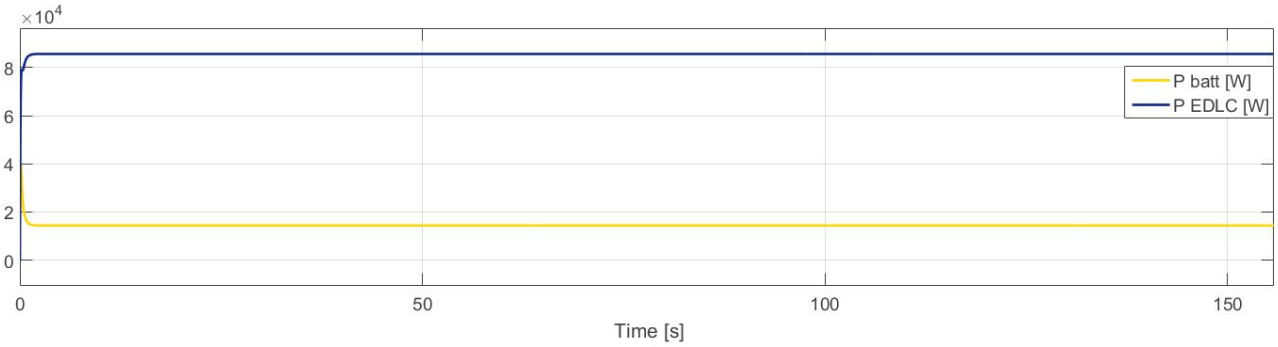

Figure 7.8: system response to a step of 100 kW with no secondary control and SOC restoration

When the SOC restoration is used, the SOC restoration block detects that the energy level of the EDLC is decreasing and changes its reference voltage in order to restore the initial energy. Therefore, at steady state, when the initial energy has been restored, the output of the EDLC is zero and the battery only provides the whole power until a new perturbation occurs. Then, the voltage deviation at the end of the transitory results to be:

- $\Delta V = m_{batt} \cdot 100 = 0.1505 \cdot 100 = 15.05\ V$

Fig. 7.8 shows the results of the simulation using a ΔSOC_{max} of 50. The initial conditions of the system are equal to those in the previous case: the voltage deviation is 2.16 V and the power sharing

the same as in Fig. 7.8. After this initial state, the SOC restoration moves the system to a new equilibrium, to let the EDLC pack recover its energy. It should be noticed that the system can still work without the secondary level. Problems arise in case of sudden perturbations, when the bus voltage may be further reduced till the DC/AC converter, which connects the system to the main grid, is no longer able to work properly.

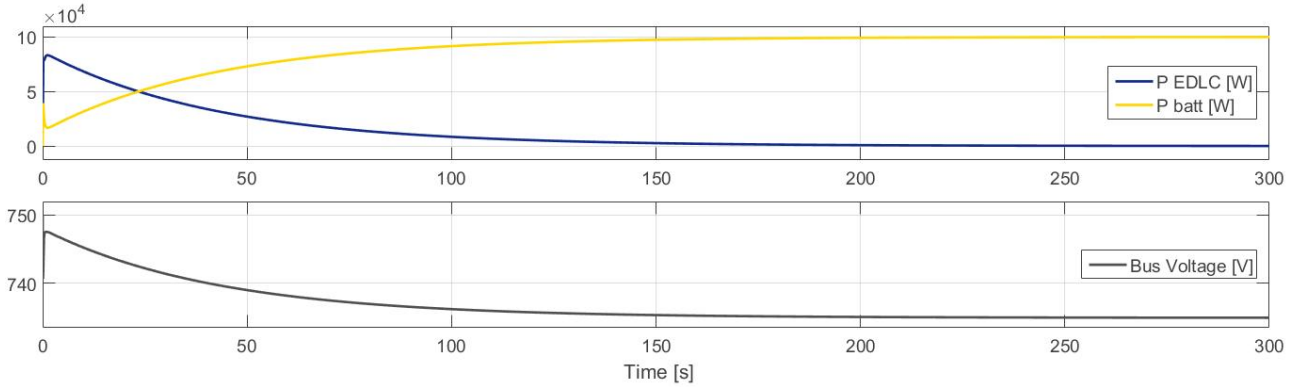

Figure 7.9: system response to a step of 100 kW with EDLC SOC restoration and no secondary control

Finally, adding the secondary control, the voltage can be quickly restored to its initial level. In fact, the same case of Fig. 7.9 but with secondary control gives:

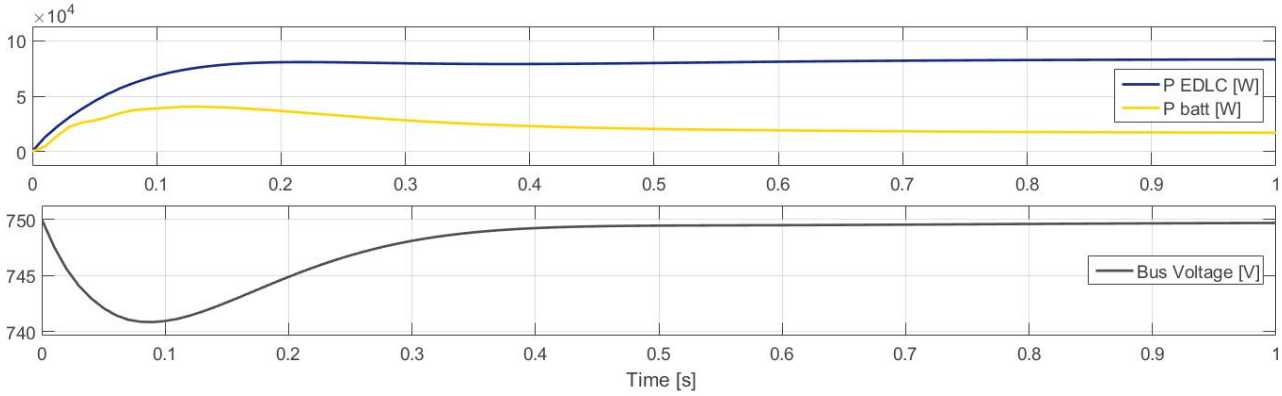

Figure 7.10: initial system response to a step of 100 kW with EDLC SOC restoration and secondary control

Once the operation of the system is clear, the different combinations can be tested with different SOC restoration factors *Ke*. Fig. 7.11 reports the results of the combinations in the area of minimum cost of Fig.7.7 while Fig. 7.12 reports the energy losses for these combinations. As expected, lower ΔSOC max lead to higher capacity fade and higher energy losses since the battery pack works in non-optimal conditions, therefore case with ΔSOC max =50 is chosen as optimal solution.

In solutions with high number of EDLC the batteries work as a support to the EDLC pack, which discharges fast and eventually is completely discharged exposing the batteries to high currents. Clearly, since the EDLC pack in this case provides most of the energy required and has an energy efficiency of around 98-99%, the energy losses are lower. On the other hand, solutions with high number of batteries do not benefit of the action of the EDLC and have higher energy losses. Therefore, the solutions close to the minimum cost in Fig. 7.7 are the optimum also from the point of view of the performance besides the cost.

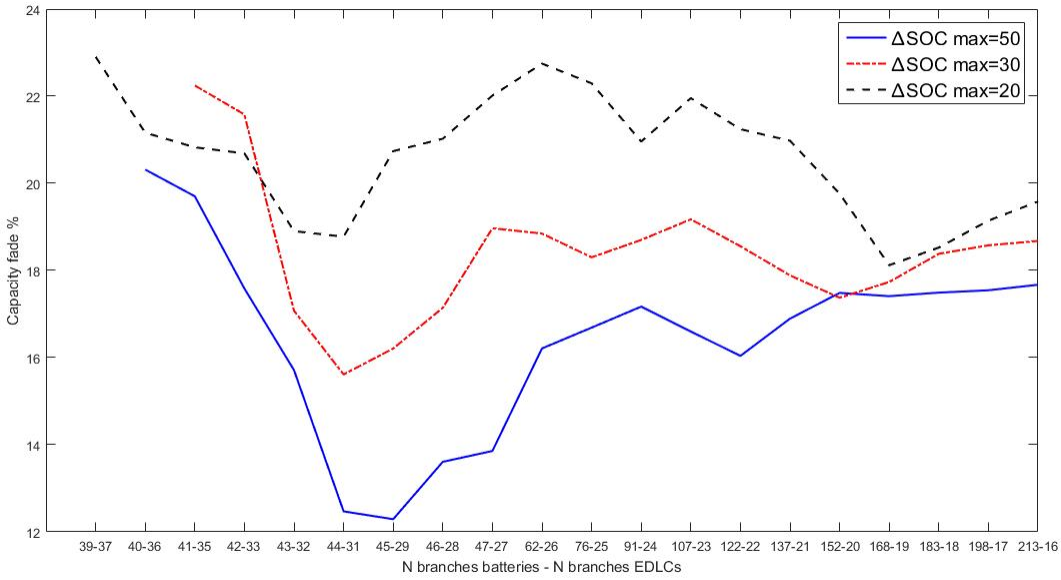

Figure 7.11: capacity fade for different combination of branches of batteries and EDLCs for 3 different ΔSOC max

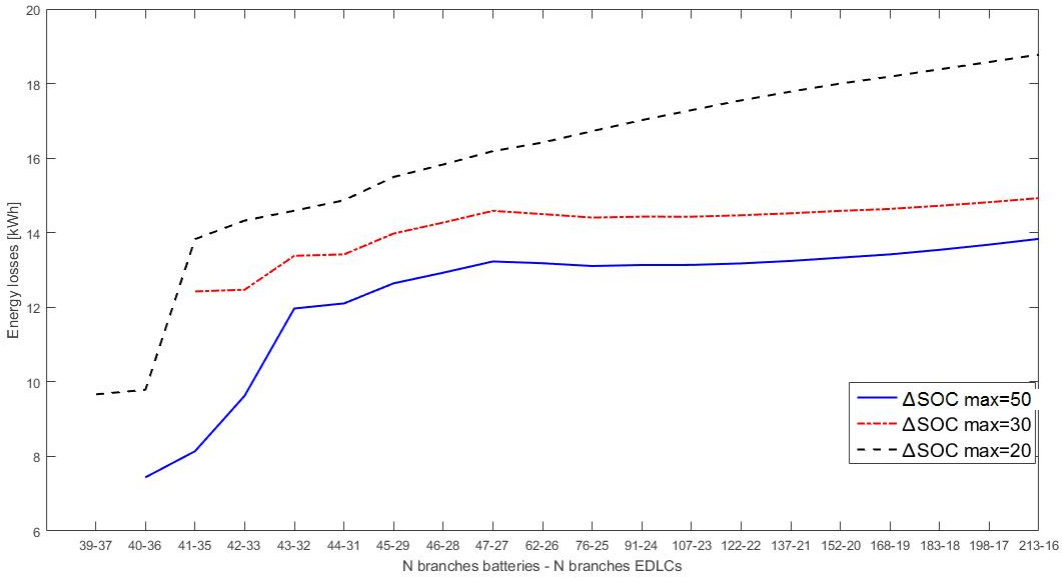

Figure 7.12: system energy losses for 3 different ΔSOC max

Finally, considering the lower cost, capacity fade and energy losses, it is possible to state that the best result is obtained when:

- Branches of batt: 45
- Branches of EDLCs: 29
- ΔSOC max: 50

These values give:

- $m_{batt} = 0.23 \frac{V}{kW}$
- $m_{EDLC} = 0.0235 \frac{V}{kW}$
- Capacity fade after 2000 cycles: 12.291%
- Cost tot: 81855 €
- Energy losses: 12.643 kWh

Figures from 7.13 to 7.15 resume the results of these set of values in terms of power profiles, battery and EDLC SOC and capacity fade.

Comparing Fig 7.13 with Fig. 7.6 it is possible to state that the battery is more subjected to rapid variation of power but the peaks, in both cases, do not exceed 500 kW. However, since the number of branches in the droop case is lower, the battery is subjected to higher currents (till 8C) as confirmed by Fig. 7.15, so the capacity fade is higher. Furthermore, despite the SOC of the battery in Fig. 7.14 and Fig. 7.7 are very similar, in the droop case the SOC variations are larger because of the higher currents, which discharge and recharge the battery faster. The larger capacity discharged contributes to increase the aging of the device.

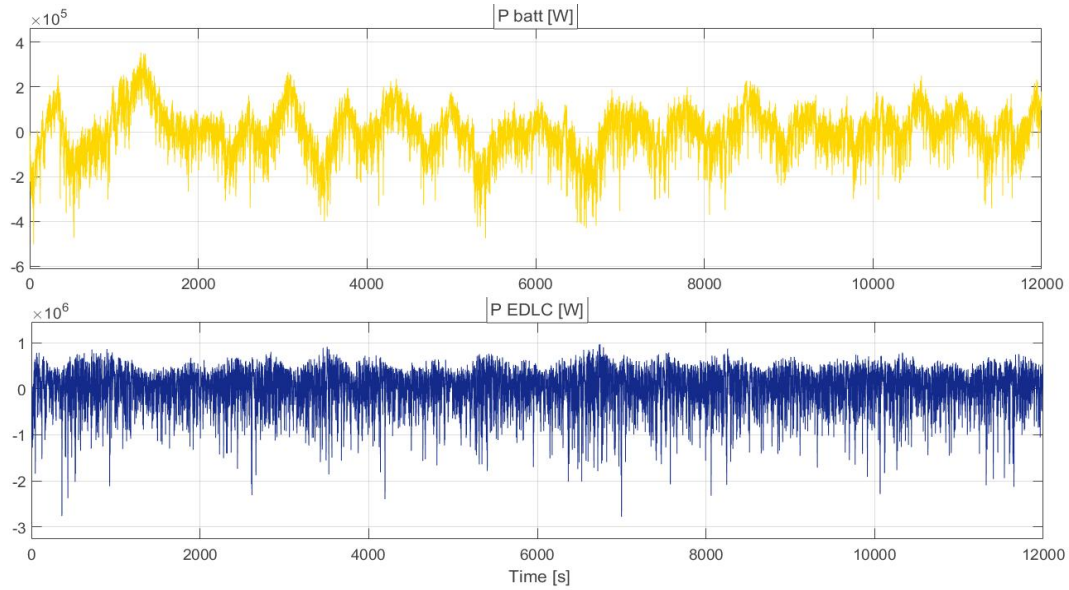

Figure 7.13: power response of battery and EDLC packs

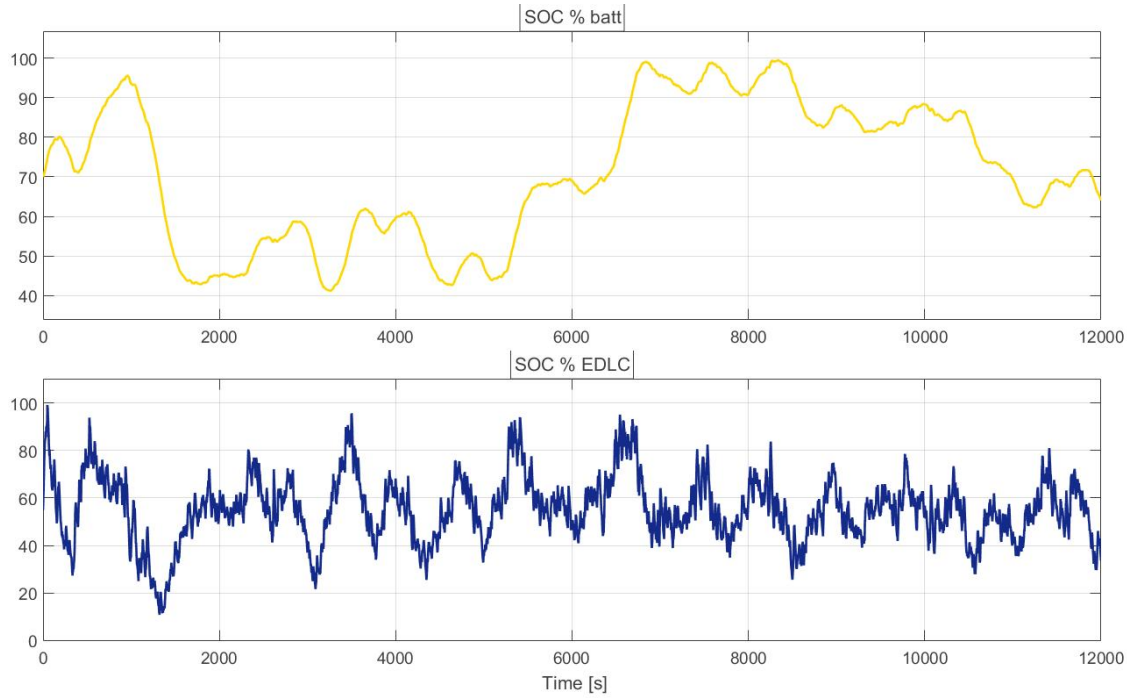

Figure 7.14: SOC variation of the battery and EDLC packs

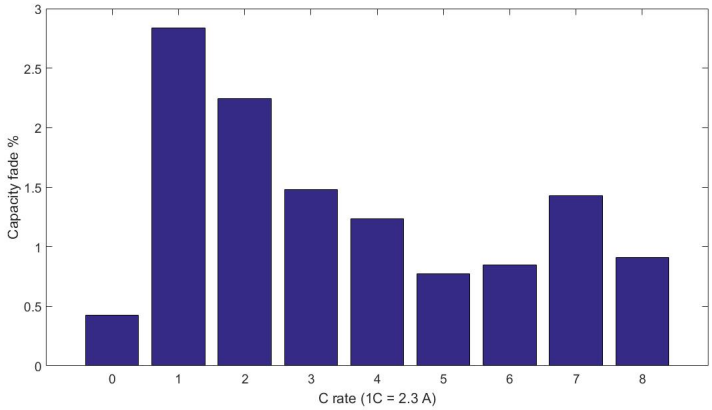

Figure 7.15: percentage of capacity fade introduced by each current rate

8 CONCLUSIONS AND FUTURE DIRECTIONS

In this dissertation, a hybrid energy storage system (HESS) made of batteries and electric double layer capacitors has been studied and modeled to manage the power generated by a renewable energy source, wave energy in this case. The aim was to demonstrate that the HESS can be more economic and performant than an energy storage made of batteries only, using the EDLC as a support for the battery pack. The key point of the study is the implementation of an effective control strategy, in order to valorize the main characteristics of each device.

Firstly, the general scheme of the system has been presented, focusing on the importance of the two DC/DC converters which allow explicit power sharing to both the two energy storages. Then, after presenting the main parameters characterizing an energy storage device, the models of battery and EDLC have been implemented using Simulink. More attention is given to the battery since it is the weaker device and the comparison is made with the case of batteries only. Therefore, the temperature and aging calculation are included into the model. More complex models may be used (especially for the EDLC) but, for the purpose of this study, it is sufficient to guarantee the different dynamic responses of the two devices.

Two control strategies have been implemented in order to coordinate the HESS. The centralized control relies on the effect of a first-order filter to split the power/current reference in low and high frequency components, used as reference signals by the two DC/DC converters. This HPF control depends on communications between the central unit and the converters so it can not work in case of communication failure. However, the system considered in this dissertation does not have a large extension in terms of area so it is suitable to this type of strategy. On the other hand, decentralized control is certainly the most studied and used one since it distributes the control functions on different levels: the first one is implemented at each local converter unit and therefore is always usable. Then, additional levels with slower dynamics can be used to coordinate the system and achieve other goals besides the primary power sharing, such as voltage restoration (which in case of droop-control is always necessary to ensure the stability of the system). Both the strategies include a state of charge control of the EDLC, since it has the lowest energy density and its discharge allocates high currents on the battery.

In order to have a comparison with the case of batteries only, a battery pack has been sized to handle the whole power and the results of the simulation give a capacity fade of almost 20% after 2000 cycles, with a cost of 180340 € and 23 kWh of losses. Then, the two strategies have been simulated, explaining the sizing procedure. In the case of HPF, once the frequency is known, it is easy to calculate the size of each pack so a brute-force approach has been used to find the best cut-off frequency. Instead, in the case of V-P droop, the brute-force approach has been used to find the best combination of branches of batteries and EDLCs since it is not possible to know the power sharing before sizing. Cost, capacity fade and energy losses have been considered the key decisional factors. Even considering a price ten times higher for the EDLC compared to the battery, both the strategies result to have lower cost and better performance than the case with batteries only. In particular, the HPF gives a capacity fade of 5.82 % with a cost of 87630 € and 13.4 kWh of losses, while the V-P droop gives 12.291% with a cost of 81855 € and 12.643 kWh of losses. Therefore, both the strategies succeeded in almost halving the cost and the losses and reducing the capacity fade, with the HPF reducing it by 5 times. From this point of view, the HPF seems to be the most effective.

The next step, since EDLC has been merely considered as a support for the battery pack and no temperature and aging effect have been considered, will be the development of a more accurate model

for the EDLC. This simplification is justified by the far longer lifetime of the EDLC compared to the battery. However, to be able to make considerations about the lifetime and cost of the whole energy storage system, a complete model is necessary. The key factor in this future model of the system may be the annual cost of the HESS, considering the lifetime of each component.

Finally, the work presented in this dissertation can be repeated considering other types of energy storage device, always coupling a technology with slow dynamic and low power density with another with fast dynamic and high power density. For instance, a future study may consider fuel cell and flywheels. These technologies are improving year after year becoming more affordable. As a prove, the EDLC capacitance has been increased by ten times in a few years and new materials are being studied to increase the maximum voltage. As the technology progresses, the price will decrease as in the case in the case of Li-ion batteries. The energy storage systems will be cheaper and cheaper, leading to a more extended penetration of renewable energy sources into the grid and possibly to a larger use of distributed generation.

9 REFERENCES

[1]: European Environment Agency (2017). *Renewable energy in Europe – 2017 Update.* Luxembourg: Publications Office of the European Union

[2]: Sang, C., Woo Young, J. (2016). *Analogical Understanding of the Ragone plot and a New Categorization of Energy Devices.* Energy Procedia, Volume 88, p. 526-530

[3]: Moreno, P., Concha, T. (2016). *Analysis and design considerations of an electric vehicle powertrain*. Madrid: Universidad Politécnica de Madrid

[4]: Tenti, P. (2012). *Convertitore buck-boost, corso di elettronica industriale*

[5]: Wens, M., Steyaert, M. (2011). *Design and Implementation of Fully-Integrated Inductive DC-DC Converters in Standard CMOS.* Springer Netherlands

[6]: Xuemei, Z. (2009). Practical PID Controller Implementation and the Theory Behind. In: *2009 Second International Conference on Intelligent Networks and Intelligent Systems.* Tianjin

[7]: Jianfang, X., Peng, W., Leonardy, S. (2016). *Multilevel Energy Management System for Hybridization of Energy Storages in DC Microgrids.* IEE Transactions on smart grid, Volume 7, Issue 2

[8]: Falnes, J., Kurniawan, A. (2015). *Fundamental formulae for wave-energy conversion*. Royal Society

[9]: emec.org.uk, (2018). *Wave devices.* Available at: http://www.emec.org.uk/marine-energy/wave-devices/

[10]: Bharat, S., Singh, S.N. (2009). *Wind Power Interconnection into the Power System: A Review of Grid Code Requirements.* Elsevier The Electricity Journal, Volume 22, Issue 5

[11]: Gayathri, N., Diksha, J., Ruchira, J. (2015). *Sizing of a Generic Hybrid Energy Storage System for Power Smoothing of a Wind Generator*. IEE

[12]: Chaofeng, L., Zachary, G., Guozhong C. (2016). *Understanding electrochemical potentials of cathode materials in rechargeable batteries.* Elsevier Materials Today, Volume 19, No. 2

[13]: Jiang, Y., Zhang, C., Zhang, W., Shi, W., & Liu, Q. (2013). *Modeling charge polarization voltage for large lithium-ion batteries in electric vehicles.* Journal of Industrial Engineering and Man, Volume 6, No. 2

[14]: Alireza, K., Zhihao, L. (2010). *Battery, Ultracapacitor, Fuel Cell, and Hybrid Energy Storage Systems for Electric, Hybrid Electric, Fuel Cell, and Plug-In Hybrid Electric Vehicles: State of the Art*. IEEE Transactions on vehicular technology, Volume 59, No. 6

[15]: Berckmans, G., Messagie, M., Noshin, O. (2017). *Cost Projection of State of the Art Lithium-Ion Batteries for Electric Vehicles Up to 2030.* Energies, Volume 10, No. 13

[16]: Minh, T., Nesimi, E., Miller, T. (2017). *The Use of Peukert Equation in Lead Acid vs Lithium Ion Battery*. World Applied Sciences Journal, Volume 35, No. 8

[17]: A123 Systems High Power Lithium Ion Cell ANR26650M1. 2008. Available online: http://www.sullivanuv.com/wp-content/uploads/2014/06/A123-Cell-Datasheet-2008-08.pdf

[18]: mit.edu, (2008). *A Guide to Understanding Battery Specifications* Available at: http://web.mit.edu/evt/summary_battery_specifications.pdf

[19]: Buja, G. (2015). *Course of Electric Road Vehicles: batteries*

[20]: batteryuniversity.com, (2018). *Comparison Table of Secondary Batteries.* Available at: http://batteryuniversity.com/learn/article/secondary_batteries

[21]: Curry, C. (2017). *Li-ion battery cost and market.* Available at: https://about.bnef.com/blog/lithium-ion-battery-costs-squeezed-margins-new-business-models/

[22]: Mousavi, S.M., Nikdel, M. (2014). *Various battery models for various simulation studies and applications.* Renewable and Sustainable Energy Reviews, Volume 32

[23]: Kyri, B., Ying, S., Christensen, D. (2017). Modeling Stationary Lithium-Ion Batteries for Optimization and Predictive Control. In*: IEEE Power and Energy Conference Champaign.* Illinois

[24]: Saidani, F., Hutter, F., Scurtu, G., Braunwarth, W. (2017). *Lithium-ion battery models: a comparative study and a model-based powerline communication.* Advances Radio Science, Volume 15, p. 83–91

[25]: Forgeza, C., Friedricha, G., Morcretteb, M., Delacourt, C. (2009). *Thermal modeling of a cylindrical LiFePO4/graphite lithium-ion battery.* Journal of Power Sources, Volume 195, p. 2961–2968

[26]: Gu, W.B, Wang, C.Y. (2000). *Thermal-Electrochemical Modeling of Battery Systems.* Journal of The Electrochemical Society, Volume 147, p. 2910-2922

[27]: Walker, W., Ardebili, H. (2013). *NASA Thermal & Fluids Analysis: New Techniques for Thermoelectrochemical Analysis of Lithium-ion Batteries for Space Applications*

[28]: Nájera, J., Moreno-Torres, P., Lafoz, M., Arribas, J.M. (2017). *Approach to Hybrid Energy Storage Systems Dimensioning for Urban Electric Buses Regarding Efficiency and Battery Aging.* Energies, Volume 10

[29]: Wanga, J., Liua, P., Shermana, E., Soukiaziana, S., Musser, J., Finamore, P. (2011). *Cycle-life model for graphite-LiFePO4 cells.* Journal of Power Sources, Volume, p. 3942–3948

[30]: Grbovic, P.J. (2014). *Ultra-Capacitors in power conversion systems.* Munich: Wiley

[31]: González, A., Goikoleab, E., Andoni Barrena, J. (2016). *Review on supercapacitors: Technologies and materials.* Renewable and Sustainable Energy Reviews, Volume 58, p. 1189-1206

[32]: Innocent, S., Iyuke, S., Ozoemena, K. (2015). *An overview of mathematical modeling of electrochemical supercapacitors/ultracapacitors.* Journal of Power Sources, Volume 273, p. 264-277

[33]: *K2 ultracapacitors - 2.7V series.* Available at: http://www.maxwell.com/images/documents/K2Series_DS_1015370_5_20141104.pdf

[34]: Cañizares, C. (2014). *Trends in Microgrid Control.* IEEE Transaction on smart grid, Volume 5, No. 4

[35]: Storey, N. (2013). *Electronics: a systems approach.* Pearson Education

[36]: Mendis, N, Muttaqi, K. M., Perera, S. (2012). Active Power Management of a Super capacitor-Battery Hybrid Energy Storage System for Standalone Operation of DFIG based Wind Turbines. In: *Industry Applications Society Annual Meeting (IAS*). Las Vegas

[37]: Hredzak, B., Agelidis, V., Demetriade, G. (2017). *Supercapacitor Sizing Method for Energy-Controlled Filter-Based Hybrid Energy Storage Systems.* IEEE Transaction on power electronics, Volume 32, No. 2

[38]: Baoquan, L.,Fang, Z., Xianwen, B. (2012). Control Method of the Transient Compensation Process of a Hybrid Energy Storage System Based on Battery and Ultra-Capacitor in Micro-grid. In: *Industrial Electronics (ISIE), 2012 IEEE International Symposium.* Hangzhou

[39]: Singha Roy, P., Karayaka, H. B., Yan, Y., Alqudah, Y. (2017). Size Optimization of Battery-Supercapacitor Hybrid Energy Storage System for 1MW Grid Connected PV Array. In: *Power Symposium (NAPS), 2017 North American.* Morgantown

[40]: Gayathri, N., Diksha, J., Ruchira, J., Senroy, N., Abhyankar, A. R. (2015). Sizing of a Generic Hybrid Energy Storage System for Power Smoothing of a Wind Generator. In: *Power & Energy Society General Meeting*. Denver

[41]: Paolucci, A. (1990). *Lezioni di trasmissione dell'energia elettrica*. Padova: Cleup

[42]: Jingang, L., Zhou, H., Wenshan, J. (2015). Synchronization of Hybrid Microgrids with Communication Latency. Mathematical Problems in Engineering, Volume 10, p. 1-10

[43]: Wang, P., Setyawan, L. (2015). *Multilevel Energy Management System for Hybridization of Energy Storages in DC Microgrids.* IEEE Transaction on smart grid, Volume 7, No. 2

[44]: Xiao, J., Xiaolei, H., Wang, P. (2015). *A Decentralized Power Management Strategy for Hybrid Energy Storage System With Autonomous Bus Voltage Restoration and State-of-Charge Recovery*. IEEE Transaction on smart grid, Volume 64, No. 9

[45]: Adhikari, S., Tang, Y., Wang, P. (2016). Secondary Control for DC Microgrids. In: *Asian Conference on Energy, Power and Transportation Electrification.* Singapore

[46]: Zheming, J., Meng, L., Guerrero, J. M. (2017). Comparative Admittance-based Analysis for Different Droop Control Approaches in DC Microgrids. In: *DC Microgrids (ICDCM), IEEE Second International Conference.* Nuremburg

[47]: Lin, P., Wang, P., Xu, Q., Xiao, J., (2017). An Integral-Droop based Dynamic Power Sharing Control for Hybrid Energy Storage System in DC Microgrid. In: *Future Energy Electronics Conference and ECCE Asia (IFEEC 2017 - ECCE Asia), IEEE 3rd International.* Kaohsiung

[48]: Wang, P., Setyawan, L. (2015). *Hierarchical Control of Hybrid Energy Storage System in DC Microgrids.* IEEE Transaction on smart grid, Volume 62, No. 8